Reach Extension for Future Optical Access Networks Based on Optical Amplification

Vom Fachbereich Elektrotechnik und Informationstechnik
der Technischen Universität Darmstadt
zur Erlangung der Würde eines
Doktor-Ingenieurs (Dr.-Ing.)
genehmigte

Dissertation

von

M.Sc.
Ali Emsia
geboren am 01.07.1986
in Teheran, Iran

Referent:	Prof. Dr.-Ing. Franko Küppers
Korreferent:	Prof. Dr.-Ing. Bernhard Schmauß

Tag der Einreichung:	16.04.2016
Tag der mündlichen Prüfung:	24.10.2016

D17
Darmstadt 2017

Preface

This dissertation is my four and half years of effort in the Institute for Microwave Engineering and Photonics, at Technical University of Darmstadt.

Firstly, I would like to express my appreciation and gratitude to my advisor **Prof. Dr.-Ing. Franko Küppers** for his endless support of my PhD study, his patience, immense knowledge, and motivation. He opened a new horizon in my life. He could not have been better and perfect than that.

Beside my Professor, I am deeply grateful to my colleague and friend **Dieter Briggmann** for the continuous support and fruitful technical discussions during the PhD study.

My thanks go to **Prof. Dr. Ivan Djordjevic** for his supervision during my 6-month visit in College of Optical Science, University of Arizona, USA.

I would like to thank **Mohammad Tanvir Haidar** for our fruitful discussions about the laser technology. I deeply appreciate my colleagues, **Mohammadreza Malekizandi**, **Sujoy Paul**, and **Dr. Quang Trung Le**, without their precious support it was difficult to conduct my research to the end.

And finally, I would like to thank my wife, my parents, and my sister for their patience and support during my study life.

To my lovely wife, parents, and sister

Erklärung laut §9 PromO

Ich versichere hiermit, dass ich die vorliegende Dissertation allein und nur unter Verwendung der angegebenen Literatur verfasst habe. Die Arbeit hat bis her noch nicht zu Prüfungszwecken gedient.

Zusammenfassung

In den letzten Jahrzehnten wurden optische Netzwerke wegen der Eigenschaften von Glasfasern, die verglichen mit Kupferkabeln eine viel größere Bandbreite bei geringen Übertragungsverlusten erlauben, immer wichtiger. Insbesondere die rasante Entwicklung des Internet durch ständig hinzukommende neue Dienste verlangt den Ausbau des Netzes, damit dem Teilnehmer die notwendige Bandbreite zur Übertragung hochbitratiger Datenströme zur Verfügung gestellt werden kann. Hierfür werden in vielen Ländern passive optische Netze (PON) als breitbandige Zugangsnetze eingesetzt, um die Bedürfnisse der Endverbraucher und der Industrie zu erfüllen, so zum Beispiel G-PON (ITU-T G.984 series [1]) und 10GEPON (IEEE 802.3ah [2]). Die G-PON-Standards, wie 10G-EPON-PRx30 ermöglichen eine symmetrische Übertragungsrate von 10 Gbps und unterstützen ein Leistungs-Budget von 29 dB. Diese Standards wurden für verschiedene Fiber-To-The-x (FTTx) Märkte definiert. Diese Standards nutzen Zeitmultiplex-Verfahren, die jedoch die Anforderungen an zukünftige Zugangsnetze nicht erfüllen. Die Herausforderung ist, in ein bestehendes PON System neue Dienste zu implementieren, die Reichweite zu vergrößern, jedoch gleichzeitig die Betriebskosten zu senken, ohne die Struktur des Central Office (CO) zu ändern [3, 4].

Wellenlängen-Multiplex für PONs (WDM-PON) ist eine vielversprechende Option für die nächste PON-Generation (NG-PON) [5]. Wegen der Punkt-zu-Punkt-Verbindung zwischen Optical Line Terminal (OLT) und Optical Network Unit (ONU) gibt es keine Bandbreiten-Beschränkungen, jedoch größere Übertragungsdistanzen und höhere Sicherheit.

Ein fließender Übergang zwischen den aktuellen PONs und den NG-PONs ist notwendig und es muss gewährleistet sein, dass beide Standards nebeneinander koexistieren können. Deswegen werden Hybrid-TDM/WDM-PONs intensiv für Full Service Access Networks (FSAN) betrachtet. Wie bereits erwähnt, muss der Übergang von aktuellen PONs zu NG-PONs fließend sein, ohne Unterbrechung der Dienste und ohne zusätzliche Kosten. Mit anderen Worten, der Einsatz der NG-PONs soll durch die Verwendung der bestehenden Glasfaserstrukturen höhere Übertragungskapazitäten zur Verfügung stellen. Netzbetreiber bevorzugen während der Übergangszeit eine Koexistenz von PON und NG-PON , um Nachteile bezüglich der Wartung und der Kosten zu vermeiden. Die Betreiber der Netze erhoffen sich durch die NG-PONs wichtige Vorteile, nämlich die Erhöhung der Übertragungskapazität, größere Übertragungsdistanzen und die Senkung der Entwicklungs- und Betriebskosten.

In dieser Dissertation werden Techniken zur Erhöhung der Reichweite, die auf Halbleiterlaserverstärkern (SOA) und Erbium-dotierten Faserverstärkern (EDFA) basieren, vorgestellt. Ziel ist es, eine geeignete Verstärker-Anordnung zu entwickeln, um mit dem NG-PONs die Reichweite und die Anzahl der Teilnehmer zu erhöhen. Des Weiteren werden neue,

kosteneffiziente Sende-Empfänger-Anordnungen vorgestellt, die im NG-PON Verwendung finden können. Chirp Managed Laser (CML) sind kosteneffektive Module für OLT/ONUs. Der CML wird direkt moduliert und kann optische PSK-Signale ohne externen Modulator erzeugen. Darüber hinaus ist eine Daten-Remodulation mit einer Fabry-Perot-Injektionssteuerung möglich. Bei der beschriebenen Verstärker-Anordnung sind die ONU-Laser nicht von den eingespeisten Wellenlängen abhängig und werden daher als transparente ONUs bezeichnet. Dies erspart zusätzliche optische Komponenten in den Sende-Empfänger-Modulen. Bei der vorgeschlagenen Verstärker-Anordnung wird ein fortschrittliches, phasenmoduliertes Signalformat (DPSK) verwendet, welches die Anforderung nach hoher spektraler Effizienz erfüllt. Diese Technik wird erstmalig genutzt, um die Anzahl der Teilnehmer deutlich zu erhöhen und gleichzeitig eine einfache Architektur anzubieten. Die Verstärker-Module bestehen aus zwei SOAs, einem Interferometer mit Verzögerungsleitung, variablen optischen Dämpfungsgliedern und zwei Zirkulatoren.

Das Konzept wurde mit Simulationen und Experimenten untersucht. Der TDM/WDM-PON-Fall wurde mit zwei verschiedenen Modulationsarten simuliert, mit DPSK und mit dem orthogonalen Frequenzmultiplexverfahren (OFDM). Die Messergebnisse bestätigen, dass die vorgeschlagene Verstärkeranordnung mehr als tausend Teilnehmer, in einen optischen Kanal, sowohl Upstream als auch Downstream (US/DS), über eine Einmodenfaser (SMF) mit einer Länge von mehr als 50 km versorgen kann. Die Ergebnisse zeigen, dass die beschriebene Verstärker-Anordnung vorteilhaft und erfolgreich in zukünftigen NG-PONs eingesetzt werden kann.

Abstract

Over the last decades, optical networks have become important for information society. Due to the features of the optical fiber as a transmitting medium, it offers larger bandwidth and lower loss compared to copper cables. Recently, the information society encountered technological advancements due to the evolution of Internet services. With increasing the demand for emerging applications and services, subscribers will require much higher bandwidth as they have today [6]. Passive optical networks (PONs) have been deployed in may countries as a strong broadband access networks. For instance, G-PON (ITU-T G.984 series [1]) and 10GE-PON (IEEE 802.3ah) [2] have been introduced and deployed to satisfy the needs of consumers and business sectors. The G-PONs standards such as 10G-EPON-PRx30 enable symmetrical 10 Gbps rate, and support 29 dB power budget. Other standards such as ITU-T G.984 and IEEE 802.3ah are also considered in different Fiber-To-The-x (FTTx) market. These standards use time division multiplexing (TDM) technology which cannot address the future access network requirements. To incorporate the legacy PON with new services while reducing the operational costs as well as central office (CO) footprints, reach extension (extended transmission distance) techniques are required [3, 4]. wavelength division multiplexing-PON (WDM-PON) appears to be an intriguing option for next-generation-PON (NG-PON) [5], because of point-to-point connectivity from optical line terminal (OLT) to optical network unit (ONU), no bandwidth limitation, higher security, and longer transmission distance.

It is necessary to make a smooth transition from the legacy PON to the NG-PONs, and to assure the co-existence of both standards. Because of this, hybrid TDM/WDM PONs is extensively considered by full service access network (FSAN). Migrating from legacy PONs to NG-PON needs to be smooth without any service interruption or extra-cost. In other words, in NG-PON deployment, the existing fiber infrastructure should be used to provide higher capacity. Network operators prefer the legacy PON and NG-PONs co-existence to avoid any inconvenient issue in terms of maintenance and cost. They consider two significant goals for NG-PONs. First, increasing capacity, and the second is reach extension to reduce the operational and deployment costs.

This dissertation reports reach extension techniques based on semiconductor optical amplifiers (SOAs) and erbium doped fiber amplifier (EDFAs). The aim is to investigate a suitable amplifier scheme to increase the reach and the number of subscribers in NG-PONs. Furthermore, new suitable cost-effective transceiver schemes are demonstrated which can be utilized in NG-PONs. One of them is the chirped managed lasers (CML). This type of laser configuration is directly modulated and can generate optical phase-shift-keying (PSK) signals without need of any external modulator. Additionally, another technique is data remodulation

with Fabry-Pérot injection locking. In this scheme, the ONUs laser sources do not depend on the incoming wavelength, they are called colorless ONUs. This allows us to remove any extra optical components in the transceiver modules at ONUs.

The proposed amplifier configuration uses advance modulation differential phase-shift keying (DPSK) signals format which is another requirement for NG-PON to have high spectral efficiency. This technique is used for the first time to increase a large number of subscriber and offer a simple architecture. The amplification module consists of two SOAs, a delay line interferometer (DLI), variable optical attenuators, and two circulators. The concept is investigated using both simulations and experiments. The TDM/WDM-PON scenario is simulated with two different modulation formats, differential quadrature phase-shift-keying D(Q)PSK and orthogonal frequency division multiplexing (OFDM). The experimental results, successfully verify the amplification scheme proposed in the dissertation can support more than a thousand of subscribers on each optical channel in upstream/downstream (US/DS) scenario transmission over more than 50 km of single-mode fiber (SMF). The results show that the amplification technique is a strong candidate for long reach NG-PONs deployments.

Contents

Chapter 1

Introduction

Passive optical networks (PONs) are favorable candidates for service providers compared to other access networks. This is mainly due to the higher bandwidth they provide by transmitting through optical fibers. In wireless access networks, WiFi (802.11 [7]) and WiMAX (802.16 [8]) are two widely used technologies. The recent WiFi (802.11n) technology has bit rate of 248 Mbps and less than 500 meters of coverage. Compared to WiFi (wireless fidelity), WiMAX (worldwide interoperability for microwave access) covers around 5 km with bit rate of 75 Mbps. Both technologies provide point-to-multipoint (P2M) access in which the bandwidth is shared by different subscribers. Nevertheless, these technologies hardly support higher bandwidth-intensive services, such as IPTV and HDTV, from which the service providers can increase their revenues. Another access technology is the copper-based digital subscriber line (DSL) (G.992/993 [9,10]) that is the most widely used access technology nowadays. There are various options of DSL, ADSL (asymmetric DSL) that provides upstream/uplink (US/UL) rate of 1 Mbps and downstream/downlink (DS/DL) rate of 8 Mbps, and reaches about 5.5 km. The ADSL2+ is the successor of ADLS with improvement in data rate, 3.5 Mbps and 24 Mbps for US and DS, respectively. The fastest DSL version is very-high-bit-rate DSL2 (VDSL2) with 100 Mbps in both directions but over shorter distances. The state-of-art DSL technology is called G.fast where G stand for ITU-G series recommendation [11]. This technology supports higher bit rates for short distance scenarios, the G.fast aims at increasing the bit rate in fiber-to-the-distribution-point (FTTdp). This technology is still under laboratory investigations.

All these technologies have bandwidth bottlenecks, rapidly increasing services, which occupy a large bandwidth, pushes the technology advancement in PONs further. Looking to the future, every access technology should have a fiber, evolution of the wireless connectivity requires a fiber-based backhaul. Fiber-to-the-x (FTTx) is an undeniable solution for the copper, cable access networks development, and for any other access technology. The PONs have won the competition in fiber-based network architecture due to following reasons:

- **Point-to-multipoint connectivity**
  This topology is inexpensive to be deployed and maintained. The passive splitters used in the network do not require power supplies, this gives the deployment flexibility. The encryption can ensure the security of the transmission line. The bandwidth is shared in this topology and is not symmetrical for US/DS direction.

- **Point-to-point connectivity**
  Each subscriber has a dedicated large bandwidth, in this case the bandwidth is not shared. This topology offers a symmetrical bandwidth for US/DS directions, which makes it more important for low-latency applications such as video-on-demand.

- **Low maintenance cost**
  As no electronics is deployed between the central office and subscribers, the maintenance cost is reduced.

- **Cost-effective**
  The PON uses minimal number of optical transceivers in OLT and ONU.

- **Data-rate flexibility**
  The data rates launched into fibers can be upgraded with technology evolution. The data rates are now going beyond 40 Gbps in next-generation PON (NG-PON).

- **Wavelength division multiplexing**
  Multiple wavelengths can be combined together to increase the transmission bandwidth using wavelength division multiplexing (WDM) technology. The WDM technology will be explained in later chapters of this dissertation.

Fig. 1.1 shows a typical PON architecture. The central office provides data, voice, and video traffic through OLT interface. The optical signals are received by the ONUs and converted to electrical signals. The ONUs boxes can be located outside building, on curbs, or inside houses. The passive splitters are optical splitters to distribute (route) optical signals to the corresponding subscriber.

The PON systems have been deployed in many places [12–14], two standards are widely available which are G-PON and EPON. The evolution of the internet and multimedia services causes the existing PONs to be upgraded. For instance, Fig. 1.2 illustrates the global IP traffic categorized by applications, we see that IP traffic will grow at a compound annual growth rate (CAGR) of 27% percent from 2014 to 2019 [15]. The numbers on each bar shows the total growth in exabyte per month. The NG-PON is being reviewed by full service access network (FSAN) as well as ITU-T to address such bandwidth growths in the future. The NG-PON2 which is the second phase of this technology should provide 40 Gbps data rate, this future standard combines both time-division multiplexing (TDM) and WDM technologies. One of the requirements for NG-PON2 is the co-existence with the existing technology, in other words, the deployment of the new technology must be compatible with the current optical distribution networks (ODNs) to reduce the **operational and deployment costs**. Another critical requirement is the **optical path loss** introduced by passive elements in the transmission. To find a technique to increase the optical power budget to compensate for the loss is challenging. These requirements pave the way for the smooth migration from legacy PON to NG-PON2 without interrupting the current connections to the subscribers. The wavelength plan should be arranged so that there exist minimum cross-talk between legacy PON and NG-PON2. Network operators desire unceasingly to reduce the operational expenditure cost of the networks. Clearly, the subscribers do not expect the price growth of their broadband lines.

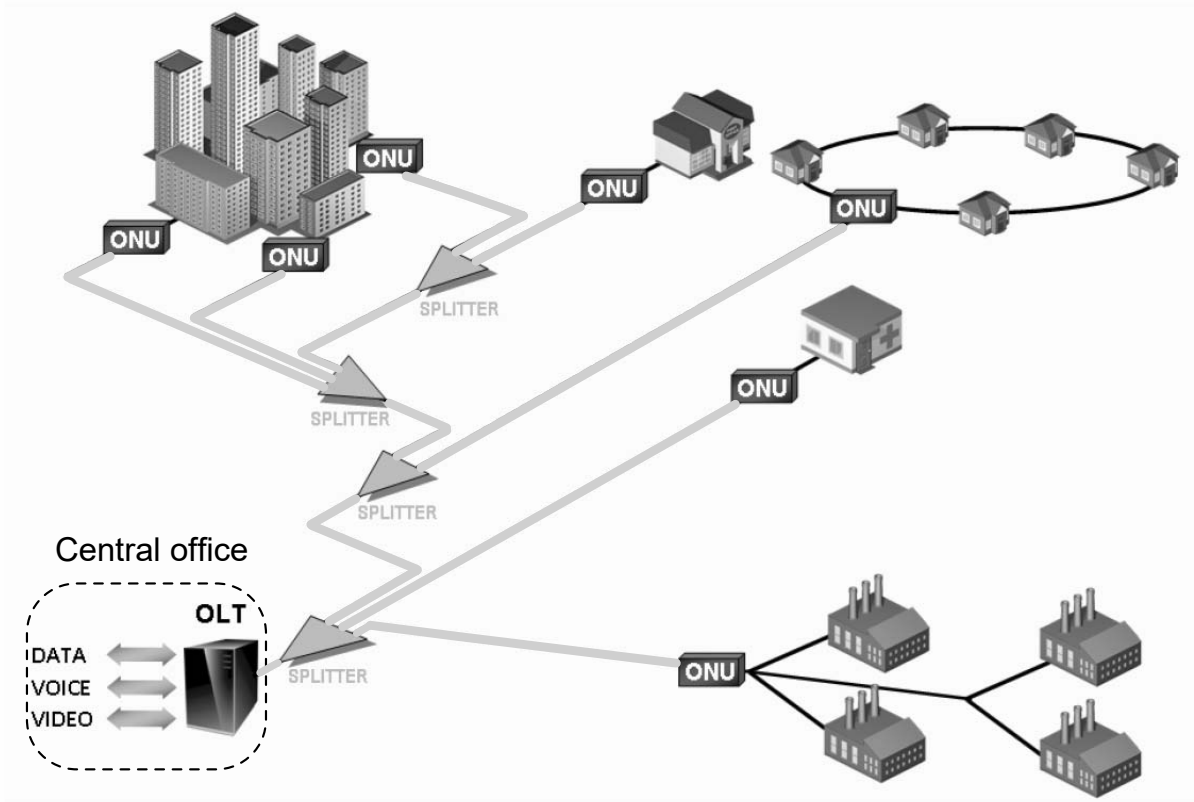

Figure 1.1: A passive optical network architecture. OLT: optical line terminal, ONU: optical network unit.

Therefore, lowering the module costs, and enlarging the bandwidth are two key factors which will be goals of this dissertation.

1.1 Motivation and Goals

To reduce the operational costs and increase the optical power budget, new transceivers need to be designed in such a way that the optical signals can be transmitted even longer distance with higher quality. Suitable selection of **amplification techniques** are required in the remote node (RN) where signals are distributed to manage the optical path loss introduced by passive splitters, fibers, and passive elements.

Several methods have been discussed in the literature for the reach extension and optical power budget improvements, the midway amplifiers such as SOAs [16], EDFA [17], and Raman amplification [18] can be mentioned. In [19] the extension strategies have been completely investigated, EDFAs and Raman techniques are not recommended for short-distance access networks due to high costs and requirement of a longer distance for optical pumping. SOAs are currently most favorable candidates among all other optical amplification methods, for the reason that they have moderate to high optical gain, they are inexpensive, integrable

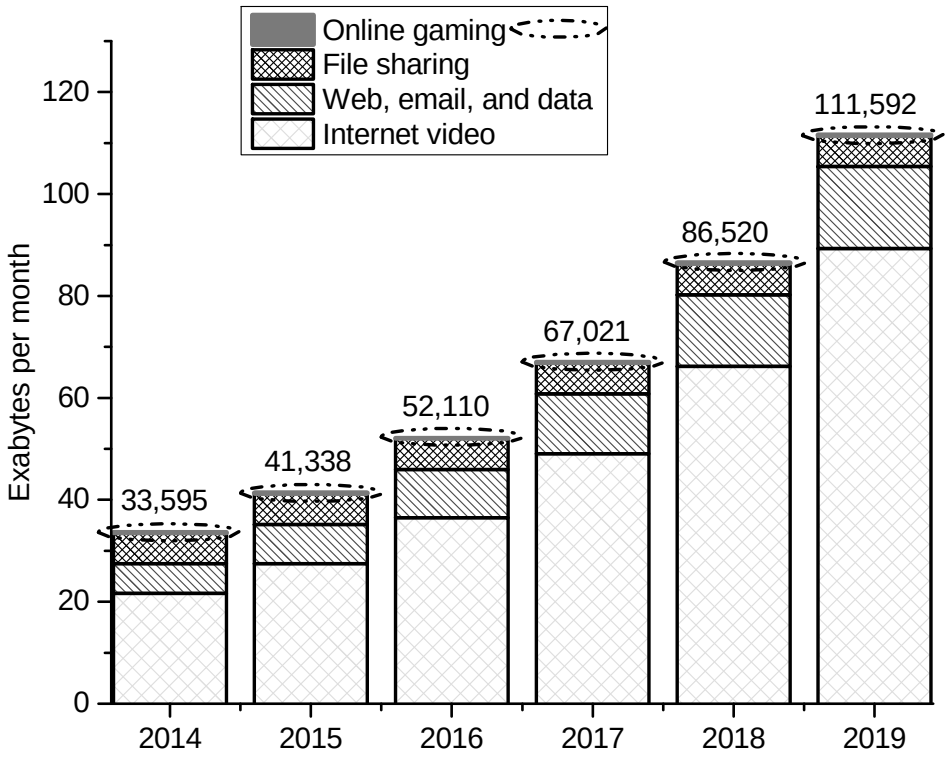

Figure 1.2: Global IP Traffic by Application Category, 2015 [15].

with photonic devices, capable of intensity modulation with high data rates, and they can be designed for a specific optical band [20]. Different techniques can be employed to extend the reach and increase the number of subscribers in PONs. Authors in [21] demonstrated noise-power extenders based on erbium doped fibers that enables $4,000$ subscribers in TDM-based PONs. They reused optical noise as a pump for the optical amplification. However, the ONUs architectures need complex modifications. In [22], 10 Gbps burst-mode upstream DWDM-TDM PONs was demonstrated that resulted in 16×512 split, distance of 100 km, however, additional SOAs were used to remedy the penalties introduced by burst-mode receivers (BMRxs). Authors in [23] demonstrated $8,192$ splitter in DWDM-TDMA PON scenario with symmetrical 10 Gbps bit-rate. They achieved 135 km transmission through SMF. The electro-absorption modulator-SOA (EAM)-SOA was used at ONUs for US transmission.

One technical problem arising in US scenario at high data rates is the complexity of receivers at OLTs. The optical packets travel through different paths, as a result, signal amplitude levels vary, therefore a receiver is needed that can track the packets power variations and their corresponding phase alignments. The BMRxs are designed to tackle this problem. To ease the design criteria and complexity of such receivers, the proposed SOA-based extender is

used to equalize the bursts from different subscribers and to compress the dynamic range (DR) in the optical domain. The proposed extender manifests a large DR compression compared to previously reported results [24] that can simplify the BMRx design complexity such as threshold and automatic gain control. The burst equalization have been studied by various others [25–27], however, their proposed techniques showed pattern effects and high dependence on bias current of the SOAs.

Another challenge is to develop a cost-effective source to enable the easy deployment of the NG-PONs. One option is DS data remodulation at the ONUs for US transmission [28]. The DS optical signal is remodulated again and transmitted to US direction. This enables using colorless sources at ONUs and avoids need for the installation of any wavelength selective source. Several techniques have been proposed in [29, 30], however, some drawbacks have been observed, e.g., the mode fluctuations of the laser limits the transmission distance and reduces the optical signal quality. Using injection locked Fabry-Péerot laser diodes can help to reduce the overall cost in PONs.

The purpose of this dissertation is to investigate the amplification techniques to provide reach extension as well as increasing splitting ratio for NG-PONs, two amplifiers are investigated SOAs and EDFAs, respectively. The Simulation and experimental results are demonstrated in multi-gigabit WDM/TDM PON scenarios. It is shown that the deployment of the proposed techniques is feasible and promising solutions for the future access networks. The amplification scheme include advanced modulation formats which in turn increase the spectral efficiency and the transmission data-rate. Cost-effective transmitters/receivers configurations are discussed as an inexpensive option for NG-PONs.
The two key requirements of NG-PONs namely, the number of subscribers and reach (distance) extension are discussed and competitive solutions are proposed. The dissertation contribution can lead to increasing the number of subscriber at each wavelength to a large value, providing inexpensive transceiver components for OLTs/ONUs, and expanding the transmission bandwidth.

1.2 Thesis Organization

The structure of the thesis is as follows,

Chapter 2 provides an overview of optical communication systems on single-mode fiber, linear and nonlinearity properties of optical fibers, and various optical components such as light sources, arrayed-waveguide grating, optical modulators, and optical amplifiers.

Chapter 3 describes the optical transmission techniques and modulation formats. It explained how the optical signals are generated from the electrical data sequence. The advanced modulation formats QPSK, and OFDM will be discussed.

Chapter 4 moves forward from fundamental explanations to broadband access networks. This chapter explains different access networks and gives a comparison between them in the market. Th wireless and wired will discussed in detail in this chapter and passive optical networks will be introduced and selected as a better option for future broadband access networks.

Chapter 5 elaborates the simulation results performed throughout this study. The SOA-

based power extender will be introduced with flexible two different modulation formats DPSK, and DQPKS. The EDFA-based extender will be investigated for OFDM modulation format. Both amplification techniques will be compared.

Chapter 6 shows the experimental results of the proposed techniques. This chapter is solely based on SOA-based amplification. The questions mentioned earlier about NG-PON requirements will be addressed here. It will be manifested that large number of subscribers can be served with high bit-rate using the proposed technique.

Finally, **chapter 7** concludes the study, highlights what has been achieved, and provides a prospective for future works in this area.

Chapter 2

Basics of Optical Communications

2.1 Electromagnetic Fields in the Optical Fiber

The technology advancement in low-loss silica fiber production, and progress in development of optical components have boomed the optical fiber communications industry in the past years. Demands for higher bandwidths due to newly emerging services makes the low-loss silica fiber optic the best solution as a medium of the transmission. The advantages of optical fibers are inexpensive, small size, enabling transmission of high bit rates. As a result of these advantages, the silica fiber optics have become one the most important transmission media in the recent century.

To define the behavior of the wave propagation in the fiber electromagnetic wave theory must be considered. The principle of electromagnetic wave propagation is based on Maxwell's equation [31]. The differential Equations in vector forms are

$$\boldsymbol{\nabla} \times \mathbf{E} = -\frac{i\omega}{c}\mathbf{B} \tag{2.1}$$

$$\boldsymbol{\nabla} \times \mathbf{H} = \frac{i\omega}{c}\mathbf{D} \tag{2.2}$$

$$\boldsymbol{\nabla} \cdot \mathbf{D} = 0 \tag{2.3}$$

$$\boldsymbol{\nabla} \cdot \mathbf{B} = 0 \tag{2.4}$$

where $\mathbf{E}$ is the electric field, $\mathbf{D}$ is the electric flux density, $\mathbf{H}$ is the magnetic field, and $\mathbf{B}$ is magnetic flux density. Here, zero conductivity, and no free charges are assumed, and $\boldsymbol{\nabla} \equiv (\frac{\partial}{\partial x}\widehat{x}, \frac{\partial}{\partial y}\widehat{y}, \frac{\partial}{\partial z}\widehat{z})$. The bold notation denotes the vector field. The above Equations can be related as

$$\mathbf{D}(\omega) = \varepsilon(\omega)\mathbf{E}(\omega) = n^2(\omega)\mathbf{E}(\omega) \tag{2.5}$$

$$\mathbf{B} = \mu\mathbf{H} \tag{2.6}$$

where n is the refractive index of the medium, μ is the magnetic permeability, and ε is the dielectric permittivity of the medium. The wave equation can be derived from Maxwell

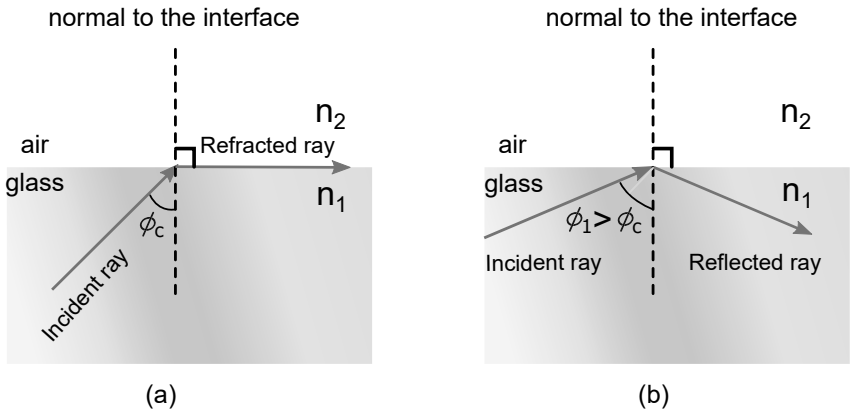

Figure 2.1: The guidance of the light ray in denser medium ($n_1 > n_2$), (a) the critical angle ϕ_c (the refraction angle is greater than the incident angle), (b) the total internal reflection (the angle of incident is greater than the critical angle).

equations by taking curl of Eq. 2.1

$$\begin{aligned}\boldsymbol{\nabla} \times \boldsymbol{\nabla} \times \mathbf{E} &= \cancelto{0}{\boldsymbol{\nabla}(\boldsymbol{\nabla} \cdot \mathbf{E})} - \boldsymbol{\nabla}^2\mathbf{E} \\ &= i\frac{\omega}{c}\boldsymbol{\nabla} \times \mathbf{B} = i\frac{\omega}{c}(-i\frac{\omega}{c}\mathbf{D}) \\ &= \boldsymbol{\nabla}^2\mathbf{E} + \frac{\omega^2}{c^2}\varepsilon(\omega)\mathbf{E} \end{aligned} \tag{2.7}$$

where $\mu = 1$. The propagation of light in the optical fiber rely on the total internal reflection (TIR) phenomenon. When the light is incident at interface with smaller refractive index, then the ray is reflected from the interface plane totally, if the angle of the incident is larger than the critical angle ϕ_c. The critical angle occurs when the angle of refraction is $90°$, so that the total ray is reflected. This phenomenon is illustrated for air-glass interface in Fig 2.1. The angles are measured from the rays to the normal line orthogonal to the interface. Figure 2.1 illustrates that the incident ray has larger angle than ϕ_c at the interface which results in TIR. Thus, according to the Snell's law

$$\begin{aligned} n_1 \sin(\phi_1) &= n_2 \sin(90°) \\ \phi_1 = \phi_c &= \sin^{-1}\left(\frac{n_2}{n_1}\right) \end{aligned} \tag{2.8}$$

Figure 2.2 shows an optical fiber consisting of a dielectric core surrounded by rarer material $n_2 < n_1$ by cladding. They both are made from glass. The core diameter is around $8\mu m$ and that of cladding is about $125\mu m$ for single-mode fiber (SMF). The core refractive index n_1 is greater than cladding refractive index n_2. The Δ is the fractional index change at the core-cladding interface which is obtained as

$$\Delta = \frac{n_1^2 - n_2^2}{2n_1^2} \tag{2.9}$$

$$\Delta \approx \frac{n_1 - n_2}{n_1} \qquad \text{If } n_1 \approx n_2 \tag{2.10}$$

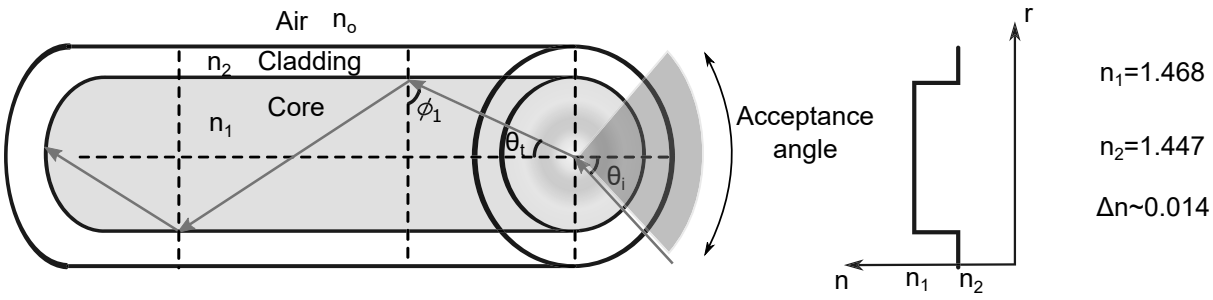

Figure 2.2: Cylindrical optical fiber.

In order to find the incident angle on the entry of the fiber input at which the light is totally internally reflected, the relation between θ_i and ϕ_1 need to be formulated. From Snell's law follows

$$\frac{\sin(\theta_i)}{\sin(\theta_t)} = \frac{n_1}{n_o} \tag{2.11}$$

$$\tag{2.12}$$

The TIR occurs when

$$\begin{aligned} \sin(\phi_1) = \cos(\theta_t) &> \frac{n_2}{n_1} \qquad (2.13)\\ \sqrt{1-\sin^2(\theta_t)} &> \frac{n_2}{n_1} \\ \sin(\theta_t) &< \sqrt{1-\frac{n_2^2}{n_1^2}} \\ \sin(\theta_i) &< \frac{n_1}{n_o}\sqrt{1-\frac{n_2^2}{n_1^2}} \\ \sin(\theta_i) &< \sqrt{\frac{n_1^2-n_2^2}{n_o^2}} \qquad (2.14) \end{aligned}$$

Therefore, in order to trap the light in the optical fiber, the incident light angle must be less than θ_i, and $\sin(i_m)$ is termed as numerical aperture (NA) of the fiber. This is shown as a cone in Fig. 2.2 (acceptance angle).

$$NA = \sqrt{n_1^2 - n_2^2} \tag{2.15}$$

Since SMF will be considered throughout this work, the ray theory cannot be used to specify the modes propagating in the SMF, thus, the Maxwell equations 2.1 and 2.2 need to be solved.

The optical modes are the solution of the wave equation in cylindrical coordinate. The step-index profile fiber is considered here. The wave equation can be written as [31]

$$\frac{\partial^2\Psi}{\partial r^2} + \frac{1}{r}\frac{\partial\Psi}{\partial r} + \frac{1}{r^2}\frac{\partial^2\Psi}{\partial\phi^2} + [k_0^2 n^2(r) - \beta^2]\Psi = 0 \tag{2.16}$$

where k_o is the wavenumber in the vacuum, and Ψ represents the field components. The cylindrical coordinated (r,ϕ,z) is used. As the refractive index only varies in radial direction, the solution the the Eq. 2.16 can be solved by separation of variables. The guided modes of a step index fiber is written as

$$\Psi(r,\phi) = \begin{cases} \frac{A}{J_l(U)} J_l(\frac{Ur}{a}) \begin{bmatrix} \cos(l\phi) \\ \sin(l\phi) \end{bmatrix} & \text{if } r < a \\ \frac{A}{K_l(W)} K_l(\frac{Wr}{a}) \begin{bmatrix} \cos(l\phi) \\ \sin(l\phi) \end{bmatrix} & \text{if } r > a \end{cases} \tag{2.17}$$

where $J_l(\frac{Ur}{a})$ is the Bessel functions of the first kind and $K_l(\frac{Wr}{a})$ is the modified Bessel functions of the second kind of order l. A is a constant for a particular fiber mode.

$$U = a\sqrt{k_0^2 n_1^2 - \beta^2} \tag{2.18}$$

and

$$W = a\sqrt{\beta^2 - k_0^2 n_2^2} \tag{2.19}$$

U and W are mode parameters of the fiber from which the normalized waveguide parameter can be obtained

$$V = \sqrt{W^2 + U^2} = \frac{2\pi}{\lambda_0} a \sqrt{n_1^2 - n_2^2} \tag{2.20}$$

A fiber that has $V < 2.405$ supports only the fundamental HE_{11} mode and is called single-mode-fiber, $V = 2.405$ is the cut-off number (normalized frequency). Wavelengths longer than cut-off show single-mode behavior $\lambda > \lambda_c$.

2.2 Linear Properties of Optical Fiber

Two important linear effects are considered in this work, the fiber attenuation, and the chromatic dispersion. Other effects will not be treated here as they are not the main concern of the work.

2.2.1 Attenuation

The silica fiber attenuates the light as it propagates though. The loss can be subdivided by intrinsic (material) and extrinsic (technological). The extrinsic loss can be inhomogeneity of the material, geometry effects (sharp bends of the fiber), bad input-output light coupling, splice loss and so forth. The intrinsic loss caused by absorption due to material impurities, Rayleigh scattering, and intrinsic absorption of the silica. The absorption coefficient over length L is given by

$$\alpha[dB/km] = \frac{10}{L} \log_{10}(\frac{P_{in}}{P_{out}}) \tag{2.21}$$

P_{in} is the launched power into the fiber and P_{out} is the output power at distance L. A typical loss of silica fibers is about 0.2 dB/km.

2.2.2 Chromatic Dispersion

As there is no monochromatic or single-frequency source, the light exhibits a band of frequencies (the linewidth is not completely zero). The spectral components travel with different velocity which introduces propagation delay between optical paths traveled by spectral components. This leads to pulse broadening at the output of the fiber. Dispersion causes an inter-symbol interference (ISI) between neighboring pulse. This limits the maximum available bandwidth in a fiber. The total dispersion can be presented as material dispersion and waveguide dispersion. The total dispersion can be written as

$$D = D_M + D_W \tag{2.22}$$

To formulate the dispersion parameter D, we start with the group delay of pulse broadening along the SMF that is given by

$$\tau_g = \frac{1}{c}\frac{d\beta}{dk} \tag{2.23}$$

where β is the propagation parameter within the core of the fiber, k is the wavenumber in the vacuum, and c is the velocity of light in the vacuum. The dispersion parameter of the first order is defined as rate of change of the group delay with respect the wavelength

$$D = \frac{d\tau_g}{d\lambda} \tag{2.24}$$

$$= -\frac{\omega}{\lambda}\frac{d\tau_g}{d\omega} = -\frac{\omega}{\lambda}\frac{d^2\beta}{d\omega^2} \tag{2.25}$$

D is in unit of [ps$\cdot$ nm$^{-1}\cdot$-km^{-1}], it expresses the pulse broadening with bandwidth of 1 nm after propagation of 1 km. Figure 2.3 shows the SMF dispersion in terms of wavelength. The dispersion is zero at 1310 nm and 17 ps/nm/km at 1550 nm, these values are commonly used in optical fiber transmissions.

2.3 Optical Components

The optical components are the key elements of PONs. This chapter will discuss about the optical components used in all experimental measurement during this thesis. The operation principle of each component will be elaborated.

2.3.1 Optical Light Sources

Fabry-Pérot Laser Diodes

The FP-LD has two partially reflecting mirrors at each end of the cavity to form a resonator. The electric field is reflected back and forth, this results in standing electromagnetic waves in

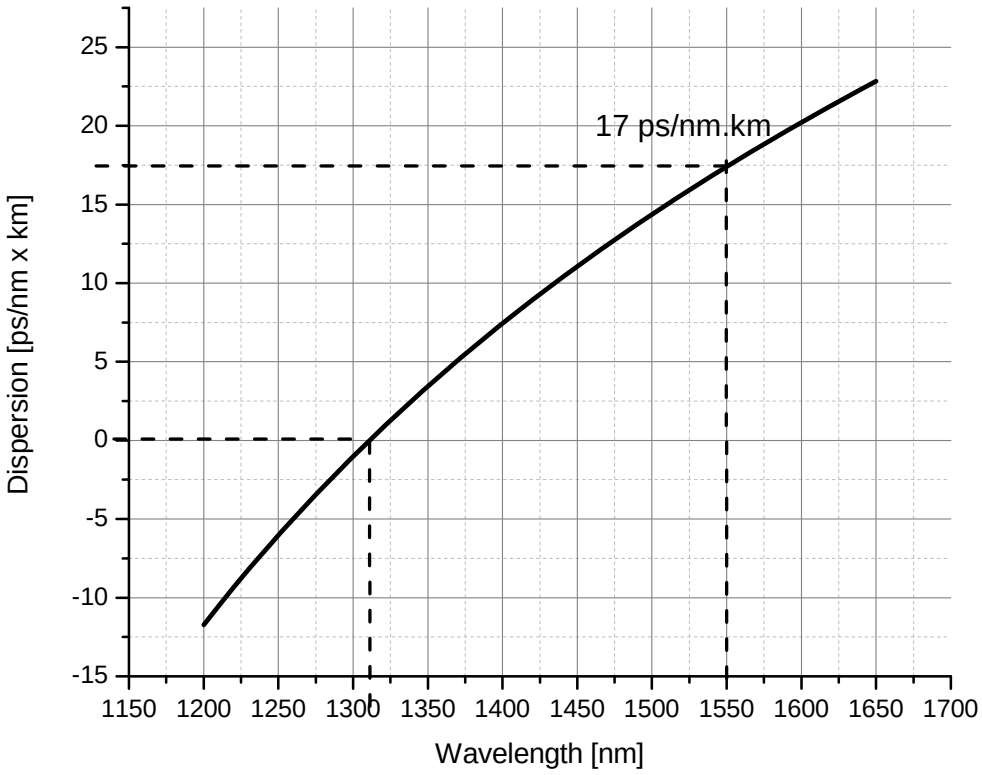

Figure 2.3: Single-mode fiber total dispersion versus wavelength, parameter are retrieved from Corning-28 [32].

the cavity. The length of the cavity is related to multiple integer of half-wavelength as follows,

$$m\frac{\lambda}{2} = L \qquad m = 1, 2... \tag{2.26}$$

$$f = m\frac{c}{2L} \tag{2.27}$$

where m is the cavity mode, L is the cavity length, and f is the resonant frequency. The frequency spacing between neighboring modes is called free spectral range (FSR). This is shown in Fig. 2.4(a). The E_0 represents the field amplitude at some instance in the cavity, and $E_1 = rE_0$ which is the reflected wave, assuming the harmonic waves, the resultant E_{cavity} is the infinite interference among all traveling waves in the cavity and can be formulated as (assuming that the reflection coefficient of the mirrors are the same)

$$\begin{aligned} E_{cavity} &= E_0 + E_1 + ... \\ &= E_0 + r^2 E_0 \exp(-j2kL) + \\ &\quad r^4 E_0 \exp(-j4kL) + r^6 E_0 \exp(-j6kL) + ... \end{aligned} \tag{2.28}$$

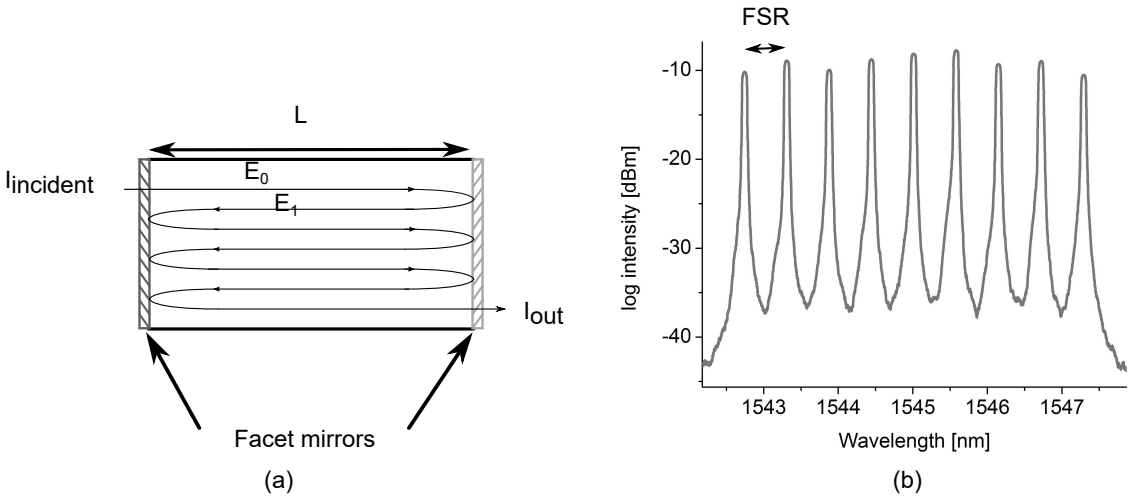

Figure 2.4: Schematic of a Fabry-Pérot laser diodes, (a) Optical cavity, (b) Log intensity versus wavelength for different modes.

The sum can be calculated using geometric series

$$E_{cavity} = \frac{E_0}{1 - r^2 \exp(-j2kL)} \tag{2.29}$$

After having evaluated the resultant electric field, the optical intensity of the cavity is calculated as

$$\begin{aligned} I_{cavity} &= |E_{cavity}|^2 \\ &= \left(\frac{E_0}{1 - r^2(\cos(2kL) - j\sin(2kL))}\right)\left(\frac{E_0}{1 - r^2(\cos(2kL) + j\sin(2kL))}\right) \\ &= \frac{E_0^2}{1 - 2r^2\cos(2kL) + r^4} = \frac{E_0^2}{1 - 2R_F + 4R_F\sin^2(2kL) + R_F^2} \\ &= \frac{E_0^2}{(1 - R_F)^2 + 4R_F\sin^2(2kL)} \end{aligned} \tag{2.30}$$

where $R = r^2$, and k is the wavenumber. The maximum intensities occur when $kL = m\pi$ in Eq. 2.30, as depicted in Fig. 2.4(b). The spectral width of each mode is evaluated as full width half maximum (FWHM), and is related to finesse F of the resonator. The following relation represents this dependency,

$$\begin{aligned} \Delta f &\approx \frac{f}{F} \\ F &= \frac{\pi\sqrt{R_F}}{1 - R_F} \end{aligned} \tag{2.31}$$

Now, if we assume $I_{incident}$ is the input incident to the cavity, the fraction of it $1 - R$ enters the cavity, and again a fraction of it $1 - R$ escapes the cavity as indicated in Fig. 2.4(a), then it

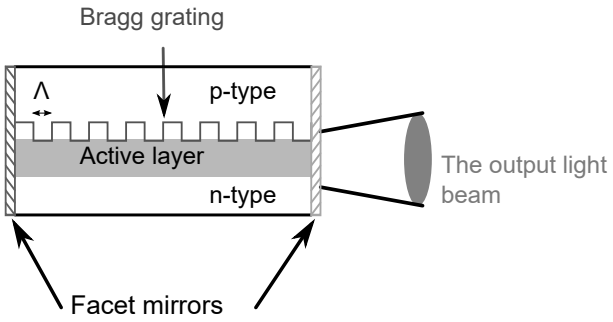

Figure 2.5: Schematic of a distributed feedback laser.

follows that

$$I_{out} = I_{incident} \frac{(1-R)^2}{(1-R)^2 + 4R\sin^2(2kL)} \tag{2.32}$$

Distributed Feedback Lasers

DFB lasers have the selective gratings inside their cavity, they are based on Bragg diffraction phenomenon in which the electromagnetic waves are coupled and propagate in forward and backward directions. The coupling between backward and forward waves are due to the periodic change of the refractive index in the active region. To create the periodic variation in the refractive index, one the hetero-interfaces needs to be corrugated. Figure 2.4 illustrates a structure of a DFB laser. The structure consists of two facet mirrors which have high reflectivity and the other end with partial reflectivity. The Λ is the period of the grating which is chosen to meet the Bragg condition for reflection in opposite and negative traveling wave directions. The Bragg condition is

$$2\beta\Lambda = 2m\pi \tag{2.33}$$

$$\lambda_B = \frac{2n\Lambda}{m} \tag{2.34}$$

where β is the Bragg propagation constant, and m denotes the diffraction order. Equation 2.33 shows that β depends on the period of the grating Λ, by changing Λ the Bragg wavelength λ_B can be shifted accordingly.

2.3.2 Mach-Zehnder Interferometer

The MZ interferometer (MZI) can be used as a Filter to separate/demultiplex two neighboring optical channels. It will be used to separate the all-optical OFDM odd and even channels (subcarriers) in this work. Figure 2.6 shows the general structure of a MZI which has two inputs and two outputs. The incoming optical signals are split into two paths, the optical path length difference introduces a phase shift of ϕ which in turn, it multiplexes the channels from

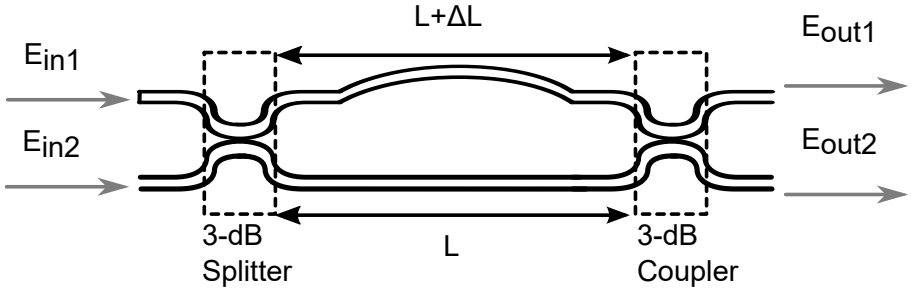

Figure 2.6: Structure of a Mach-Zehnder Interferometer.

each other at the output. The induce phases can be written as

$$\phi_1 = \frac{2\pi n L}{\lambda} \tag{2.35}$$

$$\phi_2 = \frac{2\pi n (L + \Delta L)}{\lambda} \tag{2.36}$$

The transfer function of the given Mach-Zehnder interferometer is the cascade of two optical couplers, and a phase shifter which can be obtained as

$$\begin{aligned}
\begin{bmatrix} E_{out1} \\ E_{out2} \end{bmatrix} &= T_{3-dB} \cdot T_{phase} \cdot T_{3-dB} \begin{bmatrix} E_{in1} \\ E_{in2} \end{bmatrix} \\
&= \frac{1}{2} \begin{bmatrix} 1 & j \\ j & 1 \end{bmatrix} \begin{bmatrix} \exp(-j\phi_1) & 0 \\ 0 & \exp(-j\phi_2) \end{bmatrix} \begin{bmatrix} 1 & j \\ j & 1 \end{bmatrix} \begin{bmatrix} E_{in1} \\ E_{in2} \end{bmatrix} \\
&= \frac{1}{2} \exp[-j(\frac{\phi_1 + \phi_2}{2})] \begin{bmatrix} 2j\sin(\frac{\phi_1 - \phi_2}{2}) & 2j\cos(\frac{\phi_1 - \phi_2}{2}) \\ 2j\cos(\frac{\phi_1 - \phi_2}{2}) & -2j\sin(\frac{\phi_1 - \phi_2}{2}) \end{bmatrix} \begin{bmatrix} E_{in1} \\ E_{in2} \end{bmatrix}
\end{aligned} \tag{2.37}$$

If we assume the second input E_{in2} is terminated, then the output powers can be obtained as

$$\begin{bmatrix} P_{out1} \\ P_{out2} \end{bmatrix} = \begin{bmatrix} \sin^2(\frac{\Delta\phi}{2}) \\ \cos^2(\frac{\Delta\phi}{2}) \end{bmatrix} \tag{2.38}$$

This is shown in Fig. 2.7, by changing the voltage on the electrode in the lower arm the solid curve is changed to the dashed curve, depending on the phase shift even or odd wavelengths can be recovered. The transfer function is depicted in dB scale for $\sin^2(\frac{\Delta\phi}{2})$(dashed) and $\cos^2(\frac{\Delta\phi}{2})$(solid) receptively.

2.3.3 Optical Receivers

An optical detector plays an important role in optical communication systems, since it specifies the overall system performance. It absorbs photons and converts it to electron-hole (carriers) pairs. Figure 2.8 illustrates two structures of photodetectors, (a) p-i-n diode, (b) APD. The p-i-n diode is comprised of p-type, n-type, and intrinsic (i)-type semiconductor layers. The electron-hole pair is produced when the photon has equal or larger energy than the energy bandgap of

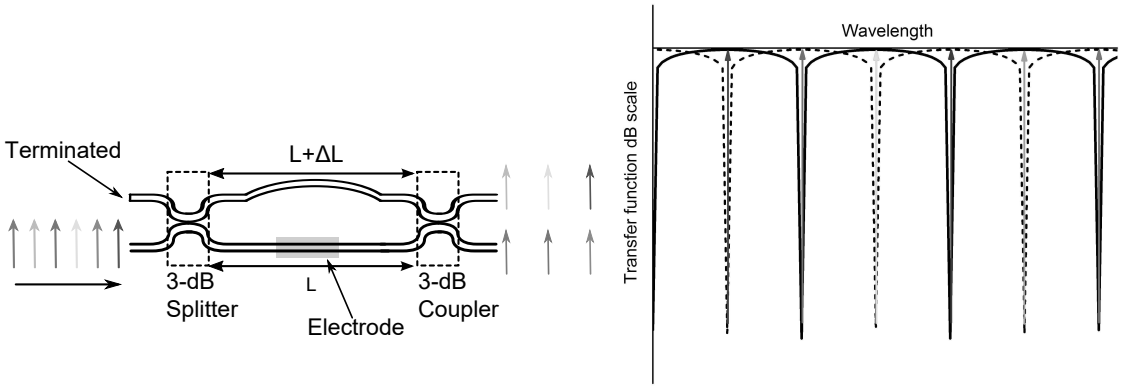

Figure 2.7: Mach-Zehnder interferometer a demuliplexer.

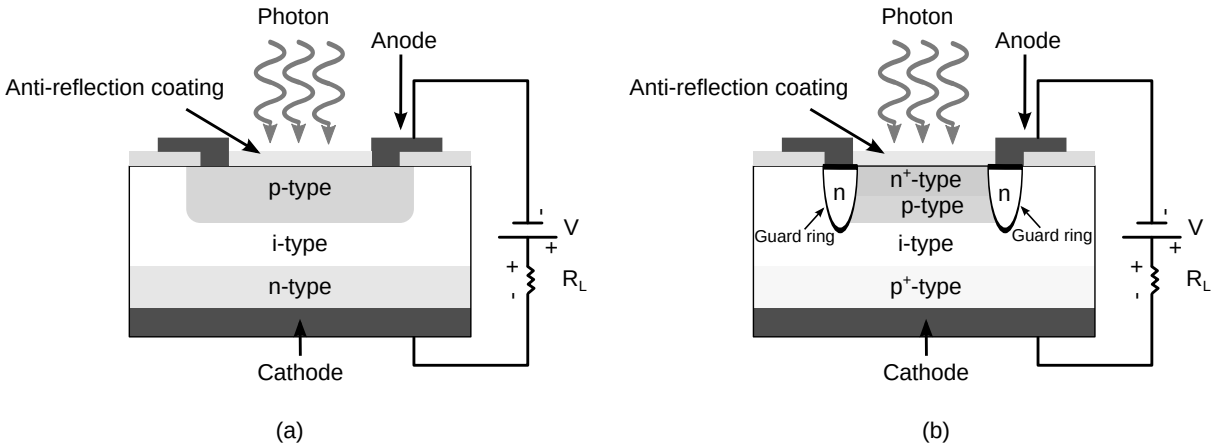

Figure 2.8: Structure of the photodetetor, (a) p-i-n photodiode, (b) avalanche photodiode (APD).

the semiconductor material. The E-field is produced across the p-i junction when the structure is reversed biased, causing the electron-hole pairs to drift away, this creates a depletion region where it is depleted of holes and electrons. Once the carriers leaves the depletion region, they move to the terminals and generation the photocurrent which is collected by the load resistor (R_L).

Unlike p-i-n photodiode, APD has an internal gain in its material, it can generate several electron-hole from a single photon absorption. The generated electron-hole pairs can generate new pair of carries if they have high enough energy from the external E-field, this is the impact ionization phenomena. The APD has more layer structure than p-i-n diodes as shown in Fig. 2.8(b), these layers are there to increase the impact ionization process. The guard rings are used to reduce the excessive leakage current at the junctions. The important parameters of the photodiodes are quantum efficiency, photodiode responsivity, the total noise, and cut-off

frequency. The quantum efficiency is the ratio between the number of photocarriers produced and the number of incident photons

$$\eta = \frac{\text{The number of photocarriers produced}}{\text{The number of incident photons}} \tag{2.39}$$

The quantum efficiency η is less than unity and represented as percentage, it depends on absorption coefficient of the semiconductor material, and it is a function of the wavelength. Generally, the optical detector must have high sensitivity at the the operating wavelength, high quantum efficiency, minimum noise, small size, and low cost. The responsivity of a the photodiode is related to η as

$$R = \frac{\eta q}{h\nu} \tag{2.40}$$

where $h\nu$ is the incident photon energy and q is charge of an electron. The responsivity increases with wavelength since there exists more photons per watt at longer wavelengths. It can also be related to the generated photocurrent (I_p)

$$R = \frac{I_p}{P_{in}} \tag{2.41}$$

In high-speed optical transmission, the photodiode must have a large bandwidth, there is a trade-off to design a wide-band photodiode. In order to increase the bandwidth, the depletion region length must be increased, while increasing the transit-time (the average time required for a photocarrier to transit the depletion region), which decreases the bandwidth.

2.3.4 Arrayed Waveguide Grating

Arrayed Waveguide Gratings (AWGs) are one of the key components of WDM-PONs. AWGs can multiplex/demultiplex 48 channels (also higher) wavelength channels with different channel spacings. In this work, 100 GHz (0.8 nm) spacing will be considered. The AWG consists of input/output waveguides, phase arrayed of multiple channels with path length difference between neighboring channels, and two focusing slab propagation region as shown in Fig. 2.9. The slabs are free propagation region where the light propagates through and then radiates to the arrayed waveguides. Each waveguide has different path length, thereby inducing phase shift with respect to neighboring channels, at the output of waveguides, the light beams interfere constructively at one focal point such as x (see Fig. 2.9 [33]) in the second slab. This phase retardation allows separation of two light beams at the output of the waveguide. For more details on theory of the AWG (please refer to [33]).

2.3.5 Amplifiers

Optical amplifiers are another key components of fiber optic communications. They compensate the loss introduced by optical paths which limits the data transmission. The amplification process is based on stimulated emission process. Optical-electrical-optical (O-E-O) conversion is another technique to compensate the optical signal loss. However, it is

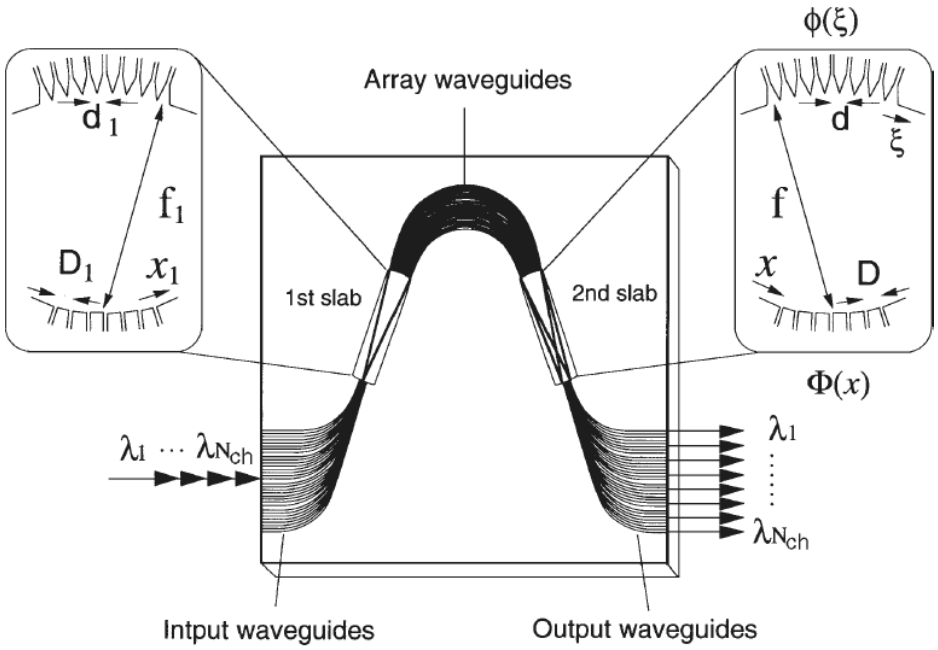

Figure 2.9: Structure of arrayed waveguide grating multiplexer/demultiplexer [33].

not a transparent techniques, namely, the line should be disconnected for the conversion. Additionally, it is bandwidth limited due to the electronics and depends on the modulation format, and finally, it is not cost-efficient. The optical amplifiers can also be used as booster amplifiers in front of the optical transmitters to compensate the loss induced by modulators, and passive elements. They can be placed in-line in long-haul optical transmission where the optical signal needs to be amplified repetitively. Another application is to use the amplifier before the optical receiver to enhance the signal to noise ratio. Two types of optical amplifiers will be used in this work, EDFA, and SOA.

SOA

An SOA operates similar to a laser. It amplifies the optical signal under a certain condition. Figure 2.10(a) depicts a p-n junction SOA from lateral view. The cleaved facets are anti-reflection coatings to prevent the light reflects back at the input/output of the SOA. The gain is produced by forward biasing the amplifier across the p-n junction. The p-type cladding includes hole carries and that of n-type has electron carries. The electrons are pumped electrically to conduction bands and thereby leaving holes in the valence bands. In the active medium the electrons and holes recombine to generate photons through amplified spontaneous emission or stimulated emission processes. The amplified optical light results from the stimulated emission process. In order to obtain light amplification, a certain number of carries are needed otherwise the incoming photon is absorbed, this is called stimulated absorption. The three physical phase are illustrated in Fig. 2.10(b).

SOAs are promising candidates in long-reach PONs due to larger bandwidth, integrability

with other photonic components, and they can be easily produced at different wavelengths. Furthermore, they can be used in wavelength conversion applications where the data signal on channel λ_1 is converted to λ_2.

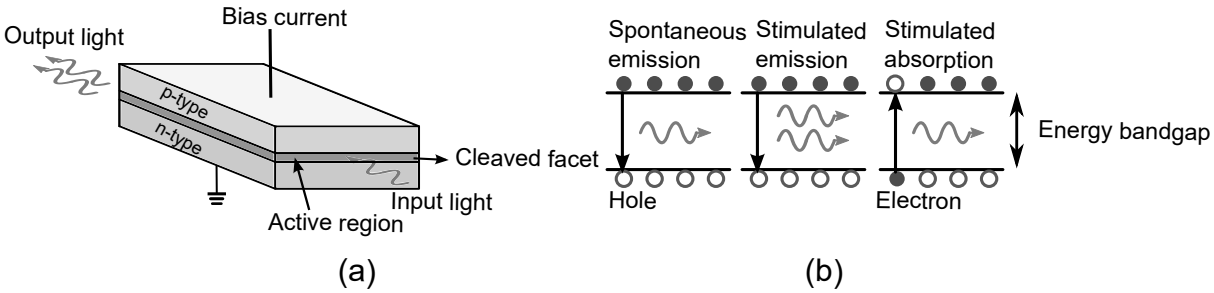

Figure 2.10: (a) Schematic of a semiconductor optical amplifier in the lateral direction, (b) stimulated and spontaneous processes.

EDFA

An erbium doped fiber amplifier (EDFA) is another widely used one in optical communication systems. EDFAs provide high gain, high optical output power, and low channel crosstalk in WDM scenario. An EDFA is comprised of a pump laser, a WDM coupler, Erbium doped fiber, and an optical isolator as shown in Fig. 2.11. The components are illustrated in Fig 2.11. The erbium doped fiber is single-mode fiber doped with Er^{3+} ion. The pump laser usually has a wavelength at 980 nm or 1480 nm, excite the Er^{3+} ions to the upper state in order to amplify the light in 1550 nm region. The WDM coupler combined two different wavelengths, incoming, and the pumped light. The setup includes two isolators which blocks the reflected light.

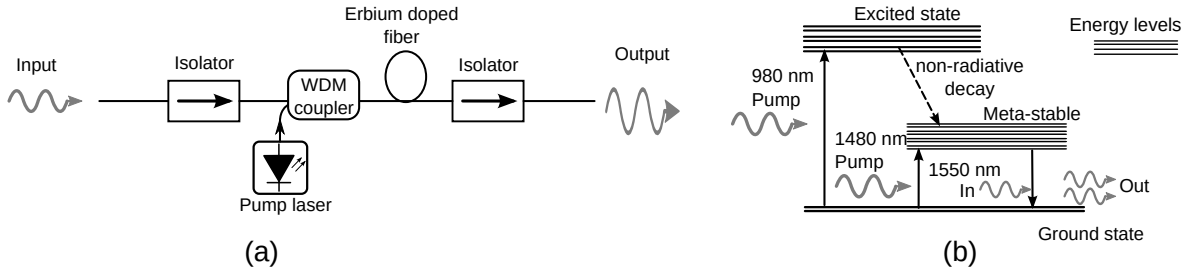

Figure 2.11: Erbium doped amplifier structure, (a) the schematic of EDFA with 980 nm (1480 nm) pump laser, (b) Energy diagram of Er^{3+}.

Figure 2.11(b) shows the energy system of the erbium doped fiber. The lines show energy state of the of the material. The pump light excites the carriers from the ground state to the excite state resulting in population inversion (stimulated absorption). The carriers drop from the excite level drop to the metastable state through non-radiative decay (spontaneous emission). Finally, after 10 msec (staying on the metastable state), the carriers move from meta-stable state to the ground state which gives rise to the emission at the amplifying wavelength (stimulated

emission). If the pump laser is constantly exciting carriers to the higher energy level, some carriers can be accumulated in the meta-stable state and the illustrated three-level system will reduce to two-level energy system. Contrary to SOAs, EDFAs are optically pumped.

Chapter 3

Optical Transmission Systems

Optical transmission technology is used in all types of communication systems to meet the never-ending bandwidth demands. In this chapter, the modulation techniques will be explained, different line-codings will be elaborated, and detection theory will be treated.

3.1 Optical Modulation

The electrical bit streams need to be converted in optical domain by modulation of the optical carrier, the modulation can be performed directly or externally. In case of direct modulation the electrical signal is part of the laser driving current, while with external modulation as physical phenomena such as electro-optic effect is used. Figure 3.1(a) illustrates the structure of the direct, and Fig. 3.1(b) external modulation. In the first scenario, the laser is turned on when high level voltage (1) is applied and ideally off when there is low level voltage (0). In contrast, in the second scenario, the continuous wave (CW) laser is first biased above the lasing threshold to turn on the laser and then the external modulator converts the electrical applied signals to optical ones. There is two advantages using external modulation; first is the high extinction ratio (ER) which is defined as the ratio between power level of the "1" (P_1) and "0" (P_0) bit ($ER = P_1/P_0$). And the second advantage is the possibility of the chirp-free operation. When the light is intensity modulated using direct modulation, the signal phase may change which results in instantaneous frequency change or frequency chirp. The frequency chirp introduces spectral boarding which inhibits long-distance transmissions. Driving the external modulation in push-pull operation as depicted in Fig. 3.1(a) will lead to chirp-free optical signals.

Mach-Zehnder modulators (MZM) are widely used in optical communication system, due to its high extinction ratio and the chirp-free option. In MZM, the incoming light is split into two paths in the waveguide, the separated lights experience phase shifts of ϕ_1 and ϕ_2 by applying driving voltages on the electrodes. The optical signals are combined together at the output of the waveguide. The electric fields interfere constructively if they are in phase and destructively if they are out-of-phase. In this manner, the constructive interference result in "1" and destructive interference will result in "0". Figure 3.2 shows a schematic of a dual arm MZM modulator. The complex envelope of the electrical field can be written as

$$E(t) = \sqrt{P(t)}e^{-j(\phi)} \tag{3.1}$$

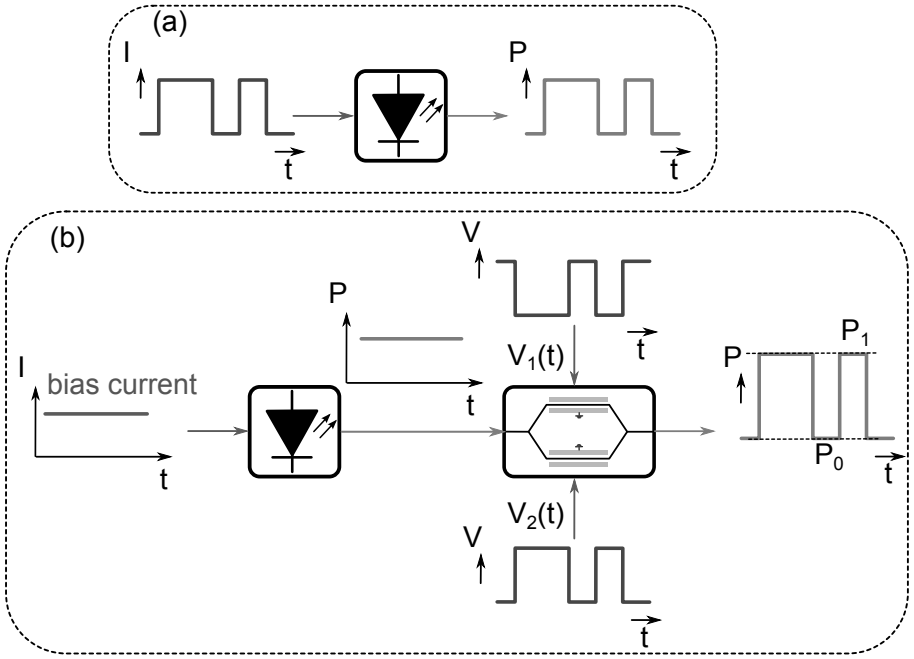

Figure 3.1: The structure of the direct and external modulation.

So the resultant electric field at the output of the modulator can be expressed as

$$\begin{aligned} E_{out}(t) &= E_{in}(t)\left(\frac{1}{2}e^{-j\phi_1(t)} + \frac{1}{2}e^{-j\phi_2(t)}\right) \\ &= E_{in}(t)e^{-j(\frac{\phi_1(t)+\phi_2(t)}{2})}\left(\frac{e^{-j(\frac{\phi_1(t)-\phi_2(t)}{2})} + e^{j(\frac{\phi_1(t)-\phi_2(t)}{2})}}{2}\right) \\ &= E_{in}(t)\underbrace{e^{-j(\frac{\phi_1(t)+\phi_2(t)}{2})}}_{\text{phase modulation}}\underbrace{\cos(\frac{\phi_1(t)-\phi_2(t)}{2})}_{\text{Amplitude modulation}} \end{aligned} \tag{3.2}$$

Obviously, the the output E-field depends on the phase difference induced by applied voltages ($V_1(t)$ and $V_2(t)$ in Fig. 3.2). The phase shift depends on electro-optic materials, geometry of the waveguide, and polarization of the incident lightwave. Lithium-niobate ($LiNbO_3$) is commonly used as the material in such modulators due to high electro-optic coefficients. Another important parameter of MZM modulators is V_π which designates the driving voltage for obtaining phase shift of π. The phase shift $\phi(t)$ can be written in terms of V_π as

$$\phi(t) = \pi\frac{V(t)}{V_\pi} \tag{3.3}$$

Looking at Eq. 3.2, the MZM can be used as intensity/phase modulation, in order to suppress the phase term, the applied voltages should be logically inverted with respect to each other, $V_1(t) = -V_2(t)$, substituting Eq. 3.3 in Eq. 3.2 yields

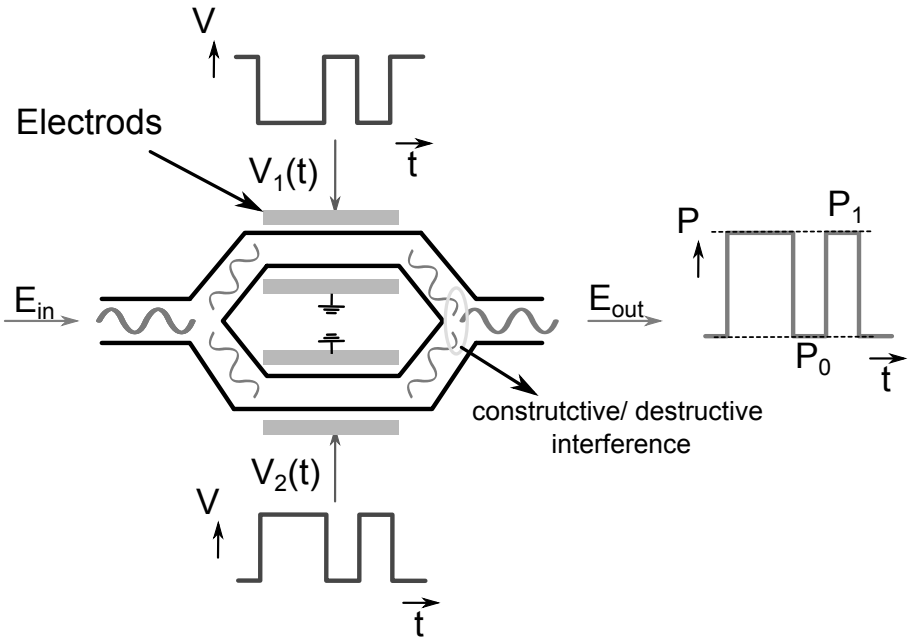

Figure 3.2: The Mach-Zehnder modulators modulator in push-pull mode.

$$\begin{aligned} E_{out}(t) &= E_{in}(t)e^{-j(\frac{\pi\frac{V_1(t)}{V_\pi}+\pi\frac{V_2(t)}{V_\pi}}{2})}\cos(\frac{\pi\frac{V_1(t)}{V_\pi}-\pi\frac{V_2(t)}{V_\pi}}{2}) \\ &= E_{in}(t)e^{-j(\frac{\pi\frac{V_1(t)}{V_\pi}-\pi\frac{V_1(t)}{V_\pi}}{2})}\cos(\frac{\pi\frac{V_1(t)}{V_\pi}+\pi\frac{V_1(t)}{V_\pi}}{2}) \\ &= E_{in}(t)\cos(\frac{\pi V(t)}{2V_\pi}) \end{aligned} \tag{3.4}$$

where $V(t)/2 = V_1(t) = -V_2(t)$, and the phase term is suppressed. Having evaluated the output E-field, the power transfer function of the MZM can be formulated as follows

$$\begin{aligned} P_{out}(t) &= |E_{out}|^2 \\ &= |E_{in}(t)|^2\cos^2(\frac{\pi V(t)}{2V_\pi}) \\ &= P_{in}(t)\left(\frac{1+cos(\frac{2\pi V(t)}{V_\pi})}{2}\right) \\ \frac{P_{out}(t)}{P_{in}(t)} &= \cos^2(\frac{\pi V(t)}{2V_\pi}) \end{aligned} \tag{3.5}$$

In above equations, $V(t) = V_{bias} + V_{pp}a(t)$, where V_{bias} is the modulator bias voltage, and $V_{pp}a(t)$ is the peak-to-peak voltage times data sequence. The transfer function of the power and E-field of the MZM is illustrated in Fig. 3.3. In order to achieve an intensity modulation, the applied peak-to-peak voltage needs to be V_π, and biased at $-\frac{V_\pi}{2}$, however, to operate the MZM as a phase modulator, the applied voltage should have $2V_\pi$ peak-to-peak voltage, and biased at null points, this is clear from the E-field transfer function, when the applied signals swing

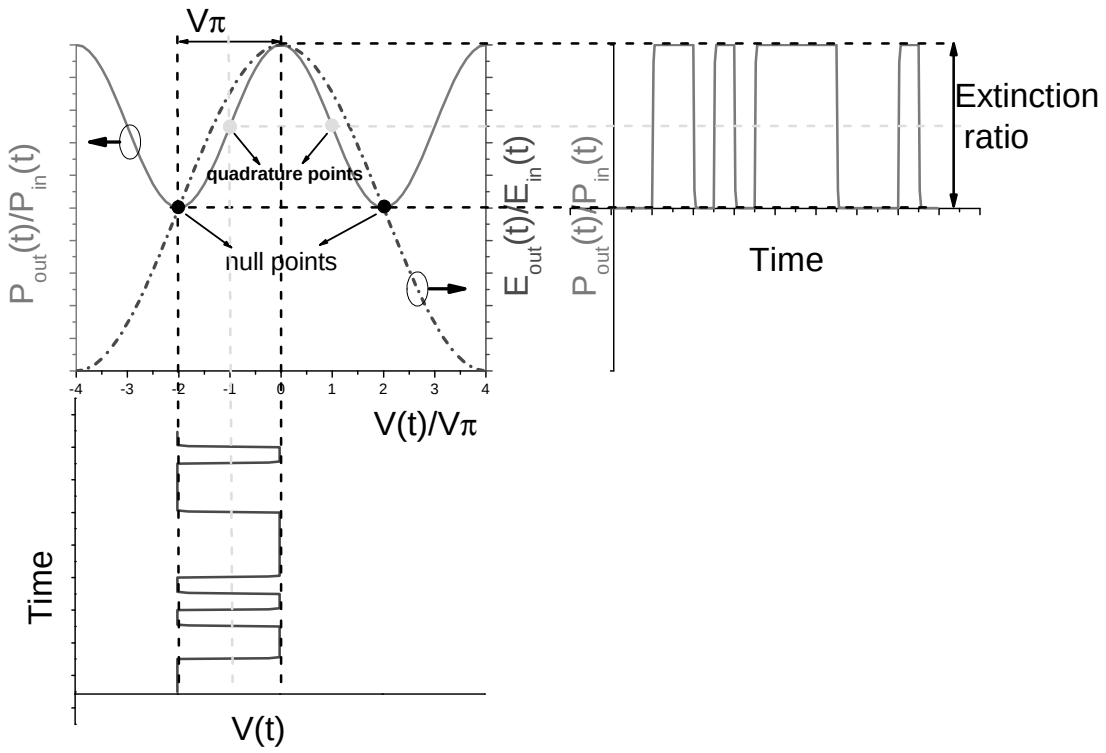

Figure 3.3: The power and E-field transfer function of the Mach-Zehnder modulators with respect to the applied voltage.

$2V_\pi$, the phase of the field changes from 0 to π, this gives rise to the phase-modulated signal. Therefore, the amplitude of the driving voltages should be adjusted according to the transfer function characteristic. Figure 3.3 depicts an example of on-off-keying (OOK) modulation.

3.2 Modulation Techniques

In order to transmit the digital data over the fiber, the electrical pulses must be converted to optical pulses, this can be achieved using direct modulation, or external modulation of the optical carrier. These modulation schemes will be explained shortly.

3.2.1 Direct Modulation

The direction modulation scheme is performed by directly modulation of the digital data steam on the laser above the threshold current. The laser should be biased appropriately such that the level of 1 and 0 bits be above the the threshold current.Figure 3.4 depicts the L-I curve characteristic of a laser diode. The direct modulation is commonly used for low to moderate bit-rates. This is because of the laser frequency chirp caused by the variation of the lasing frequency. The distorted optical signal is again affected by chromatic dispersion in the fiber

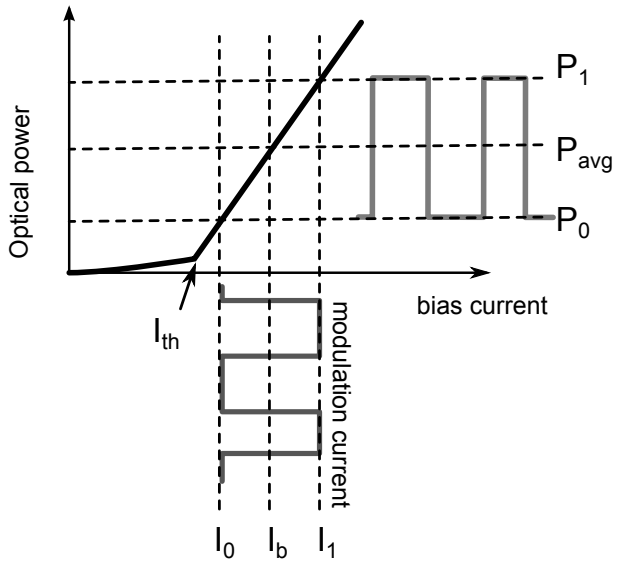

Figure 3.4: power-current characteristic of a laser diode with modulating current above the threshold.

which in turn limits the maximum achievable transmission distance. The extinction ratio also plays an important role in optical transmission systems, but direct modulation does not yield as high ER as the external modulation.

3.2.2 External Modulation

Another modulation techniques is to modulate the data on the carrier externally using an external modulator. The advantage of this technique is higher bit-rate, increase in ER, suppression of the chirp, and longer transmission, although it is not as inexpensive as direct modulation technique. In the following section we will explain how different line-codings can be used to modulate on the optical carrier.

3.3 Modulation Formats

The continuously demand for higher capacity in optical communication systems requires higher spectral efficient modulation formats. Advanced modulation formats have been always interest of research community. By encoding more bits on one symbol, higher spectral efficiency can be obtained. The modulation can be performed on amplitude, phase, polarization, or combination of three. Nowadays with the availability of the high speed electronics and coherent receivers, using different advanced modulation formats is not a difficult task to do. In the following sections we will review different modulation formats and their corresponding detection techniques which will be used in later chapter of this work.

3.3.1 On-Off Keying

On-off keying (OOK) is the mature modulation techniques which has been used in fiber communication systems as intensity-modulation/direct detection (IM/DD) for a long time. The OOK can be in NRZ/RZ format depending on the application.

Non-return-to-zero OOK

The conventional NRZ-OOK is illustrated in Fig. 3.5. The external modulation of the optical carrier setup consists of a laser which can be a DFB, pulse-pattern-modulator (PPG), an electrical driver amplifier, a bias controller electronics, and a MZM. The light source emits light into the MZM which is driven by the pulses from PPG, the drivers amplifier is required to increase the amplitude of the amplified voltage which meets the characteristic function of the MZM. If the amplitude is not adjusted, the ER will be low and transmission results in poor quality. The bias voltage needs to be adjusted on the quadrature point of the MZM transfer function to fully convert the electrical signal to the optical, this was elaborated in chapter 2. As an example, the data stream $\{1,1,0,1\}$ is shown, T_b is the bit duration, as the name NRZ stated the bits do not return to zero within the bit duration. Each isolated "1" is the inverse of the bit rate, if the bit duration is 100 ps the bit rate is 10 Gbps.

Figure 3.5(b) shows the NRZ-OOK direct modulation setup where the data stream is loaded directly on the laser. The data sequence modulates the carriers inside the active medium of the laser. The laser is modulated in the steady-state region, namely the bias current is much greater than the threshold current. As the high level (1's) is applied to the laser the carriers are depleted to produce the photons, and after that the carriers recover to their steady-state value. The transmission curve of direct modulation is shown in Fig. 3.4. The difference between direct

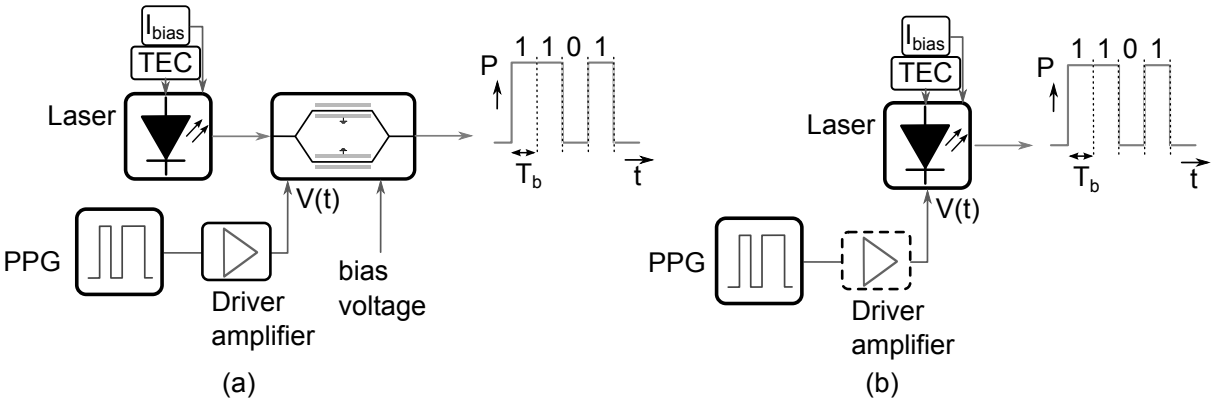

Figure 3.5: The conventional non-return-to-zero-on-off-keying modulation setup, (a) External modulation of non-return-to-zero, (b) direct modulation of non-return-to-zero

modulation and external modulation can be exhibited using eye diagram in Fig. 3.6. Obviously, the external modulation gives rise to higher extinction ratio than the direct modulation, the eye diagram are simulation results at 10 Gbps of the setups shown in Fig. 3.5. The transmission distance is limit when using direct modulation due to the reason stated above.

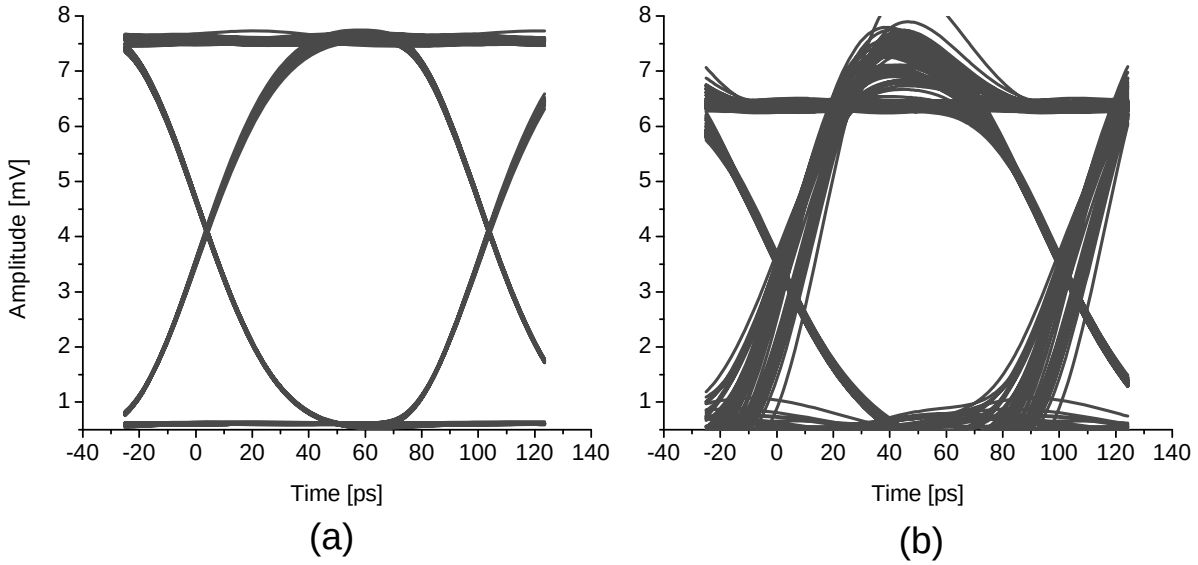

Figure 3.6: The eye diagram of external modulation using Mach-Zehnder modulator, and direct modulation for non-return-to-zero-on-off-keying at 10 Gbps.

Return-to-zero OOK

It is important to select an optimum pulse format before transmitting through the optical fiber. RZ pulses with narrow pulses resemble the soliton pulse compression in the SMF, while the adjacent "1's" of NRZ pulses are not immune against nonlinearities in the fiber. However, in higher bit-rates such as 40 Gbps the shorter RZ pulses are more sensitive to the chromatic dispersion since the group velocity dispersion is proportional to reciprocal of the square of pulse width, thus the larger the bandwidth the higher is the dispersion penalty. Therefore, there is trade-off between the chromatic dispersion and nonlinearity in the fiber. The full detailed explanation on this topic can be found in [34].

The RZ-OOK needs another MZM to produce the RZ format, the setup is shown in Fig. 3.7. The RZ pulses return to zero in on bit duration T_b, thus, they occupy larger bandwidth than NRZ pulses. The clock signal is used to carve RZ shape of the optical signal. The RZ pulse shape is more tolerant against nonlinearities introduced by fiber, however, the wider spectrum makes the RZ format less spectral efficient in WDM transmission in comparison to NRZ format. Figure 3.8 shows power spectra of RZ-OOK and NRZ-OOK pulses at bit rate of 10 Gbps, obviously RZ occupies more bandwidth than NRZ. The results are simulation of setups shown in Fig. 3.7 and 3.5 with laser source operating at 1550 nm. The alternative setup can be considered by shaping the pulse before the driver amplifier to generate RZ format, in this case only one modulator is required, but the electrical bandwidth is always limited in comparison to optical bandwidth. It is also possible to carve the NRZ pulses with different pulse durations of 33% or 67% by driving the second modulator at half frequency and biasing the carver MZM accordingly. Driving the clock at $f_b = \frac{1}{T_b}$ between the minimum and maximum transmission function gives rise to RZ optical pulses with full-width-half-maximum of 50% duty cycle. However, if the MZM is driven at $f_b = \frac{1}{2T_b}$ (half data rate) between the transfer function

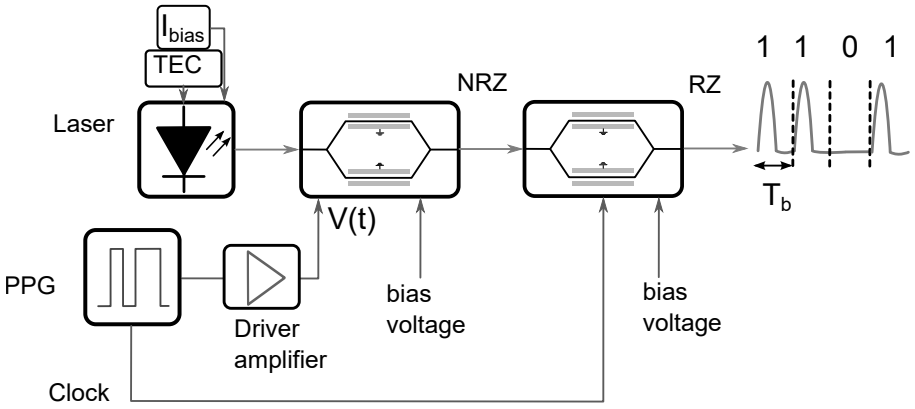

Figure 3.7: The external modulation for return-to-zero-on-off-keying.

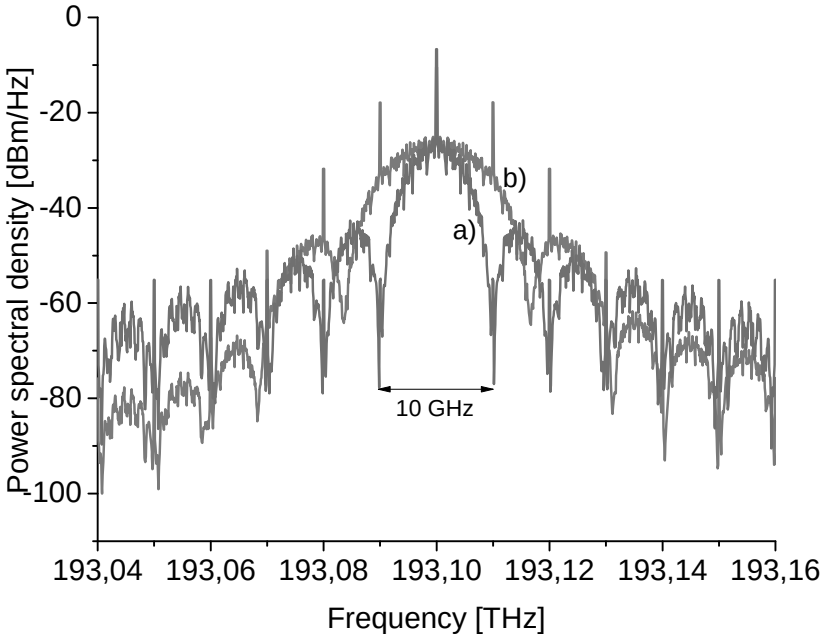

Figure 3.8: The spectra of, (a) return-to-zero-on-off-keying, (b) non-return-to-zero-on-off-keying, bit rate at 10 Gbps (simulation).

minima, 33% RZ optical pulses are obtained. Another type can be achieved by driving the MZM at half bit-rate between the maxima which results inn 67% RZ optical pulses, this type is called carrier-suppressed RZ, since the optical filed changes its sign between the maxima (see Fig. 3.9), the adjacent bits have inverted phase, therefore, the optical field envelope has zero mean which results in suppression of the carrier at optical frequency. All these operation points are illustrated in Figure 3.9. The voltage swing for different RZ formats are shown vertically on the left along with the pulse carving MZM transfer function. At output of the second MZM we see RZ optical pulses with different duty cycles on the right, and the setup is shown on the

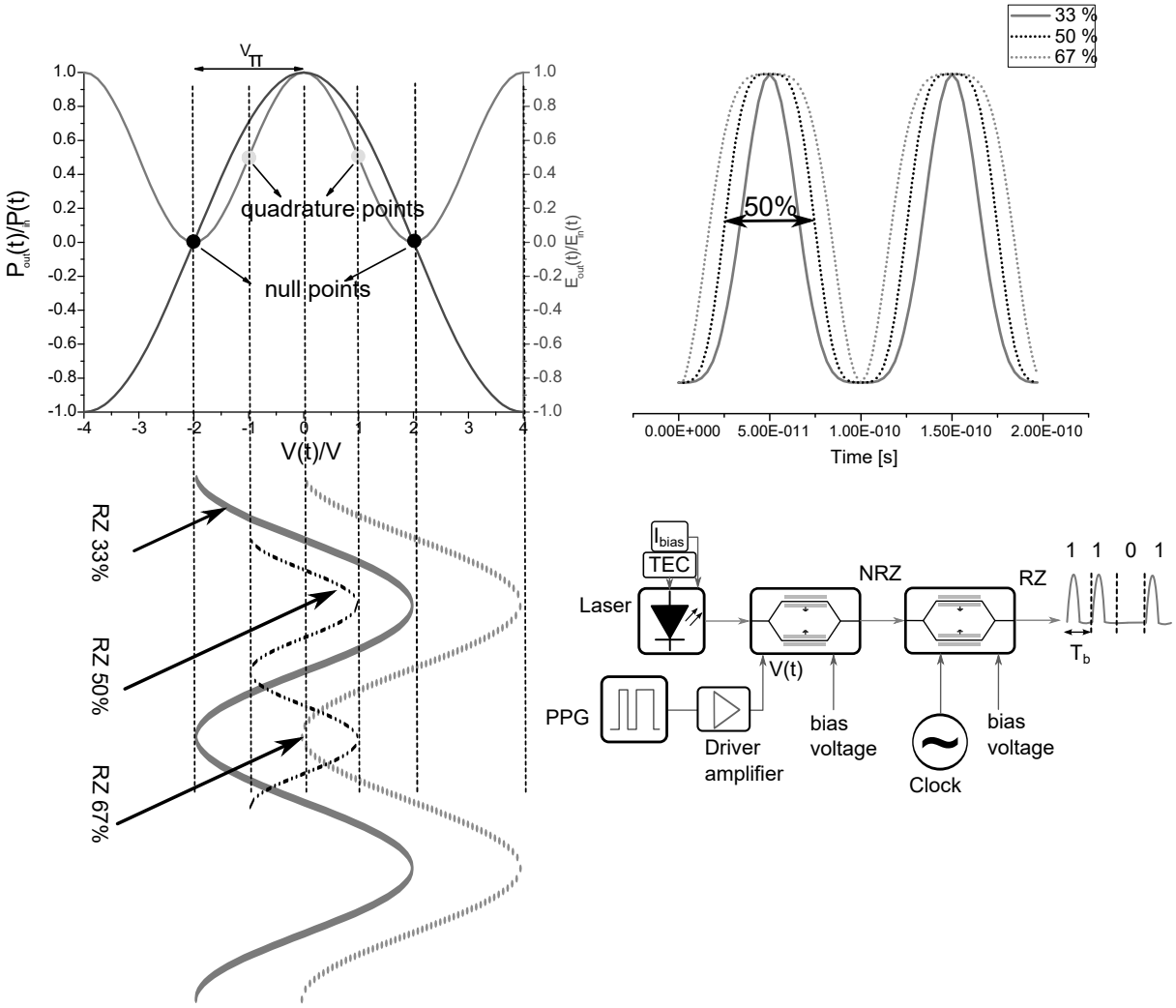

Figure 3.9: The optimum point for different return-to-zero pulse generation.

right corner.

3.3.2 Phase-shift Keying

The digital signal can also be modulated on the phase of the optical carrier to produce phase shift-keying-signal. As the direct detection cannot detect the absolute phase, in order to demodulate the phase, the phase of the preceding bit is used as a reference for the demodulation, this type of modulation format is called differential phase shift-keying (DPSK).

Differential Phase Shift Keying

Using differential phase shift keying (DPSK) enables carrying information on the phase of the optical carrier so that the data are carried in the optical phase changes of the adjacent bits. In the past, due to instability of frequency of laser sources, the optical phase modulation

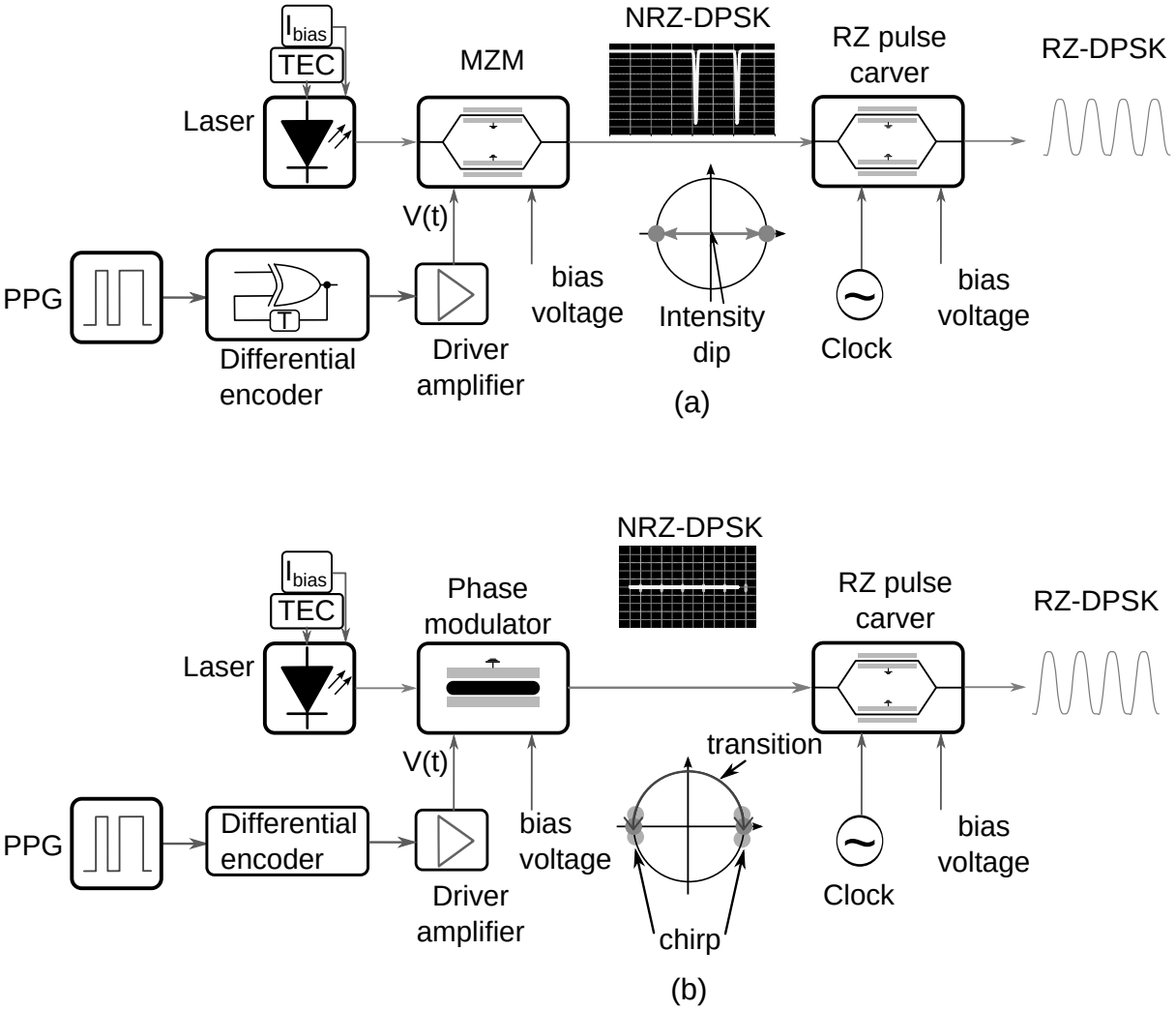

Figure 3.10: Optical differential phase-shift keying generation, a) Mach-Zehnder modulator+pulase carver, b) phase modulator+pulse carver.

was not feasible. Recent advancement of the single-frequency laser sources enables DPSK implementation in practical systems. Figure 3.10 shows two configurations of optical DPSK generation, using a MZM as phase modulator (a), or a phase modulator. The NRZ pulses are differentially encoded by DPSK precoder before being sent to the optical modulator. The precoder consists of a exclusive-OR gate with a symbol time T feedback, the relationship between the input and output data sequence is $d_k = d_{k-1} \oplus b_k$ where d_k is the output sequence, b_k is the input sequence, and $\oplus$ is the exclusive-or operator. The differential encoder output logic changes each time $b_k = 1$, however it stays the same when $b_k = 0$, in this manner, there is no phase change occurs on the signal when "0" is transmitted, but if "1" is transmitted the phase is shifted by π. The transitions (intensity dips in inset after first MZM) shown in Fig. 3.10(a) results from phase jumps of the adjacent bits, this shown in the constellation of Fig. 3.10. The driving voltage should be $2V_\pi$, and must be biased at the minimum transmission point similar to 67% RZ shown in Fig. 3.9. There is no carrier component in DPSK spectrum

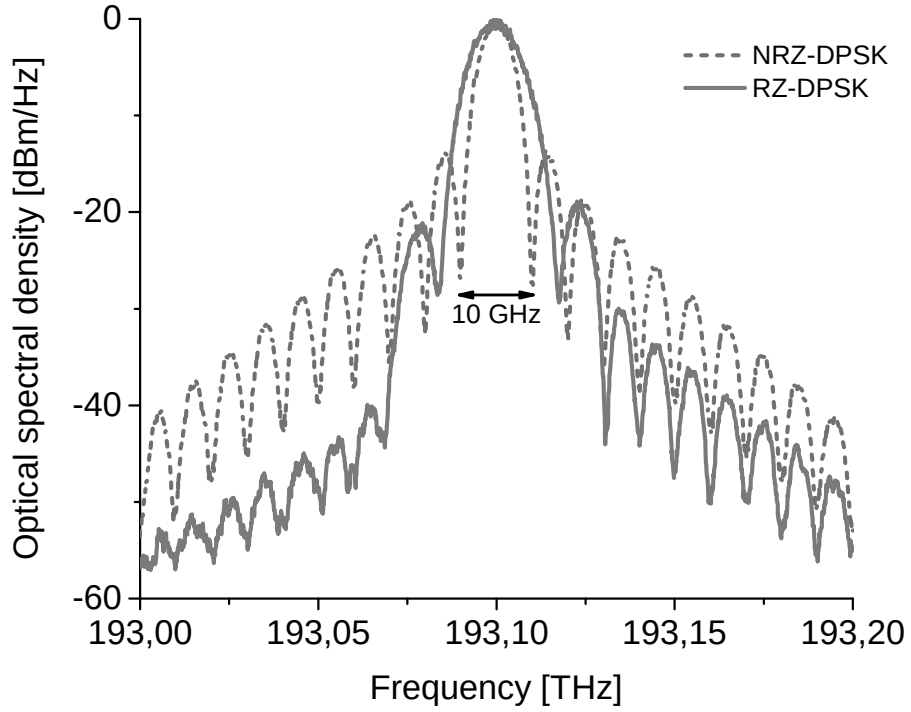

Figure 3.11: Spectra of non-return-to-zero-differential phase-shift keying and return-to-zero-differential phase-shift keying for bit rate of 10 Gbps.

as the optical field averages to zero due to the driving voltage swing between "1" and "-1". The optical spectra of NRZ-DPSK and RZ-DPSK are illustrated in Fig. 3.11, the RZ-DPSK is wider than NRZ-DPSK, the data rate is 10 Gbps in this illustration. The RZ-DPSK is more susceptible to chromatic dispersion due to the larger bandwidth. However, in general DPSK outperforms OOK and higher tolerance to SPM-GVD effect [35]. RZ modulation can be used after generation of NRZ-DPSK to suppress the intensity dips generated along with the phase shifts. This is sometimes referred as intensity modulated DPSK. The RZ-DPSK enables resistivity against to nonlinearities such as self-phase modulation (SPM).

In the second configuration, a phase modulator is used to generate the optical DPSK signal. The optical intensity is a constant value as shown in the inset of Fig. 3.10(b). As mentioned in chapter 2, the phase shift produced in electro-optic phase modulator is proportional to the refractive index change, and linearly depends on the applied voltage. Any fluctuation in driving voltage results in the phase noise, thus, it is tedious to achieve an exact phase shift of π. This phase deviation is imposed on the constellation diagram as shown in Fig. 3.10(b). This is a drawback of the configuration in comparison to the setup in Fig. 3.10(a). In order to improve the transmission distance, the pulse can be carved using the second MZM. Thus, the signal power is no longer constant.

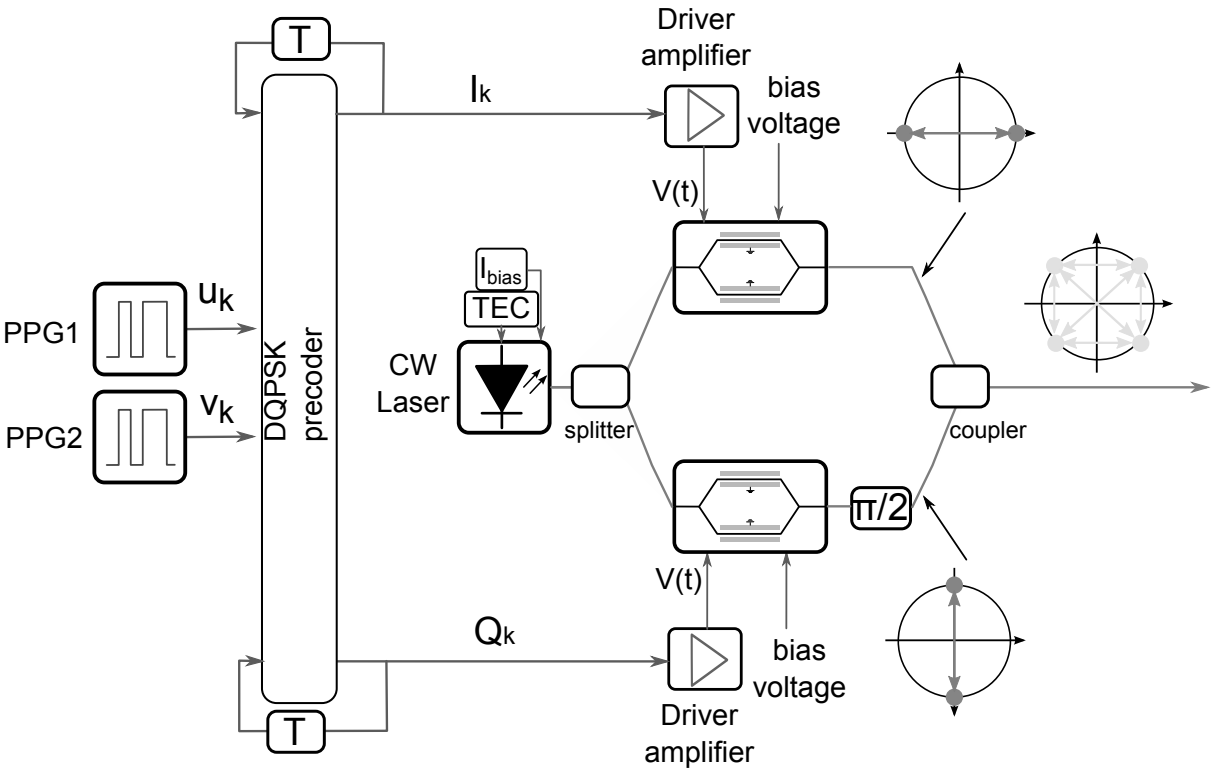

Figure 3.12: The configuration of a differential quadrature phase-shift keying optical signal generation using two Mach-Zehnder modulators.

Differential Quadrature Phase Shift Keying

Multi-level formats such as differential quadrature phase shift keying (DQPSK) are promising candidates to meet demand for higher bandwidth for NG-PONs. The DQPSK format provides robustness against chromatic dispersion as well as polarization mode dispersion. Additional, it has higher spectral efficiency in contrast to DPSK. In DQPSK format, the data sequence is encoded using a differential encoder in the differential optical phase between adjacent bits such that $\Delta\phi = [0, \frac{\pi}{2}, \pi, -\frac{\pi}{2}]$. Figure 3.12 illustrates the principle of DQPSK optical signal generation. The data sequences u_k and v_k are generated by two PPGs and sent to DQPSK precoder, The data is precoded according to the following relations [36]

$$I_k = \overline{(u_k \oplus v_k)} \cdot (u_k \oplus I_{k-1}) + (u_k \oplus v_k) \cdot (u_k \oplus Q_{k-1}) \tag{3.6a}$$

$$Q_k = \overline{(u_k \oplus v_k)} \cdot (v_k \oplus Q_{k-1}) + (u_k \oplus v_k) \cdot (u_k \oplus Q_{k-1}), \tag{3.6b}$$

where I_k and Q_k are in-phase and quadrature parts of the signals. Once the precoded data has been generated, it is sent to driving amplifiers and afterward to the MZMs. The input light from CW laser is split into two paths, one is used for in-phase part and the other for quadrature part. The MZMs biasing and driving voltage conditions are the same as DPSK generation. Using this configuration two separate DPSK signals are created at the output of each MZM (see the constellations). One output is shifted by $\pi/2$ to generate the quadrature part and then the optical signals are combined using a coupler. This type of configuration is called dual parallel Mach-

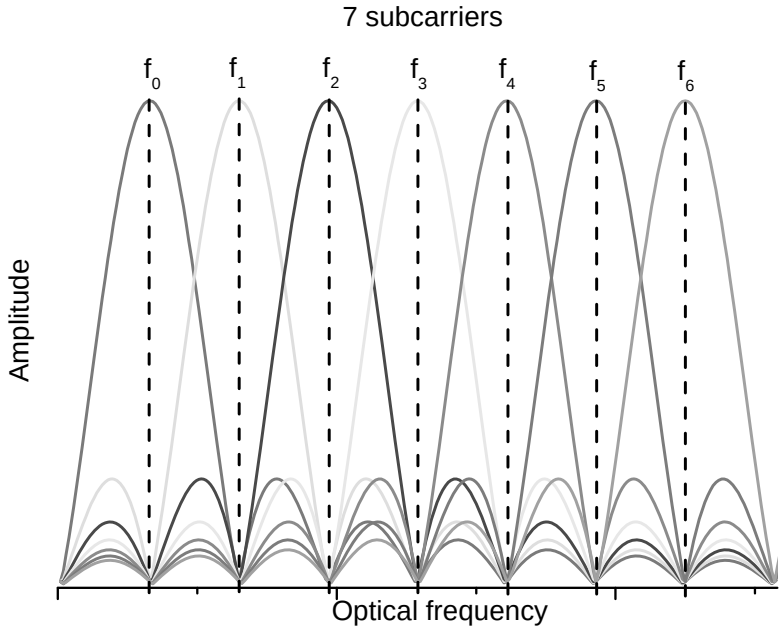

Figure 3.13: The spectrum of orthogonal frequency-division multiplexing signals, 7 subcarriers.

Zehnder modulator (optical quadrature modulator). The output results in DQPSK optical signal as displayed on the constellation with transition arrows.

3.3.3 Orthogonal Frequency Division Multiplexing

Orthogonal frequency-division multiplexing (OFDM) is classified as multi-carrier modulation (MCM) in which the information is carried on lower rate subcarriers. OFDM is robust against nonlinearities and chromatic dispersion. The OFDM uses as many narrow-band orthogonal subscribers to transmit information in parallel. The high spectral efficiency can be achieved by orthogonally overlap the spectra. This is shown in Fig. 3.13, the subcarriers are orthogonal to each other, all the subcarriers have a finite duration T_s. The condition for orthogonality between two subcarriers is [37]

$$\begin{aligned}\delta_{kl} &= \frac{1}{T_s}\int_0^{Ts} s_k s_l^* dt = \frac{1}{T_s}\int_0^{Ts} \exp\left(j2\pi(f_k - f_l)t\right) dt \\ &= \exp\left(j\pi(f_k - f_l)t\right) \frac{\sin(\pi(f_k - f_l)T_s)}{\pi(f_k - f_l)T_s}\end{aligned} \tag{3.7}$$

if $f_k - f_l = m\frac{1}{T_s}$, then two subcarriers are orthogonal. The spectrum can be considered as sum of shifted sinc functions. To modulate/demodulate OFDM signals inverse discrete Fourier transform (IDFT)/discrete Fourier transform (DFT) is used. In practice IDFT/DFT can be efficiently replaced by IFFT/FFT.
In optical communications many OFDM configurations have been proposed which are based on high speed electronics. But, all follow the same transmitter and receiver structures. Figure 3.14

illustrates a basic electrical-optical OFDM configuration. At the transmitter side, OFDM transmitter consists of serial to parallel conversion (S/P),data to symbol mapper (Mapper), an IFFT block to modulate symbols on subcarriers, a parallel to serial converter, a guard interval block to create a gap between adjacent symbols to avoid symbol interferences, this redundant information is removed at the receiver side, and a digital to analog converter. There exists many electrical processing in the OFDM transmitter, the electronics limits the bandwidth and speed of OFDM. Once the OFDM signal is generated, it is modulated on the MZM. The OFDM symbols can be detected directly and then demodulated by off-line processing (DSP). The OFDM demodulator performs reverse processing on the received symbols. Time/frequency synchronization play an important role in OFDM systems to preserve the orthogonality of the subcarriers. Additionally, OFDM signal has high peak-to-average power ratio (PAPR), which needs to be controlled to avoid high sensitivity against non-linearities [37].

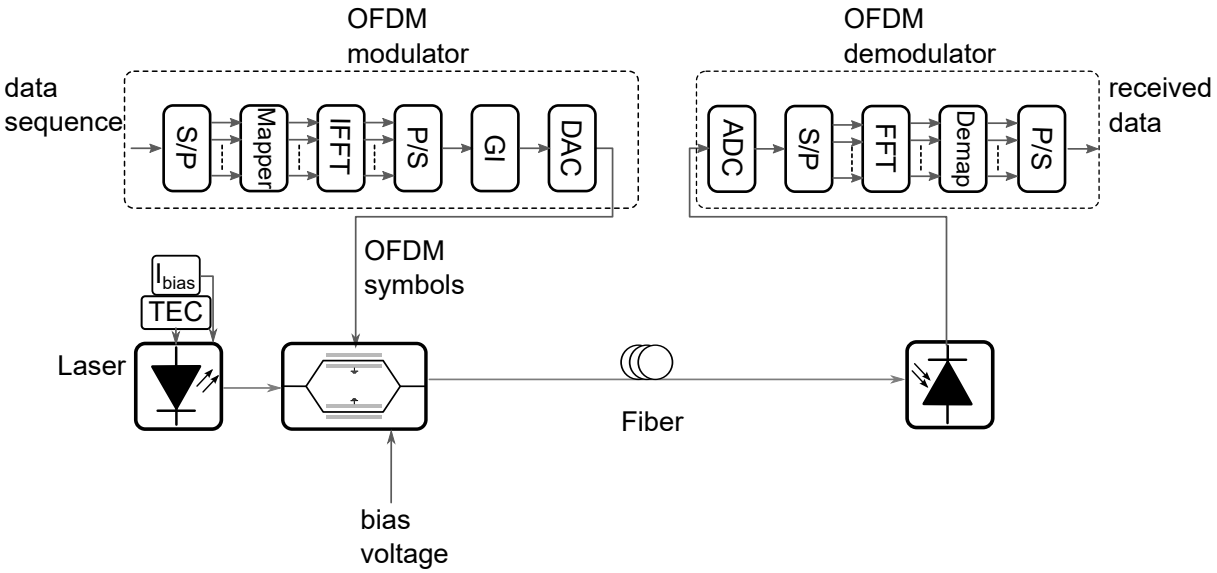

Figure 3.14: Schematic of one possible electrical-optical orthogonal frequency-division multiplexing system, S/P: serial-to-parallel converter, Mapper: data to symbol mapper, P/S: parallel-to-serial conversion, GI: guard interval, DAC: digital to analog converter, ADC: analog to digital converter, Demap: demapper.

Chapter 4

Broadband Access Technologies

In our daily life, we are consuming a large amount of bandwidth by surfing on the internet, watching high-definition (HD)TV, playing online games, setting a visual phone calls and so on. The services and applications are converted from electrical domain to optical domain at some point to benefit from higher bandwidth feature of an optical channel. The fiber to the home (FTTH) council Europe in Warsaw FTTH's conference 2015 [38] announced that the number of subscribers using FTTH/Building (B) technology increased 50% over the year 2014, there exists 15 million FTTH/B subscribers in Europe. Moreover, Cisco's Visual Networking Index 2014 report shows that the file sharing on the internet in year 2014 was about $6,548$ Petabyte per month and estimated to reach $6,875$ Petabyte/month. Furthermore, the IP traffic will reach 131.9 exabytes (1,000,000,000 gigabytes) per month in 2018 which is equivalent to transferring 45 million DVDs (digital video discs) each hour [15]. Therefore, network operators and enterprises need to cope with these traffic challenges by providing enough bandwidth for rapidly emerging services. The existing access networks need to be upgraded in order to deliver higher bandwidths to the subscribers. The broadband access networks is available as follows, powerline communications, satellite, digital subscriber line (DSL), hybrid fiber coaxial cable, optical fiber. This chapter overviews the broadband access technologies in some details.

4.1 DSL

The copper-based digital subscriber line (DSL)(G.992/993) [9] is the most widely used access technology nowadays. There are variants of DSL, asymmetric DSL (ADSL), and symmetric DSL (SDSL). ADSL has different data rates for both directions which upstream (US) rate of typically 1 Mbps and downstream (DS) rate of 8 Mbps, and reaches about 5.5 km (ITU-T 1999a). The ADSL2+ is the successor of ADLS with improvement in data rate, 3.5 Mbps and 24 Mbps for US and DS respectively (ADSL 2++ is also introduced with DS data rate of 52 Mbps). SDSL includes also different technologies such as HDSK, and SHDSL (H stands for high bit rate). For the sake brevity all the DSL standards are summarized in Table 4.1. The fastest DSL version in terms of data rate is very-high-bit-rate DSL2 (VDSL2) with 100 Mbps in both directions but over the short distances. The state-of-art DSL technology is called G.fast where G stand for ITU-G series recommendation. This technology supports higher bit rates in

shorter distance scenarios, the G.fast aims at increasing the bit rate in fiber-to-the-distribution-point (FTTdp) scenario. In DSL the bandwidth is not shared as the dedicated twist pair is used.

Standard	Downstream [Mbps]	Upstream [Mbps]	Reach [km]
SDSL	2.3	2.3	3
SHDSL(two wire pairs)	4.6	4.6	5
HDSL	2.048	2.048	3.7
ADSL	10	1	5.5
ADSL 2	12	1	5.5
ADSL 2 +	20	1	3
VDSL	52	16	1.2
VDSL2 17a	100	50	0.3
VDSL2 30a	100	100	0.3

Table 4.1: DSL standards comparison in terms of bit rate and reach.

4.2 Hybrid Fiber Coax

Hybrid fiber coax (HFC) is another broadband access technology that was originally developed for TV signals distribution. But after evolution of the fiber optics communication the system was upgraded to HFC. The TV signals are transmitted using optical fibers from the master headend to distribution nodes, then coaxial cables are deployed to serve around $2,000$ subscribers. The data rate for DS direction is 40 Mbps and 10 Mbps is for US direction. The bandwidth is shared by the subscribers using the network.

4.3 Broadband Power Line

The broadband power line (IEEE 1901) (BPL) the data signals are transmitted through optical fibers to the low-voltage power lines, and split with coupler to each households. The advantage of BPL communication is to provide internet services in rural areas where DSL connection is not feasible. The electricity is available almost everywhere so BPL could be ubiquitous. The data rate can be from 256 kbps to greater than 1 Mbps and it is the shared medium restricting the bandwidth used by each subscriber. The BPL technology bottleneck is the noise and data rate in contrast to DSL technology.

4.4 Wireless Access Networks

Another widely used broadband access technology is wireless access networks. It provides flexible data services to fixed and mobile subscribers. The wireless network are also ubiquitous.

The flexibility, scalability, and deployment cost makes the wireless access technology attractive. The wireless networks are classified according to their coverage area, Wireless personal area networks (WPANs), wireless local area networks (WLAN)s, wireless metropolitan area networks (WMANs), and wireless wide area networks (WWANs). As the names imply, WPANs covers in-house distances to few meters, WLANs cover areas within few hundred meters, WMANs covers an area of a couple of city blocks to the area of an entire city, WWANs can cover cities or countries through satellite and mobile systems such as LTE (long term evolution), UMTS (Universal Mobile Telecommunications System), GSM (Global System for Mobile), the 4G LTE can provide up to 1 Gbps. The data rates and the corresponding wireless access standards are outlined in Table 4.2. The data rates are the maximum achieved data rates specified by the manufacturer, in practice lower rates can be delivered.

Network	Data rate [Mbps]	Standard	Reach [km]
WPAN (Bluetooth)	1	IEEE 802.15.1	0.01
WLAN (WiFi)	2	IEEE 802.11	0.1
	11	IEEE 802.11b	
	54	IEEE 802.11a/h/j	
	54	IEEE 802.11g	
	150-600	IEEE 802.11n	
	1,300	IEEE 802.11ac	
WMAN (WiMAX)	134	IEEE 802.16	greater than 5

Table 4.2: Wireless access networks standard, data rate, and coverage area.

4.5 Passive Optical Networks

Although, the DSL technology and wireless access networks have been growing continuously, they may not meet the enormous data traffic increase in the near future, therefore, PON is the only solution to the services such as IPTV, HDTV, 3DTV, video-on-demand (VoD), interactive online gaming, and internet cloud to mention a few. The PON architecture supports point-to-point (P2P) or point-to-multipoint (P2M) connectivity. In P2P scheme, a fiber is purposed for each subscriber. Each subscriber has a direction connection to OLT, most deployed P2P connections use Ethernet, the P2P architecture is used by the business subscribers due to higher costs. In P2M architecture the single optical fiber is utilized by several subscribers in the network. Figure 4.1 shows the PON architecture which may be categorized into fiber-to-the-home (FTTH), fiber-to-the-curb (FTTC), and fiber-to-the-building (FTTB). The PON architecture has three main parts, optical line terminal (OLT) located in a service provider's central office (CO), this unit is an interface between PON and backbone network. The second element is an optical network unit (ONU) which provides interface between the services and the end subscribers. The fiber used in this area is called access fiber. The OLT is connected through optical distribution network (ODN) which is comprised of fibers and passive optical splitters

to ONUs. The fiber that runs from the OLT is named as feeder fiber. The ODN connects the OLT to ONUs using fibers and passive optical splitters near subscribers locations, the ODN may have tree structure formed by passive splitters as shown in Fig. 4.1. The split ratio highly depends on the optical power budget and the distance from the OLT. Typically the splitter is $1:32$. But the growth trend of subscribers urges higher number of splitters. One of the major discussions of telecom industries are the ability to serve higher number of customers.

In FTTH each subscriber is connected to a passive splitter and from there to the OLT through the shared feeder fiber in P2M scenario. FTTB is equipped with a termination box in the building where the connection is not optical fiber anymore but copper based (Ethernet transport). The connection from splitters to OLT is the shared feeder fiber similar to FTTH. The FTTC cabinets in the streets include switches or DSL access multiplexer (DSLAM), the connection between a subscriber and the cabinet can be copper based using VDSL2. This type of the network architecture is often called Active Ethernet since there exist active component in the link.

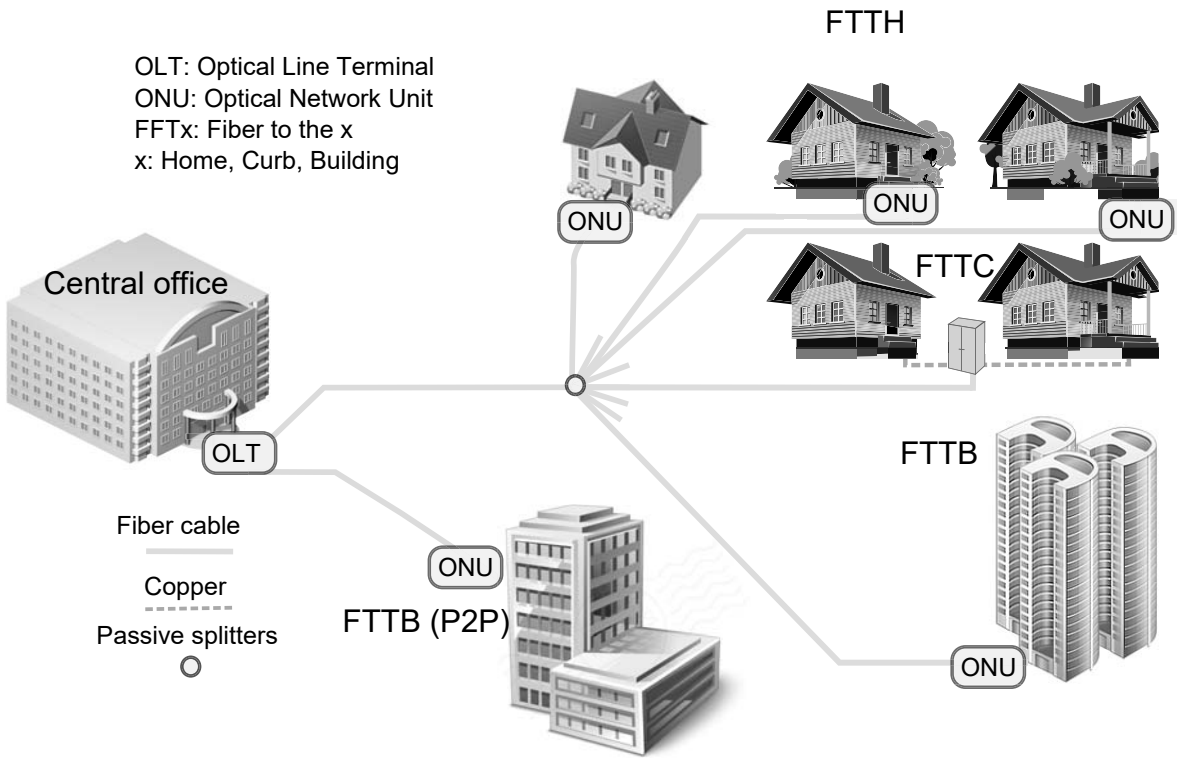

Figure 4.1: Passive optical network architecture with access to fiber-to-the-x.

Time division multiplexing (TDM), and wavelength division multiplexing (WDM) are the data multiplexing techniques widely used in PON. TDM-PON is widely deployed and mature technology. In TDM-PON, the US and the DS data are multiplexed in time on a wavelength, each subscriber has a dedicated time slot and share the total bandwidth with the others.

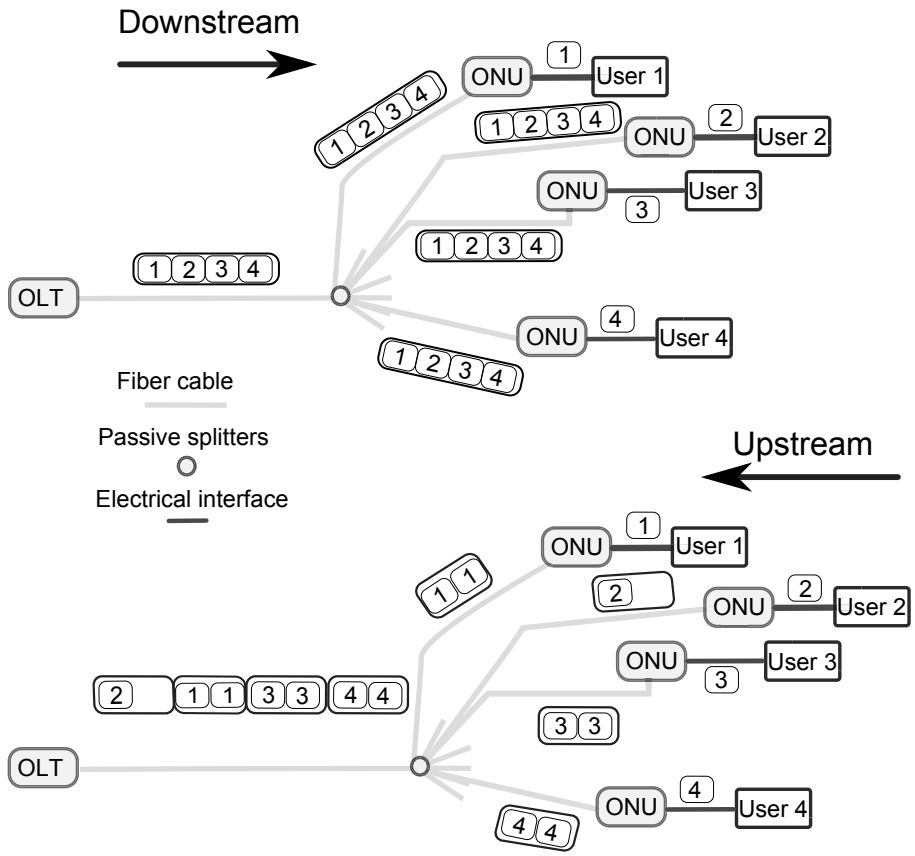

Figure 4.2: The conventional time-division multiplexing-PON architecture, (top) downstream, and (bottom) upstream direction.

4.6 TDM-PON

The TDM-PON can have different standards, asynchronous transfer mode (ATM) PON (APON) with the bit-rate of 155.52 Mbps for both directions, broadband (B)PON with 622.08 Mbps it is the enhanced version of its predecessor, gigabit (G)PON with 2.488 Gbps/1.244 Gbps DS/US bit rates, Ethernet (E) PON, 10G-EPON, and NG-PONs. Full service access network (FSAN) standardized APON,BPON, GPON (ITU-T G.984), and NG-PONs. The FSAN is world's leading telecommunication service providers that aims for advancement in broadband access technologies. The IEEE 802 group standardized EPON and 10G-EPON. All these technologies have specific frame structures which need a careful timing and synchronization between adjacent frames.

TDM-PONs are cost-effective since inexpensive optical components are used, and the DS wavelength is at 1490 nm and that for the US is 1310 nm. At these optical windows the attenuation is very low and optical components are well-developed. The TDM-PON has been largely deployed in Asia, Europe, and North America, EPON is the dominant technology in Asia, while B/GPON being used in North America as well as Europe.

Figure 4.2 illustrates TDM-PON network architecture, four users are assumed in the

network, each user has a time slot to send/receive data from the data center. The data are encapsulated into the frames and bandwidth allocation is managed by the central office. The interface between ONUs and users can be ADSL modems or Ethernet cards.

4.7 WDM-PON

Since the higher bandwidth is required, by employing WDM in both directions, the operators may supply the subscribers ideally unlimited bandwidths. WDM-PON can be a good solution to meet the bandwidth requirement of the future PON. This technology is able to serve each subscriber with a dedicated wavelength rather than splitting it among many subscriber as in TDM-PON. So, the subscriber has full bandwidth usage of the transmitted data. If only one wavelength is dedicated to each subscriber, the architecture offers higher security, because only the dedicated subscriber receives his signal. The P2P connectivity of the architecture makes each communication link work at different speeds which gives higher network flexibility and upgrade-ability, you pay in accordance with the line-rate.

Besides the advantages which mentioned above, WDM-PON has cost constraints, due to wavelength-specific sources used in ONUs. This feature introduces more requirements on lasers in ONU side. To reduce the cost and deployment hindrance, different solution have been proposed, such as using reflective-SOA as modulator in ONUs or directly modulation of the Fabry-Pérot laser diodes. In these techniques the downstream wavelength is reused to modulate the upstream data. Another solution is to put the burden on the OLT side, namely, locating the laser sources for the upstream in the OLT.

Figure 4.3 illustrates a simple WDM-PON architecture, separate channels are used for US and DS directions λ_{xUS} and λ_{xDS} respectively (x stands for the ONU's number). This architecture is a P2P architecture which OLT is connected directly to each ONU. In this topology, every ONU can operate at a different data rate and can utilize the complete dedicated bandwidth. The OLT has a set of transmitters/receivers. In remote node (RN) an arrayed-waveguide grating is used instead of the passive splitters. The AWG enables DS and US transmission at the same time since it can be operated over many free spectral ranges. Each ONU has a transmitter (Tx) and a receiver (Rx) that communicate with their corresponding Tx/Rx in the OLT. Every Tx in ONU can have either wavelength tunable source that matches to a certain AWG channel or wavelength independent source (colorless). There exist different types of wavelength tunable sources, such as vertical cavity surface-emitting lasers (VCSELs), distributed feedback laser (DFB) , distributed bragg reflector (DBR), external cavity lasers, and FP lasers (FP-LD). To minimize the operational costs, direct modulation of the laser source is required. As the high bandwidth services play a major issue in the access networks, the laser sources need to support high speed data modulations. The external cavity laser cannot provide high speed direct data modulation, since the cavity is large and inhibits the fast modulation. The VCSELs are inexpensive solutions and the tuning range can be more than 100 nm with fast tuning speed, an array of VCSELs can be manufactured and be used for different ONUs.

Using the wavelength-specific sources are expensive. Several techniques have been investigated, such as injection-locked FP lasers [29], reflective SOAs [20], spectral sliced broadband (BLS) light sources [30, 39]. The US wavelength is selected by external sources,

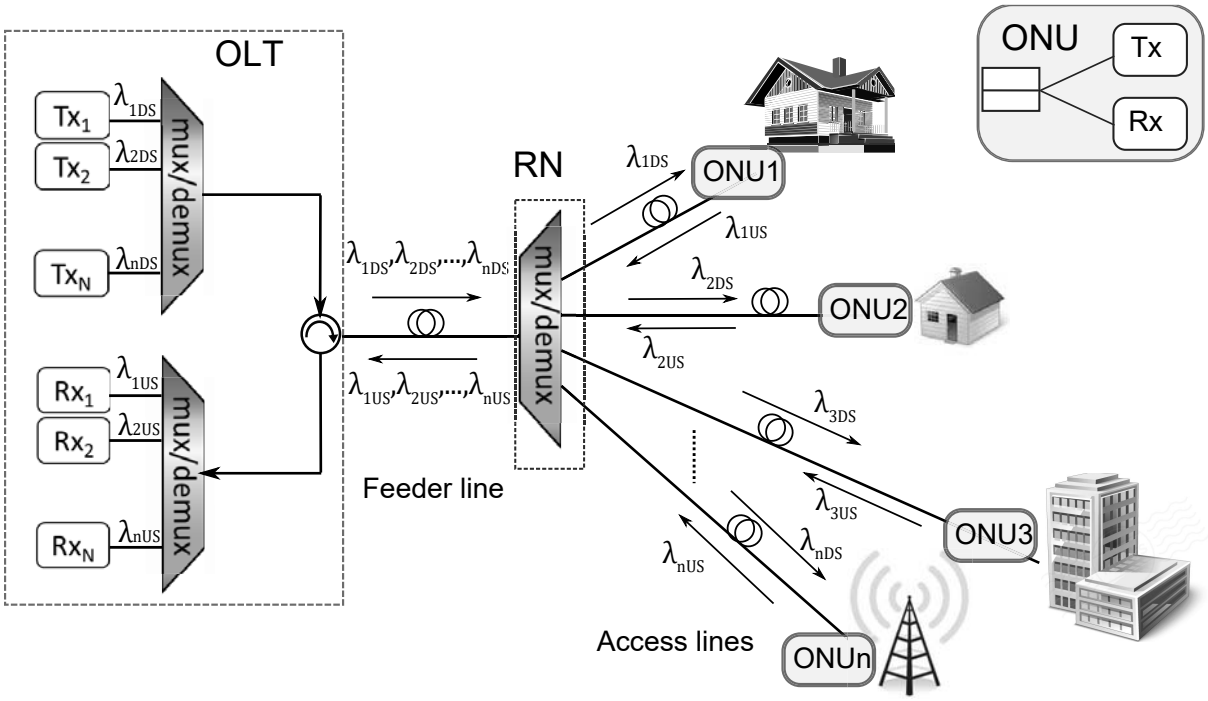

Figure 4.3: A wavelength-division multiplexing-PON architecture.

injected lights, and passive filters. Therefore, the wavelength selection management are simplified in ONUs. The DFB laser support high speed direct modulation and the tuning range of about 100 nm. They have been used for a long time in high speed optical fiber communications.

The injection of signals into to FP-LD with multiple longitudinal-modes, suppresses the side modes and a single mode can be extracted from the laser. The laser mode which is closest to the peak wavelength of the incoming light is locked and after a couple of round trips in the cavity emerges as a single mode laser. The injected optical light can be generated from a laser source in the OLT or a spectral sliced BLS. The output power of the source needs to be very high if it is located far from the ONUs, in this case the Fresnel reflections and Rayleigh backscattering limit the performance of the transmission. This scheme will be explained in detail in the following chapters of the thesis.

The spectral sliced BLS source can be a FP laser, an EDFA, or a LED which can be located at the ONU or the OLT. The spectra from different ONUs are sliced by the AWG channels located at the RN and then the multiplexed data are transmitted to the OLT. The output power of the BLS source mus be large enough to compensate the losses introduced by the mux/demux and the feeder fiber. Furthermore, the mux/demux must be temperature insensitive otherwise cross-talk may appear and deteriorate the signals quality. This Tx architecture is cost-effective, although the transmission distance and data rate is limited due to the broadband sources used in ONUs. Another limitation of this scheme is the low integrability of the setup to the existing TDM-PON technology, since the spectra of different ONUs should be sliced before being combined, otherwise incoherent lights may interfere with each other. For example if

WDM is integrated into a distributed split TDM-PON architecture, since multiple stage passive couplers/splitters are used before the AWG (US direction), if the data are combined in the power combiners before becoming sliced, collision can occur on US data stream.

4.8 NG-PON

Services such as cloud computing, triple-play, and internet-based application, which consume large amounts of bandwidth, have been constantly emerging, therefore, FSAN and ITU anticipate two stages for PONs evolution. First stage is NG-PON1 which is a short-term, and is based on XG-PON1. The FSAN task group submitted XG-PON1 (X is the Greek letter and stands for 10) specifications to the ITU-T for standardization of G.987 in 2010 with 10 Gbps DS and 2.5 Gbps US capacities. The short-term stage seems not to address the capability of higher speeds, so the market is moving toward NG-PON2 technology.

Three options were assessed by FSAN for NG-PON2, TDM-PON, dense (D)WDM-PON, and TWDM-PON technologies. TDM-PON is not considered by FSAN as a cost-efficient solution, since it is expensive to operate ONUs at full data rate of 40 Gbps, this data rate is envisaged to be far beyond the bandwidth requirement of an individual home subscriber. Additionally, some technical challenges such as, chromatic dispersion is difficult to manage at this speed for this technology. The second option is DWDM-PON, in which each subscriber can have a dedicated bandwidth with symmetrical 1 Gbps data rate. However, the high operational costs and inability to provide bandwidth sharing among subscribers, FSAN discontinued this option as well. The FSAN primary choice is the combination of both technologies, and in 2012, named it as TWDM-PON, which provides four or more wavelengths per fiber, and enables symmetrical or asymmetrical bit rates of 2.5 Gbps or 10 Gbps. This technology is selected for the implementation of the NG-PON2 architecture.

TWDM-PON increase the capacity by merging XG-PONs with four or more wavelengths. This provides 40 Gbps and 10 Gbps DS and US bit rates respectively. The GPON and radio frequency (RF) video overlay can coexist with this technology. As an example, Figure 4.4 shows a general NG-PON2 architecture in parallel with existing standards. In NG-PON2 CO, multiple OLTs can be included, which can be comprised of new and coexisting technologies. TWDM and P2P technologies are the new technologies which will be used in NG-PON2. four pairs of OLT-TWDM$_n$ (n: number of channels) are employed in the architecture. Each OLT-TWDM is comprised of a tunable laser, and a tunable receiver. The DS and US channels are not at the same wavelengths, therefore, there exists eight channel for bi-directional transmission. The RF video can be provided on-demand on the same OLT. The P2P WDM overlay enables a dedicated wavelength to each ONU, this is useful for low latency services such as mobile backhaul, and business, additionally, the network operators can benefit from unused spectrum to assign P2P WDM channel in a flexible way when needed. The line rates of P2P WDM varies from $1 - 10$ Gbps for symmetrical transmission.

The channels from GPON and XG-PON1 can be combined together with those from the TWDMs, and the P2P by a coexisting passive element (mux/demux). Then, the channels are split using a passive splitters, and later each channel is transmitted to its corresponding ONU. The NG-PON2 ONU transceivers are the key components of the new architecture. The

tunable colorless sources must be deployed in each NG-PON2 ONU. The tunable transmitters need to be stable over the temperature while tuning the OLT channels, otherwise the network fails. Thermally tuned DFBs are selected as reliable sources for ONUs, since they are more wavelength stable over temperature in comparison to injection tuned DBRs. The tunable receivers in ONUs are available such as, dual cavity etalon, thermally tuned FP filters, and thermally tuned thin film filters.

Moreover, it is necessary to take into account the best wavelength planning of the NG-PON2, in order to coexist with GPON, XG-PON1, and RF video. The US wavelength bands occupy the C-band where the optical components are commercially available and inexpensive, two options are defined, narrow and wide bands. The channel spacing of 50, 100, and 200 GHz can be provided. The DS wavelengths occupy the L-band with a fixed 100 GHz grid. The spectral flexibility plays a significant role in NG-PON2 wavelength planing. In P2P WDM case, the spectrum can be either shared or expanded. In the shared spectrum option, the P2P WDM coexist with legacy PON technologies, while the expanded spectrum enables operators to assign the channels which are not used in a specific deployment. So, The spectral flexibility provides services for different types of subscriber within the same infrastructure and makes an efficient use of the spectrum.

Figure 4.5 represents the wavelength plan for NG-PON2 coexisting with legacy PON for both US and DS directions. The high loss fiber introduced by water absorption is not used. The arrows show the shared and expanded spectrum respectively. In the expanded spectrum, the P2P-WDM can be utilized, when some parts of the spectrum is unused. For instance, a channel

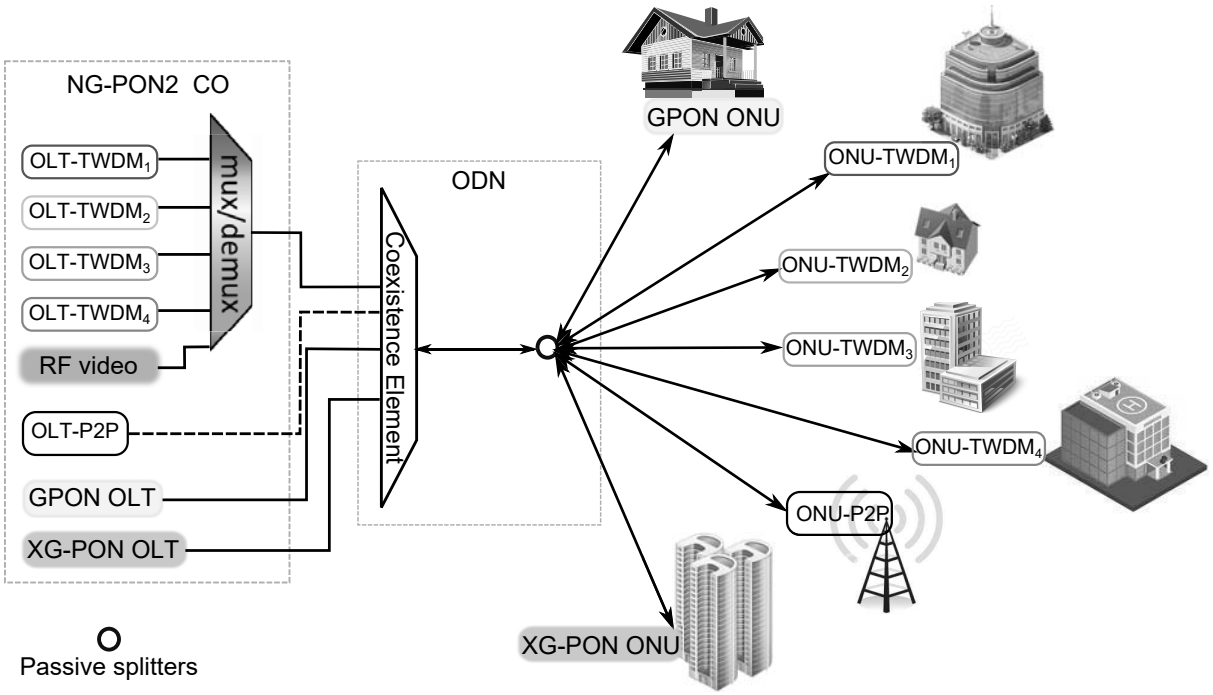

Figure 4.4: NG-PON2 general architecture including legacy PON. CO: central office, ODN: optical distribution network, P2P: point-to-point.

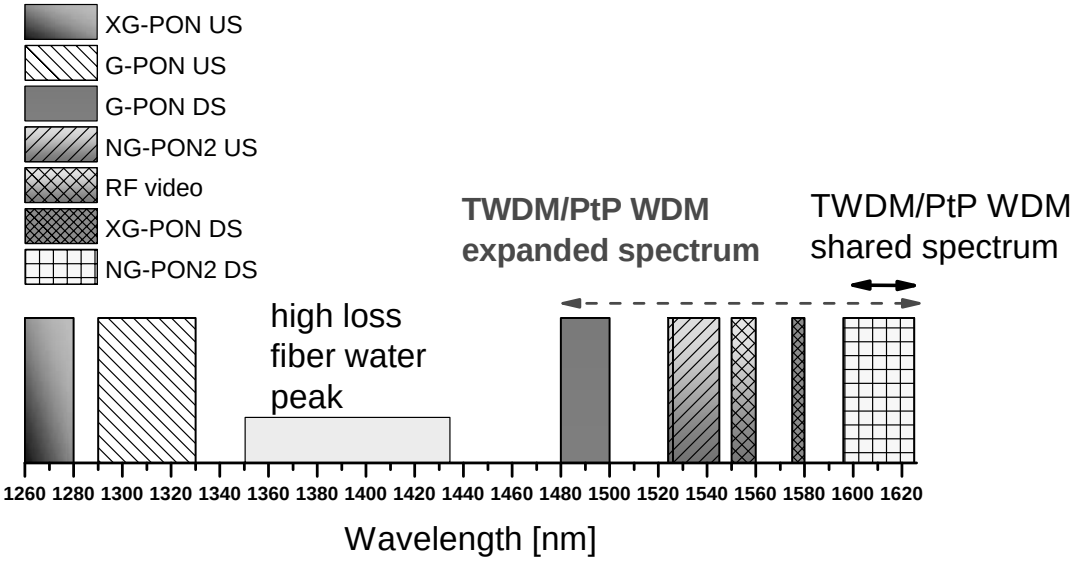

Figure 4.5: The complete wavelength plans for NG-PON2, DS: downstream, and US: upstream directions. In the shared spectrum, P2P WDM and TWDM share the spectrum and in the expanded spectrum (dashed arrow), P2P WDM is used when the specified spectrum is unused.

which is not occupied in GPON DS, the network operator can assign a wavelength to a ONU as demanded.

In the shared spectrum (small arrow, see Figure 4.5), the sub-band is already dedicated for P2P-WDM from 1603 nm to 1625 nm, the channels are always available to be assigned to a ONU.

This chapter focused on the PON technologies starting from legacy TDM-PON to the state-of-art NG-PON2. The PON architectures were illustrated in details with their corresponding bit rates. WDM-PON was suggested as promising option for NG-PON because of it higher capacity and security. It was shown that the NG-PON2 agreed on combination of WDM and TDM technologies as their final decision. In response to customers requirements, PONs are inevitable choice, and the only solution for the future broadband access networks.

Chapter 5

TDM/WDM Power Budget Extension: Simulations

The internet traffic is emerging on daily basis and is anticipated to increase in the future [15]. The demand for larger bandwidth has been expanding from old telephone line services to internet, HDTV, online gaming applications, video-on-demand, and so on. The challenges are increasing the bit rate, the number of customers, the distance to ONUs, and co-existence of the old, current, and the future PON infrastructures. It is desirable to accommodate different services using a single platform to reduce the operational costs and central office (CO) footprints.

We represent simulation results for different amplification techniques achieved in this work. The experimental results will be shown in the following chapter. Before delving into various configurations we start will SOA model.

5.1 Traveling Wave Laser Amplifier Model

The SOA model is based on time and space dependent traveling-wave equations [40–42]. In this model, the spontaneous emission noise is defined as traveling-wave power equation while the signal is defined as traveling-wave amplitude equation. The signal amplification relies on the amplified spontaneous emitted noise in the cavity, since the noise power reduces the electron population and yields to the gain saturation. The noise is distributed with random phase over wideband of wavelengths, it is defined as discrete set of wavelengths at the position of resonances. The SOA is a laser without mirrors, thus to investigate the dynamic behavior of the traveling wave in the cavity, we use the following rate equations [40]

$$\frac{dn_e}{dt} = \frac{qJ}{ed} - \frac{n_e}{\tau_{sp}} - \frac{c}{n_g \eta} \sum_{\nu=0}^{N} g_\nu S_\nu \tag{5.1}$$

$$\frac{dS_\nu}{dt} = \frac{\gamma}{\tau_{sp}} D_\nu n_e + \frac{c}{n_g}(g_\nu - \alpha) S_\nu \tag{5.2}$$

$$g_\nu = \frac{n_g \eta}{c} A(D_\nu n_e - H_\nu n_o) \tag{5.3}$$

These are two coupled differential equations for carrier and photon density respectively. When the current J is injected, the carrier concentration increases, the factor q corresponds to injection efficiency of the current into the conduction band. The second term is the ratio of the carriers to the electron life time, this term decreases because of spontaneous emission of photons. The last term shows that the carrier density increases if we have photon emission (positive sign) and decreases in case of photon absorption (negative sign). D_ν is the electron distribution function. This function is used to model correctly the spectral hole-burning (homogeneously broadening)of the laser. The function does not depend on n_e, S_ν, and J. Its summation over all modes is unity. H_ν is also a distribution function.

In Eq. 5.2 γ is a fraction of the spontaneous emitted photon coupled into the guide mode, this terms increases the photon density due to the spontaneous emission. The second term causes photon population either decrease due to the losses in the SOA (material internal losses), or increase when gain g_v is larger than the loss. η is the ratio of junction width d to effective width of guided mode. The rest of parameters are defined in the list of symbols at the end of the dissertation.

Under the steady-state the Eq.(5.1) is obtained as

$$0 = \frac{qJ}{ed} - \frac{n_e}{\tau_{sp}} - \frac{c}{n_g \eta} \sum_{\nu=0}^{N} g_\nu S_\nu \tag{5.4}$$

$$\overline{n}_e = \tau_{sp}\left(\frac{qJ}{ed} - \frac{c}{n_g \eta} \sum_{\nu=0}^{N} \overline{g}_\nu \overline{S}_\nu\right) \tag{5.5}$$

where overbar denotes the steady-state. As we mentioned earlier in the text, the photon density depends on spatial coordinate (here z), thus we assume backward and forward traveling waves for photon density

$$S_\nu = S_\nu^+ + S_\nu^- \tag{5.6}$$

We write Eq.(5.2) in total derivative form as

$$\frac{dS_\nu}{dt}^{\pm} = \frac{\partial S_\nu^\pm}{\partial t} \pm \frac{c}{n_g}\frac{\partial S_\nu^\pm}{\partial z} \tag{5.7}$$

We are interested in the steady-state of the photon density

$$\begin{aligned}
\frac{dS_\nu}{dt}^{\pm} &= 0 \pm \frac{c}{n_g}\frac{\partial S_\nu^\pm}{\partial z} \\
\frac{c}{n_g}\frac{\partial S_\nu^\pm}{\partial z} &= \pm\frac{\gamma}{2\tau_{sp}} D_\nu n_e \pm \frac{c}{n_g}(g_\nu - \alpha) S_\nu^\pm \\
\frac{\partial S_\nu^\pm}{\partial z} &= \pm\frac{n_g \gamma}{2\tau_{sp} c} D_\nu n_e \pm (g_\nu - \alpha) S_\nu^\pm
\end{aligned} \tag{5.8}$$

The spontaneous emission factor γ is halved, since only half of it travels in each direction. The solution to Eq.(5.8) is proved in the appendix

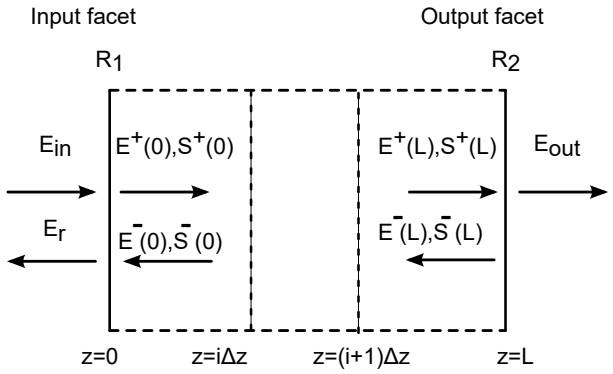

Figure 5.1: The diagram of semiconductor optical amplifier model. It is divided into small Δz sections.

$$S_\nu^+(z) = \frac{\frac{n_g \gamma D_\nu}{2\tau_{sp} c} \int_0^z (\exp\{-\int_0^z (g_\nu(x) - \alpha)dx\} n_e(y))dy + S_\nu^+(0)}{\exp\{-\int_0^z (g_\nu(x) - \alpha)dx\}} \tag{5.9}$$

$$S_\nu^-(z) = \frac{\frac{n_g \gamma D_\nu}{2\tau_{sp} c} \int_0^z (\exp\{\int_z^L (g_\nu(x) - \alpha)dx\} n_e(y))dy + S_\nu^-(L)}{\exp\{\int_z^L (g_\nu(x) - \alpha)dx\}} \tag{5.10}$$

where $S_\nu^+(0)$, and $S_\nu^-(L)$ are photon densities at left and right boundaries, respectively, as shown in Fig. 5.1, $E^+(z)$ is the traveling wave signal, and $S^+(z)$ is the spontaneous emission. R_1 and R_2 denote the reflectivity of the input and the output facets. The amplifier is divided into several section, and the carrier density is numerically calculated in the center of the cavity according to Eq. 5.1. The Eq. 5.1 can be modeled with finite difference time domain or using Runge-Kutta method. The output noise and internal noise distribution can be determined by Eqs. (5.9), (5.10), and (5.5). $S_\nu^+(0)$, and $S_\nu^-(L)$ are solved in the appendix, they are subject to boundary conditions in Fig. 5.1.

After describing the spontaneous emission wave traveling in the SOA, we add the signal to our model as the following.

The traveling waves in both directions can be written as

$$\frac{dE^+(z)}{dz} = -i\beta E^+(z) + \frac{1}{2}(g_s - \alpha)E^+(z) \tag{5.11}$$

$$\frac{dE^-(z)}{dz} = i\beta E^-(z) - \frac{1}{2}(g_s - \alpha)E^-(z) \tag{5.12}$$

where g_s is the gain coefficient, and $beta$ is the propagation constant. The gain changes as the noise and intensity of the signal changes. The solution to the above equations are

$$E^{+}(z) = E^{+}(0)\exp\{-i\beta z + \frac{1}{2}\int_{0}^{z}(g_s(x) - \alpha)dx\} \tag{5.13}$$

$$E^{-}(z) = E^{-}(L)\exp\{-i\beta(L - z) + \frac{1}{2}\int_{z}^{L}(g_s(x) - \alpha)dx\} \tag{5.14}$$

$E^{+}(0)$, and $E^{-}(L)$ are obtained using boundary conditions, these steps are shown in the appendix. We are ready to add the traveling spontaneous emission and the signal to get the total photon density.

$$S_{tot} = g_s(|E^{+}(z)|^2 + |E^{-}(z)|^2) + 2\sum_{\nu=1}^{N} g_\nu(S_\nu^{+}(z) + S_\nu^{-}(z)) \tag{5.15}$$

This equation now can be used to calculate the carrier density in Eq. (5.5). We consider two polarization with factor 2 before the summation of Eq. 5.15.

This model allows the signal propagation from opposite sides of the SOA. In this way, we can simulate the proposed co-propagating scheme. The OptiSystem software enables us to program and use the built-in modules to model our configurations. The traveling wave SOA amplifier module from the software is used with necessary modifications.

In the simulations, the nonlinear Schrödinger equation (NLSE) is numerically solved through split-step Fourier method to model the SMF. This is a fast method to understand the nonlinear behavior of the SMF as suggested in [43]. The linear and nonlinear effects of the SMF are taken into account in the model (built-in module in Optiwave system software).

5.2 SOA-based Power Extender

The purpose of this section is to demonstrate the simulation results carried out during the research time. Many optical component models are available in the Optiwave software, and some have been modeled in MATLAB by the author. In the following subsection, D(Q)PSK, and OFDM signals will be investigated using different schemes, SOA, saturated collision amplifier (SCA), and EDFA. The selection of PSK signals is due to their better tolerance to SPM-GVD, and resistivity to nonlinearities.

5.2.1 DPSK

We start with DPSK signals. Figure 5.2 shows simulation setup of for four-channel downstream transmission WDM-PON. Each channel operates at 10 Gbps. The purpose of the setup is to evaluate the DPSK performance in a PON scenario using a SOA in the RN. The data is generated using a pulse pattern generator (PPG) which clocks at 10 Gbps. The PRBS $2^{31} - 1$ is generated. In order to de-correlate the data streams on each channel, a 1:4 way splitter (lossless) divide the bits into four separate streams, this setup is used on purpose as in the experiment there is only one PPG available. There is four DPSK transmitters, each of which is composed of a

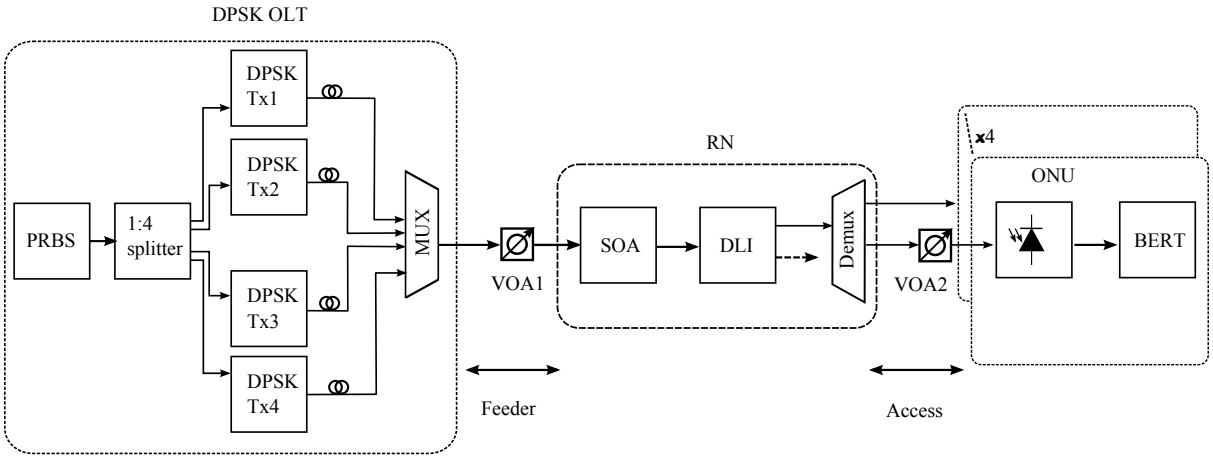

Figure 5.2: 4×10 Gbps downstream WDM-PON simulation configuration setup.

continuous wave (CW) laser, a MZM, and a pulse carver to create RZ-50%. The CW lasers emit at 1537.3 nm, 1543.9 nm, 1553.2 nm, and 1554.1 nm.

Word length	2^{31}-1
RZ	50%
Tx extinction ratio	10 dB
Laser output power	10 dBm
AWG 3-dB BW	50 GHz
SOA I_{bias}	350 mA

Table 5.1: Simulation parameters.

The optical channels are multiplexed together using an AWG and sent to feeder variable optical attenuator (VOA1) which emulates the losses introduced by feeder line (feeder fiber loss). The RN is composed of a SOA, a DLI and a demuliplexer. The optical signals are amplified and converted from DPSK to OOK at the same time. The optical channels are separated using a demuliplexer. The receiver is followed by a VOA denoted as VOA2 which emulates the fiber loss in the access lines. A BER analyzer is used to estimate the Bit Error Ratio (BER). The simulation parameters are summarized in Table 5.1.

Fig. 5.3 shows the BER curves of four channels versus received power in back-to-back scenario. The results show consistency with each other. The receiver sensitivity at BER 10^{-3} (FEC limit for DS scenario) is -24.6 dBm. The input power to the feeder line is 2 dBm, therefore, the total optical power budget is calculated to be 26.6 dB. Fig. 5.4(a) illustrates a so-called isoBER curves for back-to-back scenario. The curves are obtained by changing VOA1 in the setup by 2 increments and record the BERs. We consider forward error correction (FEC) limit throughout this work which allows us to work with $\log_{10}$BER at -3 and -4 for DS and US respectively. The dashed line depict isoBER curve corresponding to $\log_{10}$BER of -3 with the total optical power budget of 50 dB (24 dB feeder budget, and 26 dB access budget). This access budget enables splitting ratio of $1:32$ (17 dB loss), loss compensation of 5 dB

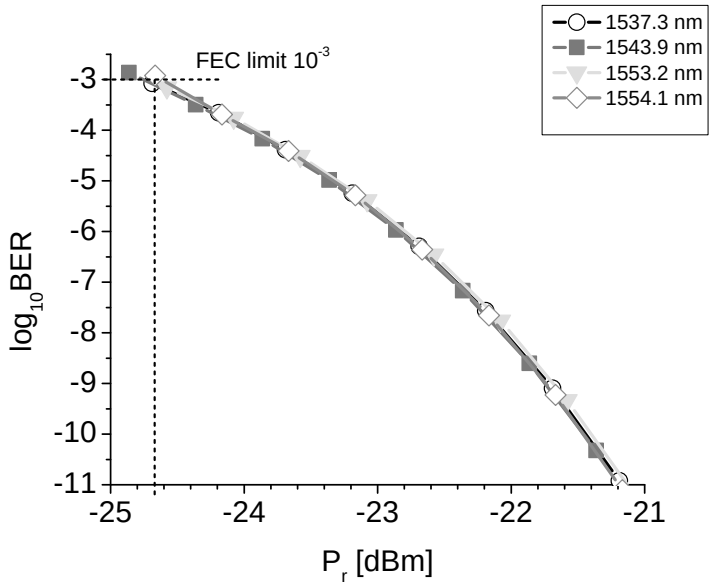

Figure 5.3: Back-to-back logBER versus received power 4×10 Gbps.

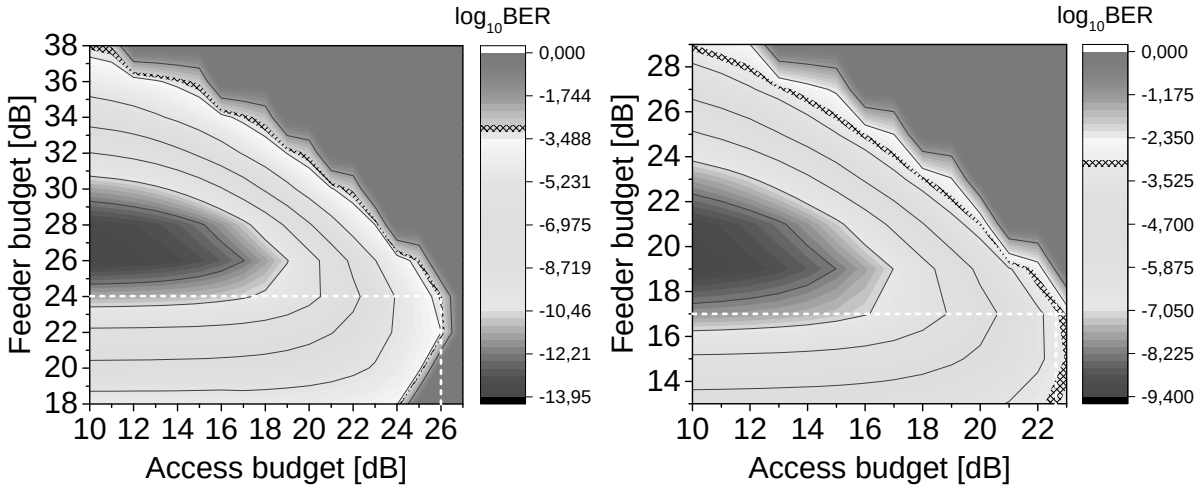

Figure 5.4: IsoBER curves 4×10 Gbps DPSK, (a) back-to-back, (b) including 50 km of single-mode fiber (40 km feeder and 10 km access).

introduced by the demultiplexer, and 4 dB reserved for the access fiber. The feeder budget can be used to compensate passive components such as optical fibers, splitters, and so forth in the feeder line. It is crucial to select the maximum achievable access budget in the curves, since the splitters are located in the access lines.

Fig. 5.4(b) is isoBER curves when total of 50 km single-mode fiber is inserted in the simulation setup, 40 km feeder and 10 km access fiber. The total optical power budget is shown as a dashed line representing 40 dB. This optical power budget allows splitting ratio of

$1:16$ (14 dB loss), 5 dB demultiplexer loss, and 4 dB optical margin reserved.

The isoBER curve is a very strong and useful tool for network operators to calculate their optical power budget at any BER. You can select any point on the curve which meets your network architecture requirements.

The SOA in the RN can increase the optical power budget by 23.4 dB in back-to-back scenario and 13.4 dB when 50 km of SMF is used. The input power to the SOA should be controlled, the optical signals with lower input powers are affected by ASE-noise of the SOA, and higher input powers are influenced by nonlinearities. As the signals are phase modulated, it is very critical to select the input power to the SOA. For high power inputs, the optical signal will be chirped (phase deterioration) by the nonlinear effect of the SOA and the data will be distorted. Additionally, all these impacts are translated on the intensity of the optical signal after the DLI. This is the drawback of this amplification setup. One may think of locating the SOA after the DLI, but this modification does not offer a cost-efficient solution, since two SOAs are needed for each outputs.

On isoBER curves the maximum value is considered as the access budget due to high losses in passive optical splitters, the aim is to achieve high number of subscribers. The feeder budget is limited by the saturation power of the SOA, the gain of the SOA, and the access budget is by ASE-noise and receiver sensitivity. The operating areas on the curves are limited by SOA gain, ASE-noise, and receiver sensitivity. Hence, at lower feeder budget the curves start to bend due to optical receiver saturation and SOA noise figure.

5.2.2 DQPSK

To achieve a better bandwidth efficiency DQPSK is proposed. We investigate in this setup, how the SOA operates when we have more symbols in our data. Fig. 5.5 illustrates the DQPSK simulation setup. The OLT consists of four DQPSK transmitters (DQPSK Tx_1) and a multiplexer. The DQPSK sequence generator has been explained in chapter 3. The VOA1 emulates the losses of the feeder fiber. Once the optical signals have propagated through the feeder line, they enter the RN for the amplification. The RN has a SOA, and a DQPSK demodulator. The optical channels are amplified simultaneously in the SOA and demodulated through DQPSK demodulator. The optical demodulator has four outputs, I_1, I_2, Q_1, and Q_2. Each output is demultiplexed and can be processed individually for each ONUs. The ONU includes a photodiode, an electrical amplifier and bit error ratio tester.

The isoBER curves are depicted in Fig. 5.6. The part (a) is back-to-back scenario, the dashed line shows an example of total optical power budget of 50 dB. The access budget can compensate loss of $1:32$ (17 dB) splitters, 5 dB mux, and 1 dB reserved for the fiber. The DQPSK configuration doubles the splitting ratio, as each output can be used separately to serve the subscribers.

Figure 5.6(b) illustrates isoBER when total of 50 km of SMF, 40 km in feeder line, and 10 km in access line are considered. The total optical power budget 42.5 dB. The access budget can serve 16 subscribers, 5 dB mux loss compensation, 1 dB optical margin. The total number of users in this case is $4 \times 4 \times 16 = 256$ users.

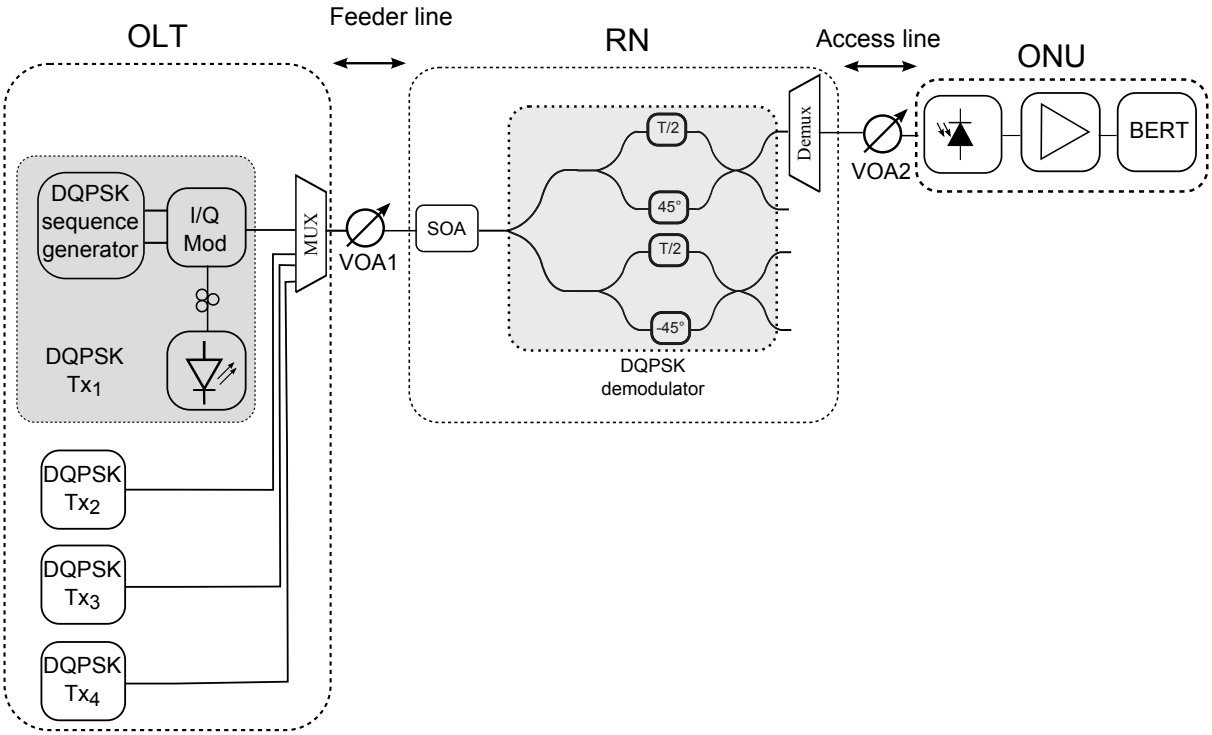

Figure 5.5: 4×10 Gbps DQPSK simulation setup.

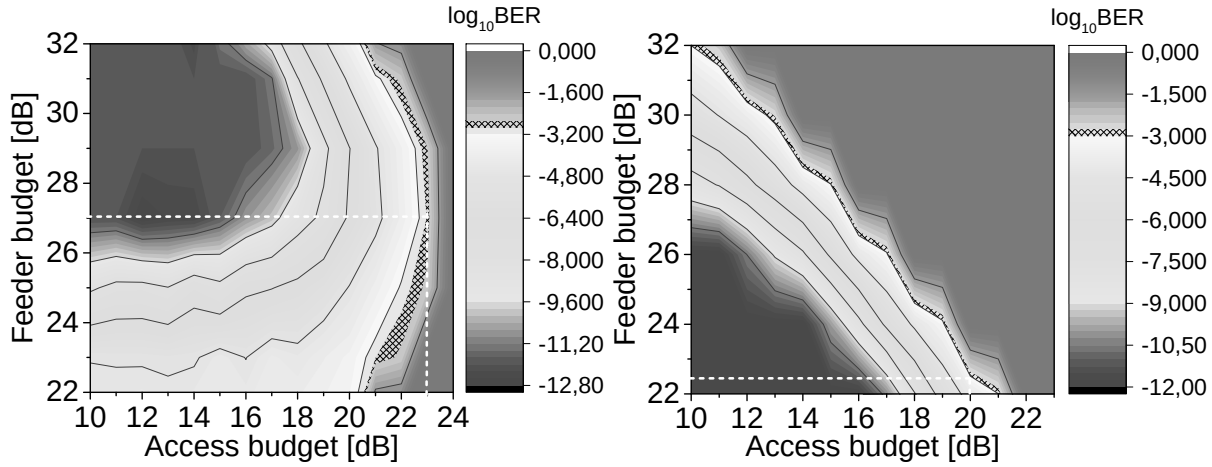

(a) (b)

Figure 5.6: IsoBER curves 4×10 Gbps DQPSK simulation, (a) back-to-back, (b) including 50 km of fiber (40 km feeder and 10 km access).

5.3 1-Tbps TWDM-OFDM

In this section we present optical power budget extension techniques for 1-Tb/s WDM/TDM-OFDM-PON. We demonstrate our simulations results for $25\lambda \times 40Gbps/\lambda$ in two different

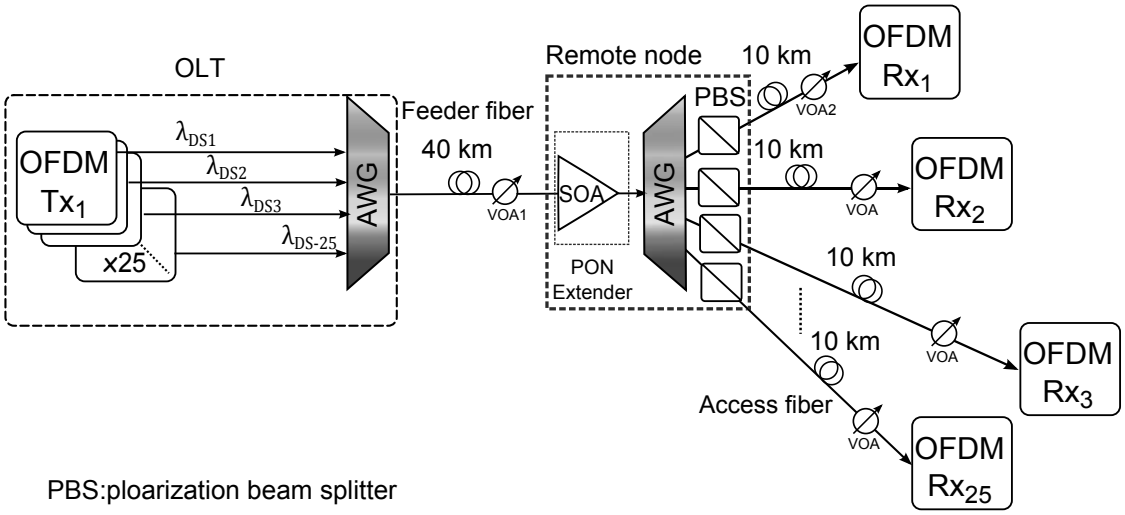

Figure 5.7: 1 Tb/s WDM/TDM-OFDM-PON SOA-based power budget extension simulation setup.

configurations. In the first configuration an SOA is used before the Remote Node (RN) as a PON extender, however in the second setup an EDFA is used. We employ different polarizations for neighboring channels to alleviate the nonlinear impacts of SOA on our OFDM symbols.

Figure 5.7 shows simulation setup of 1-Tb/s WDM/TDM-OFDM-PON. The OLT consists of 25 transmitters and an AWG with 100 GHz channel spacing. The OFDM transmitter has OFDM components explained in chapter 3, a CW laser, a Mach-Zehnder Modulator, and a band-pass optical filter to produce Single-Sideband (SSB)-OFDM. The CW lasers are divided into X and Y polarization for SOA-configuration only, odd:$\{\lambda_{DL1}, \lambda_{DL3}, ..., \lambda_{DL25}\}$, and even:$\{\lambda_{DL2}, \lambda_{DL4}, ..., \lambda_{DL24}\}$. This approach is used to decrease the impacts of nonlinear SOA on the OFDM symbols. Additionally, there is polarization beam splitter (PBS) at receiver side to remove the unmodulated polarization. There is 40 km of SMF in the feeder line, and a Variable Optical Attenuator (VOA1) to emulate the loss from OLT to RN.

In the RN, an SOA is used to increase the optical power budget for all 25 channels simultaneously. The access line encompasses a VOA designated as VOA2 for each channel to control the loss of the link and a 10 km fiber. At ONU side, direct detection is used as it is a cost-effective solution in comparison to coherent detection. In case of EDFA configuration, the SOA in the RN is replaced by an EDFA and there is no need for PBS in the access lines. The DQPSK data are modulated on OFDM symbols, 512 subcarriers are used in this simulation.

The SSB-OFDM is used to increase the bandwidth efficiency. Depending on reach, dispersion parameter and frequency of subcarriers, each subcarrier may show a different power penalty, which results in shorter transmission distance, and low quality signals in a conventional OOFDM. The SSB-OFDM can obviate this problem [44]. Furthermore it has been already shown [45] that the SSB system has stronger robustness to IQ imbalance than the dual-sideband (DSB) [46]. The optical spectrum of one channel before the APD receiver is illustrated in

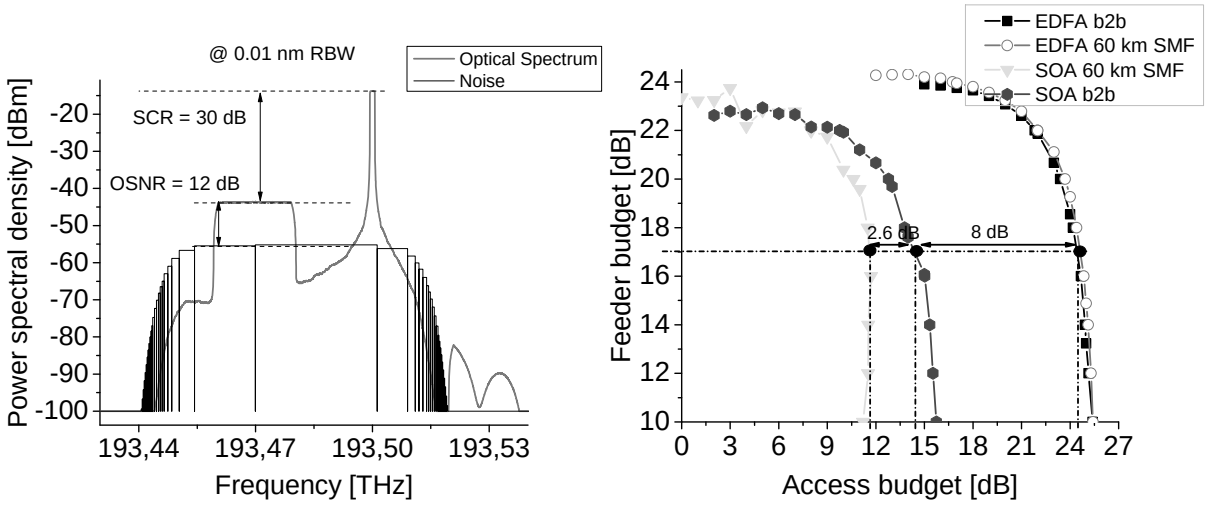

Figure 5.8: 1 Tb/s WDM/TDM-OFDM-PON simulation results, a) optical spectrum (SCR: subcarrier-to-carrier ratio, OSNR: optical signal to noise ratio, RBW: resolution bandwidth), b) isoBER curves for different cases.

Fig. 5.8(a). The subcarrier-to-carrier ratio (SCR) is 30 dB and the OSNR is 12 dB at BER 10^{-3}. The dashed lines depict the noise content of the OFDM spectrum. The isoBER curves are illustrated in Fig. 5.8(b). We assume here FEC standard, therefore, the contour curves are at BER 10^{-3}. The Feeder budget is the losses of the feeder line and the access budget is those of the access line. For each configuration two cases are considered, back-to-back, and 50 km SMF. Comparing the SOA-based with EDFA-based setup, the access budget in the first scenario is less by 8.5 dB. Furthermore, if we look at back-to-back results, the first configuration has the same access budget at the specified point (squares), however, the second configuration has 2.5 dB lower access budget. This is due to the nonlinearities as well as higher noise contribution produced by the SOA. The higher number of subcarriers can be used to cope with the nonlinear phase distortion caused by the SOA.

In EDFA-based configuration the total optical power budget of 41 dB (17 dB feeder budget, 24 dB access). This power can serve up to 64 (20 dB loss) customers with $0.625/40$ Gb/s/λ guaranteed/peak bit rate, plus 10 km fiber (3 dB loss), and 1 dB reserved for optical margin. In total, $25 \times 64 = 1,600$ can be supported. On the other hand, the total optical power budget of SOA configuration is 32.4 dB which can be used to serve up to 16 users (loss of 14 dB) with $0.625/40$Gb/s/λ guaranteed/peak bit rate. The above results show that power budget extension configurations perform differently when different modulations formats are used. The major factor here is the optimization of the SOA input power, if the input power is low the ASE noise dominates, on the other hand, if the input power is high, nonlinearities result which are not desired for phase modulated signals.

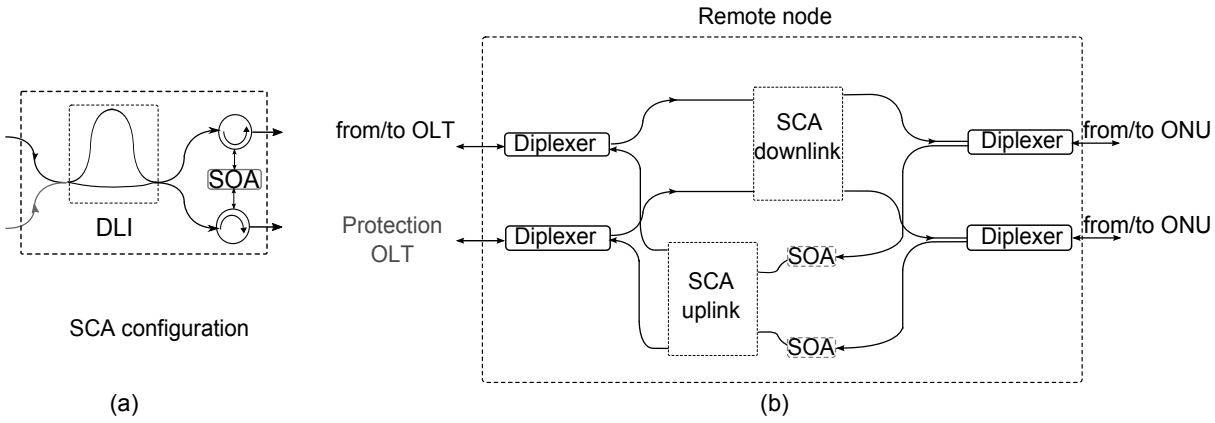

Figure 5.9: The mid/span PON extender, (a) saturated collision amplifier (SCA) configuration, (b) utilization of the mid-span in the remote node for bidirectional transmission.

5.4 SCA-based Power Extender

As shown in Fig. 5.9, the saturated collision amplifier is composed of a delay line interferometer (DLI), two circulators, and a high-gain SOA. The setup is designed for D(Q)PSK signals as they have higher tolerance against nonlinearities of the system compared to OOK signals. The signals are first converted from DPSK to OOK using DLI. The input signal to the NG-PON extender enters the DLI to convert the DPSK to OOK signals. The DLI free spectral range (FSR) matches the channel bit rate and it enables the phase-to-intensity conversion for any number of channels at the same time. The output signals from the DLI are logically inverted. These two signals co-propagate and enter at the same time into the SOA. The high level signal enters from one side and the low level signal consisting of noise enters from the other side which lets the SOA saturate, and deplete the gain medium. The SOA should be bidirectional with same gain in both directions. Due to the nonlinear gain of the SOA the fluctuations of the pulse peak intensity is decreased . As the SOA is in the saturation regime, both marks ans spaced experience the same nonlinear gain since the combined optical signals power saturate the gain medium. Furthermore, the mark is always entered from one side which modulate the noise thereby reducing the intensity variation. Additionally the optical gain depends on the sum of the marks and spaces. As a result, the SOA works as a limiting amplifier and lowers fluctuations of the high level signals. Also the eye diagram will remain open. We name our configuration the “saturated collision amplifier” (SCA), as it needs to operate in saturation region and signal “collision” occurs due to the counter-propagation. In this way, the extinction ratio of the signal is increased. Since DPSK signals have a constant optical power in each bit slot, the input power to the SOA is stable. As a consequence, the SCA configuration has only minimal bit-pattern effects [47].

5.4.1 DPSK

Figure 5.10 shows the 4×10 Gbps DPSK simulation setup including SCA extender in the RN. The only difference between this setup and Fig. 5.2 is the extender configuration in the RN,

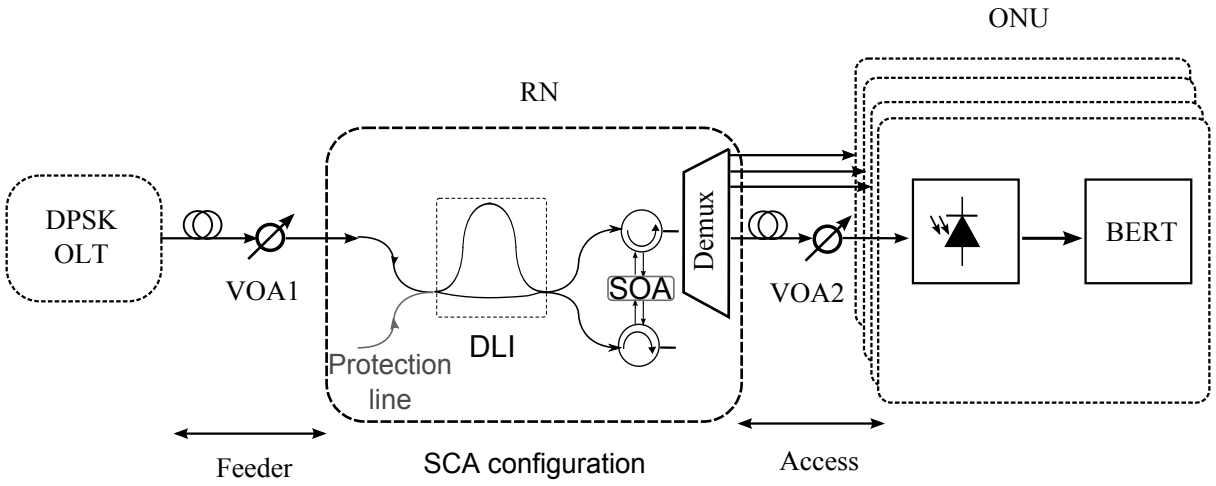

Figure 5.10: 4×10 Gbps DPSK simulation setup with SCA configuration.

the rest of the setup remained unchanged. To investigate the optical power budget extension efficiency of the SCA, two configurations are considered in the simulation. The isoBER curves of these configurations are illustrated in Fig. 5.11(a). The dashed lines and crosses depict the BER of 10^{-3}, in back-to-back scenario, the total optical power budget is 43 dB, where 28.8 dB is the access budget which enables $1:64$ (21 dB loss) splitting ratio, 5 dB mux loss compensation, and 2.8 dB reserved for the SMF in access lines. This configuration supports up to $4 \times 2 \times 64 = 512$ subscribers.

Fig. 5.11(b) is the second scenario where 50 km of SMF is used in the simulation, 40 km in the feeder line, and 10 km in the access line. The access budget shows a lower value since now the fiber is used in the link. The optical power budget in this case is 40 dB, 3 dB less than

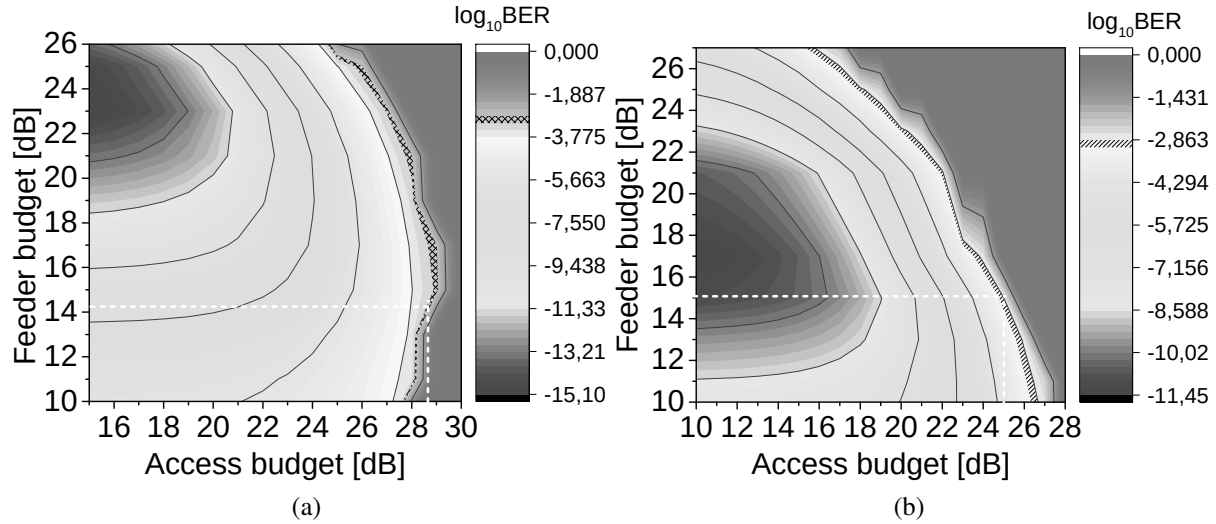

Figure 5.11: IsoBER curves for 4×10 Gbps DPSK simulation setup with SCA configuration, a) back-to-back, b) 50 km SMF.

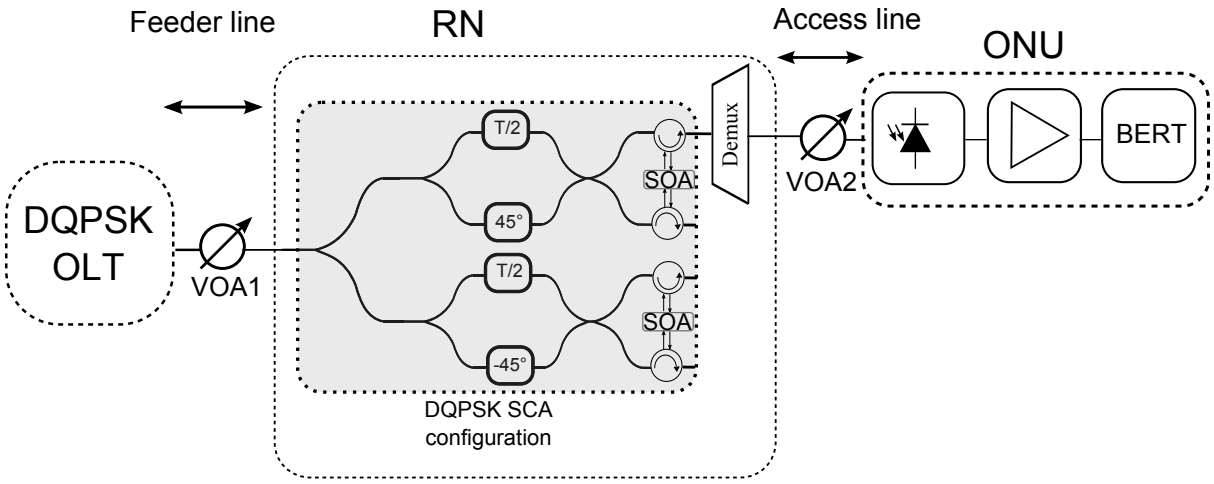

Figure 5.12: 4×10 Gbps DQPSK simulation setup with SCA configuration.

back-to-back at feeder budget of 15 dB. The access budget allows $1:32$ (17 dB loss), splitting ratio, 5 dB mux loss compensation, and 3 dB reserved for optical margin.

5.4.2 DQPSK

The simulation setup of 4×10 Gbps DQPSK is shown in Fig. 5.12. Now the SCA is utilized in the RN, the optical signal is converted to in-phase and quadrature parts and each part counter-propagates from opposite side in the SOA. The principle of amplification is already explained in the previous section. Once the optical signals are amplified, each is demultiplexed by the demux and distributed to the ONUs. The DQPSK is the highest order M-ary modulation format with 2 bits per symbol that can be used in the SCA configuration. For higher order modulation formats coherent receiver must be used and the amplification scheme needs to be altered.

Figure 5.13 displays the isoBER curves of 4×10 Gbps DQPSK setup with SCA configurations in back-to-back and 50 km of the SMF. The total optical power budget in both scenarios (Fig. 5.13(a) and (b)) is 42 dB. Obviously, adding 10 km of a SMF in access line does not change the access budget remarkably. The access budget in both cases is 27 dB, we can consider 64 subscribers in the access lines for each channel, 5 dB loss compensation of a demux, and 2 dB optical margin.

Table 5.2 summarizes the simulation results of the amplification techniques explained in this chapter. The SCA configuration enables higher number of subscribers in the network, since the amplification happens after modulation format conversion which has lower phase-noise to intensity conversion penalty. The SCA needs to be run in the saturation region to benefit from this advantage, otherwise both configuration manifest similar performance., another is used before the SCA to let it operate in the saturation. The DPSK-SCA configuration serves total of 64 subscribers on each channel which is double the number of subscribers in DPSK-SOA setup, this is due to the lower eye penalty, and higher quality of the received signals. The DQPSK-SCA supports 256 subscribers, in contrast, the DQPSK-SOA enables service delivery to 128 subscribers. The bit rate for each channel in case of DQPSK is 5 Gbps as we consider

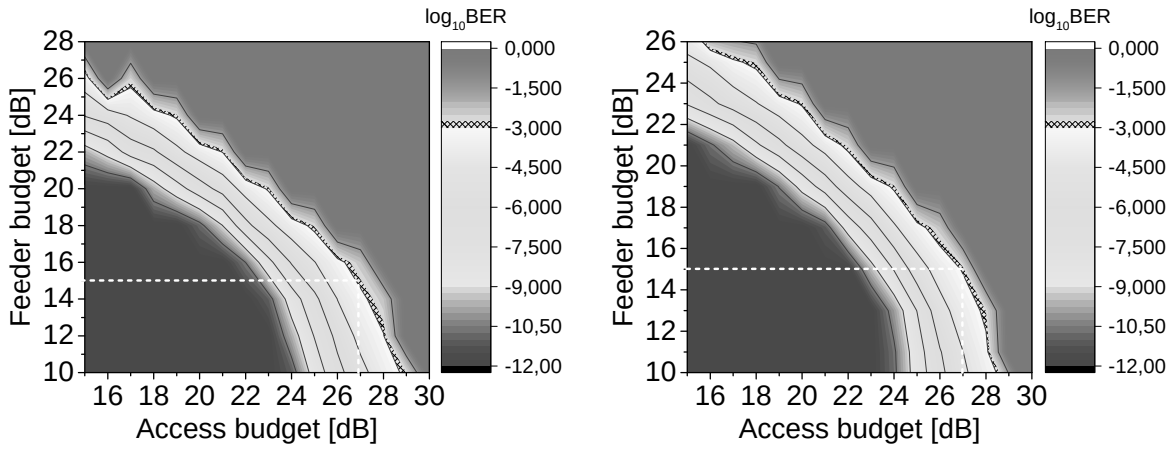

Figure 5.13: IsoBER curves of 4×10 Gbps DQPSK simulation setup with SCA configuration, (a) back-to-back, (b) 50 km of a SMF.

only in-phase part of the signal, in contrast to DSPK configuration, we have higher bandwidth efficiency. The SOA shows a penalty in case of OFDM modulation format, this is due to the time-constant limit (carrier liftime) of the SOA that cannot follow the OFDM symbol duration fast enough, the carrier in the amplifier needs more time to reach to their steady-state..

Modulation format	Technique	Total distance [km]	# of subs.	$R_b \backslash \lambda$ (Gbps)
DPSK	SOA	50	2×16	10
DQPSK	SOA	50	4×16	5
DPSK	SCA	50	2×32	10
DQPSK	SCA	50	4×64	5
OFDM	SOA	50	8	40
OFDM	EDFA	50	64	40

Table 5.2: The summary of amplification techniques for different modulation formats.

Chapter 6

Experimental Verifications

In this section the experimental results of TDM/WDM PON is presented for DS as well as US scenarios, DPSK, DQPSK, all optical OFDM, and self-seeded WDM/TDM will be elaborated. Two different transmitter configuration for the DPSK signal generation will be shown, chirped-manage laser-based and conventional DPSK generator.

6.1 SOA-based Experimental Results

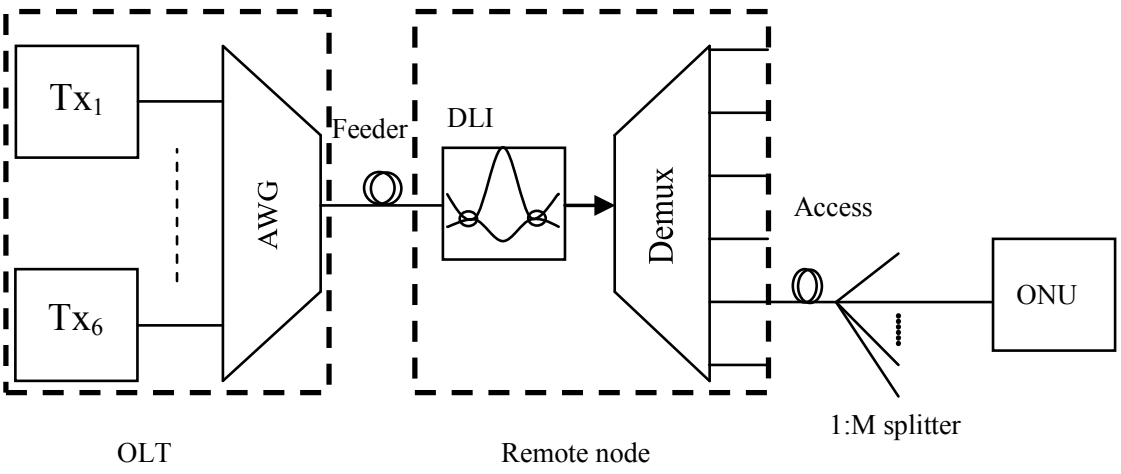

Figure 6.1: 6×10 Gbps DPSK downstream WDM PON architecture.

The proposed architecture is depicted in Figure 6.1. It consists of five parts: 1) OLT, 2) the feeder line, 3) the remote node, 4) splitters and the access line, and 5) ONUs. The DPSK signal is considered in DS scenario, the advantages over OOK modulation format are high tolerance to fiber dispersion and non-linearities as mentioned earlier. The OLT consists of 6 DPSK transmitters. If we look at US direction, each subscriber has a dedicated time slot to

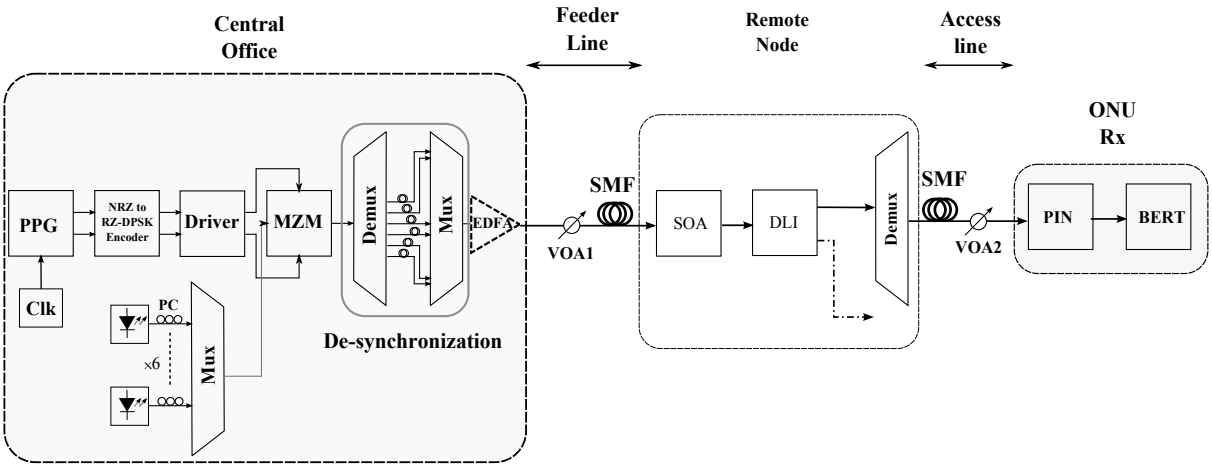

Figure 6.2: 6×10 Gbps DPSK downstream measurement setup.

transmit his data, this indicates TDM technology. This configuration allows to demodulate the channels at the same time using only one DLI, this is done in the RN. Since we perform direct detection, the demodulation is required to convert the signals back to OOK format, otherwise we cannot receive the phase information of the optical signal. The duty of the demux is to split the channels, in this configuration $1 : M$ is used. Different configurations can be used to implement DPSK transmitters in DS direction, direct phase, or frequency modulated lasers [48, 49]. The purpose of this setup is to show the power budget extension by using a SOA before the signal format conversion. The possibility to use a saturated collision amplifier (SCA) [50] is discussed in the next sections.

6.1.1 DPSK

The measurement setup is shown in Figure 6.2 where six DS channels of 10 Gbps PON are at 1537.3 nm, 1542.9 nm , 1543.6 nm, 1553.3 nm , 1554.1 nm, and 1556.5 nm generated by DFB laser diodes. The channels are combined by an AWG and modulated by a single MZM. The modulator operates in push-pull mode and generates RZ-DPSK signals at 10 Gbps (PRBS of $2^{31} - 1$). In order to have uncorrelated data on each channel, they are demultiplexed and transmitted through different fiber lengths and again multiplexed by a multiplexer. The mux/demux have 100 GHz channel spacing and 50 GHz 3-dB bandwidth. The EDFA is used to compensate the loss of the mux and the demux, each channel has 8 dBm power at the input of feeder variable optical attenuator. The line between OLT and the RN is termed as feeder line and the one between remote node and ONU is the access line.

A DLI is used in the RN to convert DPSK into OOK signal. The receiver is a PIN photodiode with sensitivity of -17 dBm at BER 10^{-9} and -22 dBm at 10^{-3}. The Figure 6.3 illustrates the BER versus optical received power for all six channels for the constructive output of the DLI. The measurements are performed in back-to-back scenario in the absence of the SOA. There is no big difference among the channels BERs. This shows the EDFA in the setup acted almost equally on each channel. The shaded area shows the optical received power of different channel at BER 10^{-3}, we assume FEC correction. The total optical power budget is

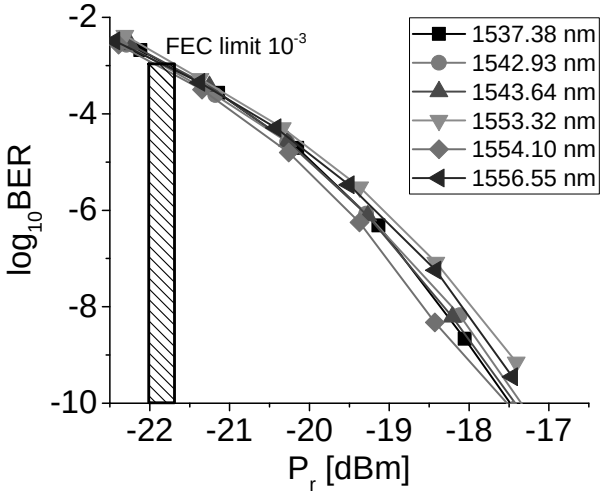

Figure 6.3: 6×10 Gbps BER curves, back-to-back for downstream scenario.

30 dB and 29.75 dB at the best and worst case. The total optical power is calculated as the difference between the input optical power at the transmitter side to the received optical power corresponding to a specific channel. The Figure 6.4 shows the optical spectrum of the channels with nearly the same power (the spectrum is acquired after DLI, refer to Fig. 6.2). The peak at the beginning of the spectrum result from the ASE noise in EDFA used after the second mux in the setup. At the time of this experiment there was only 6 DFB lasers available, that's why there is a gap between the central channels, this also validates the BER curves in Fig. 6.3. The SOA is

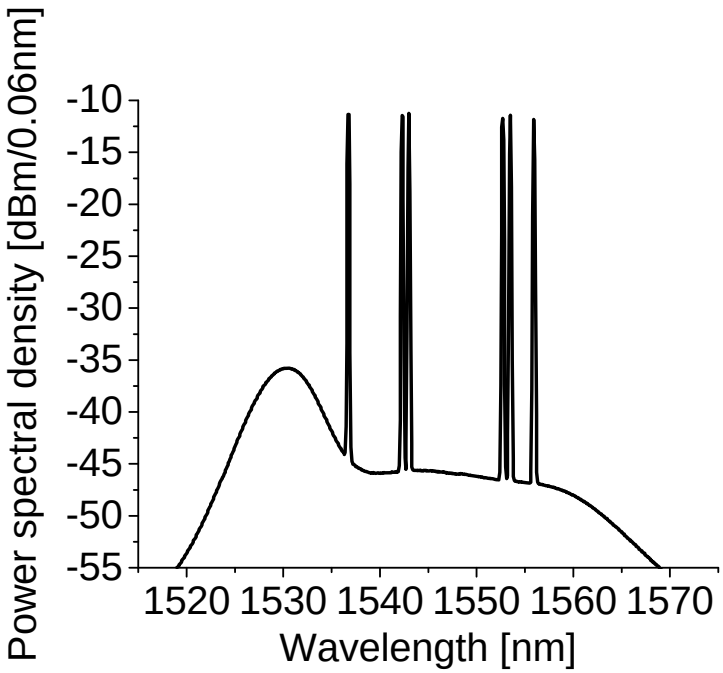

Figure 6.4: The spectrum of 6×10 Gbps DPSK downstream, RBW 0.06 nm.

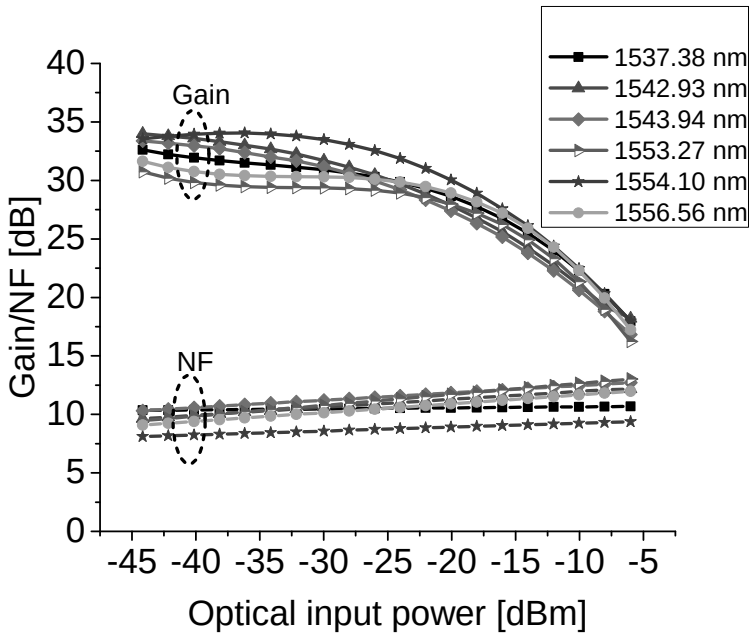

Figure 6.5: Characterization of the SOA, the noise figure (NF) and gain of the SOA.

now inserted in the setup as shown in Fig. 6.2 in order to investigate how it improves the optical power budget of the link. The bias current of SOA is set to 300 mA at the temperature of 17.2 °C. Figure 6.5 depicts the gain and noise figure of the SOAs (each measured separately) used in the experiment for various channels. The highest gain of 34.8 dB is achieved at 1554.1 nm with NF of 8.5 dB. This measurement would roughly say how the gain and noise contribution would be on each channel. The Figure 6.6 illustrates the BER curves over access budget for different values of optical feeder budget considering one channel (1543.6 nm). The legend indicates the feeder budget values. For larger values of feeder budget, the BER decreases. This is due to domination of ASE noise produced by the SOA, and the receiver limitation. On the other hand, lower values of feeder budget show worse performance, this may be a result of non-linearities caused by the SOA.

The Figure 6.7 illustrates BER map for 1543.6 nm. So, the BER of 10^{-3} can be used. In this case, at the feeder budget of 17.5 dB the access budget is 18.5 dB. Therefore, the total optical budget is 36 dB. This optical power budget can serve 16 subscribers at the ONU, and 2.5 dB reserved for the fiber and a circulator.

An APD can be used to further increase the access budget of the system, since it has higher receiver sensitivity than a PIN diode. In the absence of SOA, the maximum feeder budget is 21 dB, however, with SOA a higher feeder budget is obtained. For instance, in Fig. 6.7 at feeder budget of 30 dB we have access budget of 16.8 dB, this gives total optical budget of 46.8 dB.

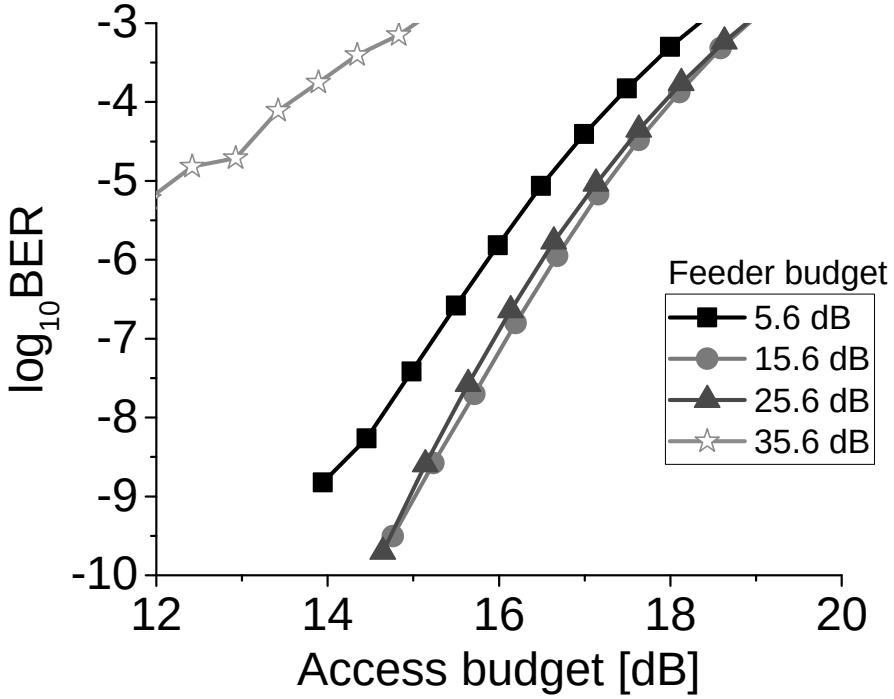

Figure 6.6: $\log_{10}$BER versus access budget for different feeder budget values.

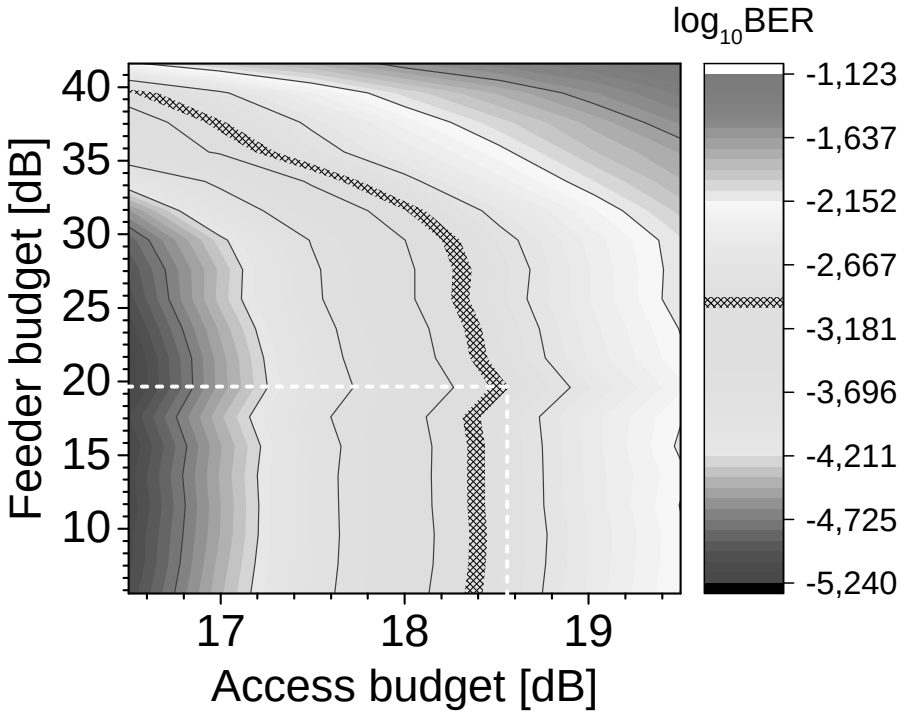

Figure 6.7: IsoBER curves of 60 Gbps WDM-DPSK conventional SOA, back-to-back scenario.

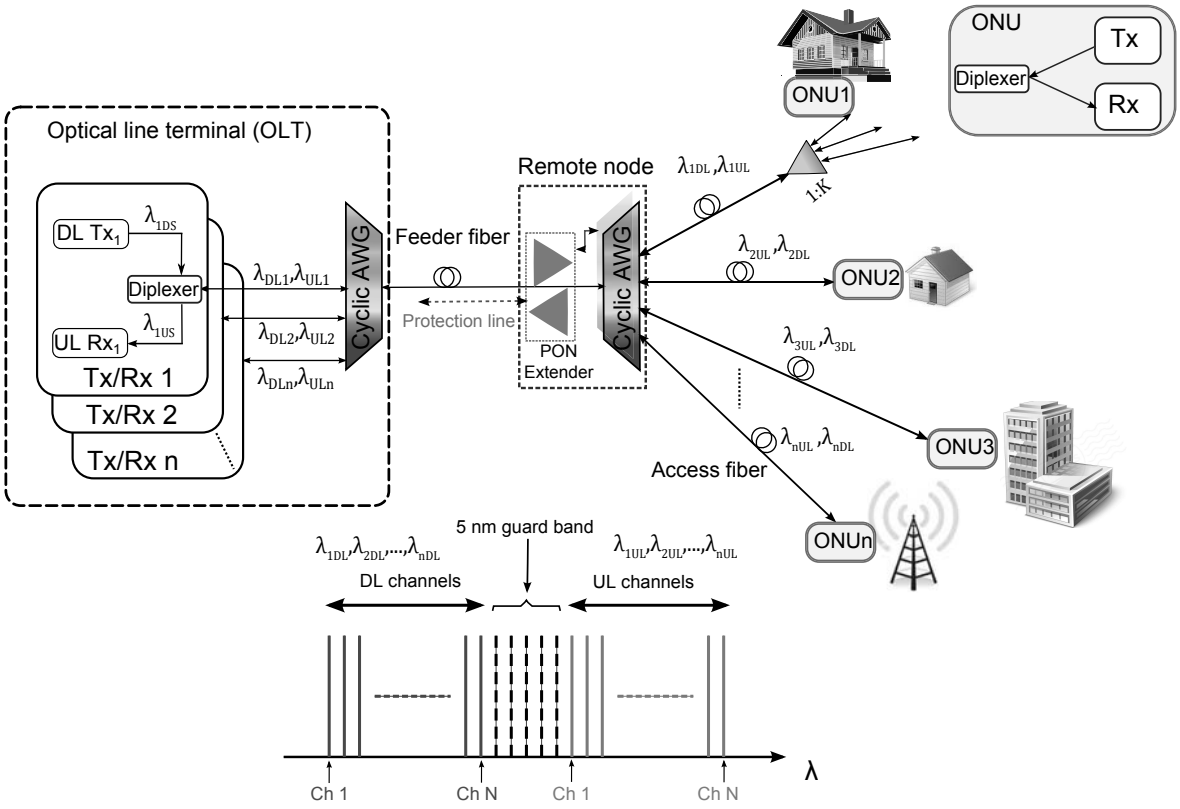

Figure 6.8: Hybrid DWDM/TDM Network Architecture.

6.2 SCA-based Experimental Results

Figure 6.8 depict the proposed hybrid DWDM/TDM architecture. This architecture consists of an OLT, a feeder fiber SMF which is the connection between OLT and the RN. The PON extender in the RN consists of two SCAs one dedicated for DL and one for UL. The OLT comprises N DPSK-transmitters for DS direction (DL Txn) and receivers (UL Rxn) for UL direction. The channels are in the C-band with 5-nm guard interval between DL and UL channels. This allows the channels to be easily separated using the cyclic arrayed waveguide gratings (AWGs) in the network. The diplexer separates DL and UL signals simultaneously, this component has an insertion loss of less than 2 dB. The architecture can be either point-to-point or point-to-multi-point, this gives the data rate flexibility in the network. The passive splitters (also called PON trees) are used in point-to-multipoint scenario. The losses introduced by these passive components throughout the network lowers the optical power budget remarkably. Therefore, the optical PON extender is necessary to compensate this loss and ensure the signal quality for transparent communication. Table. 6.1 summarizes the passive components used in the proposed architectures and their corresponding insertion loss values. The feeder line corresponds to the link between OLT transmitter/receiver and the PON extender. The access line corresponds to the link between the PON extender and the ONU transmitters/receivers. The optical path loss of the feeder line is introduced by two diplexers to separate UL and DL signals, one at the OLT and one at the RN (2×2 dB), one AWG at the OLT (5 dB), the

Table 6.1: Passive components in considered network architecture.

Feeder		Access	
Components	IL [dB]	Components	IL [dB]
2 Diplexers	2 x 2	2 Diplexers	2 x 2
AWG	5	AWG	5
Fiber	0.3 dB/km	Fiber	0.3 dB/km
DCF if needed	4	Splitters	
		1:16	14
		1:32	17
		1:64	20

feeder fiber (0.3 dB/km), and dispersion compensating fiber (DCF) to partially compensate for the chromatic dispersion in a long reach scenario. To the best of our knowledge, DCF is not in any deployed PON system, an insertion loss of 4 dB (C-band insertion loss for 40 km of DCM) is considered here as an example for this component. In a similar manner, the optical path loss of the access line is introduced by one AWG, two diplexers, the access fiber, and the power splitters with different splitting ratios. The inevitable advantage of using an optical amplifier as PON extender in DWDM/TDM-PON is the simultaneous amplification of every channel. Consequently, the deployment and the operational costs of the network can be reduced. However, with a shared amplifier, increasing the number of wavelength channels does not proportionally increase the number of subscribers. The SOA has a maximum output power which is, in an ideal case, equally divided for each channel. When more wavelengths are turned on in the architecture, the power per channel decreases. This relation can be formulated in the logarithmic scale as following,

$$P_{\lambda}[mW] = \frac{P_{out}}{N} \tag{6.1}$$

where P_{out} is the SCA output power, P_{λ} is the power per wavelength, and N is the number of active wavelengths in the architecture. The difference between each (P_{λ}) and the receiver sensitivity (P_{sen}) results in the optical access power budget for each wavelength ($PB_{Access/\lambda}$).

$$PB_{Access/\lambda} = P_{\lambda} - P_{sen} \tag{6.2}$$

Higher number of wavelengths result in lower power per channel and thus lower $PB_{Access/\lambda}$. As a consequence, less subscribers can be served by one channel. It should be mentioned that, the total number of subscribers is

$$N_{total} = N \times N_{sub/\lambda} \tag{6.3}$$

where $N_{sub/\lambda}$ is the number of clients per wavelength. When N is doubled, P_{λ} is reduced by 3-dB which is a factor of two, this means that $N_{sub/\lambda}$ is half as much and N_{total} remains unchanged.

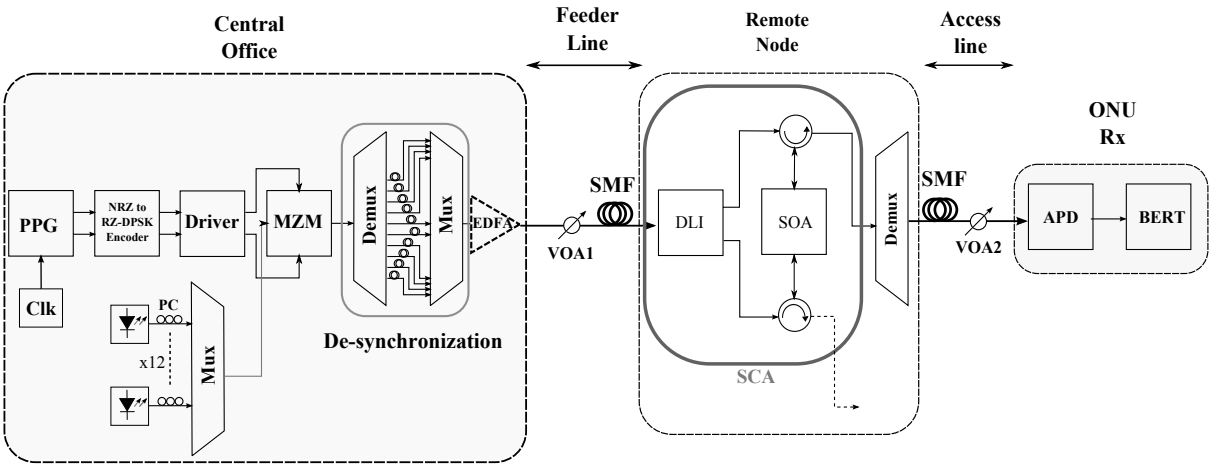

Figure 6.9: Downstream experimental setup.

As an example, a typical SOA output power is 15 dBm, with 12 active wavelengths, and P_λ is 4.2 dBm. For comparison, this power corresponds to the OLT transmitter power of XG-PON1 N2 class (minimum OLT transmitter power of 4 dBm). With the ONU receiver sensitivity of -28 dBm, the access budget is 31 dB with 1 dB margin, which can serve up to 64 subscribers. With less wavelength channels, more subscribers can be served per channel which reduces the system cost, however the sustained bandwidth per subscriber will consequently be lower. With higher number of wavelengths, the total number of subscribers stays the same, but the guaranteed bandwidth per subscribers will be increased.

6.2.1 DPSK

DS configuration

The DS experimental setup is shown in Fig. 6.9, twelve channels are used. The channels are randomly distributed over 100 GHz-spacing ITU grid [16] in order to investigate the wide gain bandwidth of the SOA. Twelve DFB lasers emit at the following wavelengths: 1537.3 nm, 1538.9 nm, 1540.5 nm, 1542.9 nm, 1544.9 nm, 1550.1 nm, 1550.8 nm, 1551.7 nm, 1552.5 nm, 1553.3 nm, 1554.1 nm, 1556.5 nm. The modulation format is return-to-zero (RZ)-DPSK data signals at 10 Gbps. One MZM is used to modulate all the channels at the same time. To have de-synchronized data patterns on each channel, the signals are demultiplexed and transmitted through SMF of different lengths and multiplexed again. To compensate the loss introduced by the pattern de-synchronization scheme, an EDFA is used similar to the simulation case in chapter 5. The variable optical attenuator denoted as VOA1 in the feeder line emulates the optical losses from OLT to RN, a DCF if needed, and a diplexer in the RN (Table 6.1). The SCA is placed in RN as depicted with the red box in Fig. 6.9. VOA2 emulates the losses introduced on the access line. Finally, the ONU receiver is modeled by an APD and a bit error ratio tester (BERT). Table 6.2 outlines the optical path losses of XG-PON1 classes [51]. N denotes “nominal” PON budget and E denotes “extended” PON budget. This table will be taken into account as the power budget references and enables a comparison with the demonstrated

Table 6.2: Power budget values of XG-PON1 classes [51]

Class	Opt. path loss [dB]
N1	29
N2	31
E1	33
E2	35

experimental results in the section. Figure 6.10 shows the measured BERs of 12 channels in back-to-back (without PON extender in the RN) scenario. That is 12×10 Gbps DWDM-PON scenario. The horizontal dashed line is the BER at FEC limit and the vertical dashed lines are receiver sensitivities at this BER. The lines manifest different slopes which arises from the EDFA used in the OLT that gain contributions and ASE noise with respect to each wavelength differs from each other. Therefore, some channels show higher receiver sensitivities than the others. For instance, the Rx sensitivity at 1553.3 nm is -32 dBm. However, at the same BER (10^{-3}) the channel 1556.5 nm achieves -31.4 dBm. The power at the output of OLT is 0 dBm so the total optical power budget of these cases are 32 dB and 31.4 dB respectively. Each single channel meets the power budget requirement of XG-PON1 classes N1 and N2a (see Table 6.2). To enhance the optical power budget and the total distance from the OLT to the ONUs, the SCA now is inserted into the experiment as shown in Fig. 6.9. For certain feeder budget values, the BER vs. access budget was measured. The measured BER map at the wavelength 1556.5 nm at BER 10^{-3} is depicted in Fig. 6.11. The graph outlines the range of operation limit (feeder budget and access budget) where BER lower than 10^{-3} can be assured. Different areas highlight with colorful rectangles which show the power budget of XG-PON1 classes. We see that the SCA configuration can potentially extend the power budgets by 9 dB, 20.8 dB, 24.5 dB, and 27.5 dB for E2a, E1, N2a, and N1, respectively. From this map, different operation points of

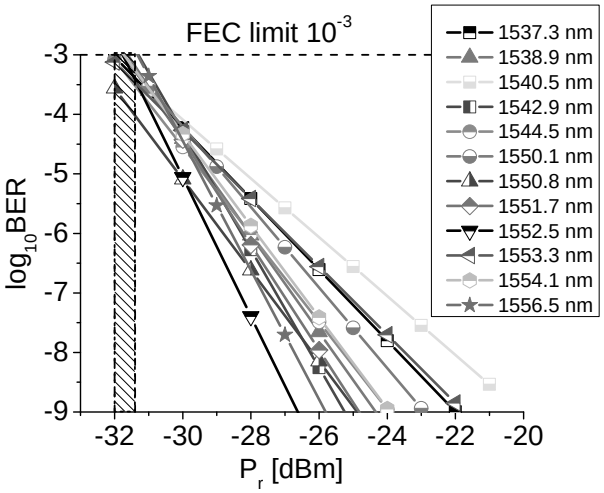

Figure 6.10: Measured BER curved of 120 Gbps DWDM-PON downstream setup, back-to-back scenario.

the extender corresponding to different network scenarios can be considered:

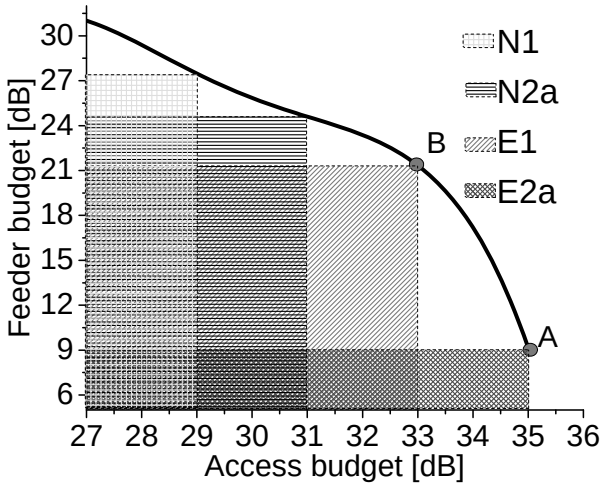

Figure 6.11: BER map at 10^{-3} for channel 1556.5 nm after using SCA PON extender.

An urban scenario (point A in Fig. 6.11): The feeder budget can be as low as 9 dB corresponding to 20 km of feeder fiber (6 dB), one diplexer at the RN (2 dB) and 1 dB margin (the feeder budget is emulated by the VOA1 after the multiplexing of DWDM channels, the insertion loss of AWG and a diplexer in OLT is excluded). In that case, the PON extender is in saturation and yields maximal output power, and an access budget of 35 dB can be obtained. This access budget allows the transmission over an AWG demux (5-dB loss), 10 km of fiber (3-dB loss), $1:64$ splitting ratio (20-dB loss), two diplexers (one at extender output, and another at ONU input) to separate up- and downlink signals (2×2 dB) and 3 dB margin. Consequently, with two outputs of the SCA and 12 wavelengths, the number of served clients can be up to $1,536$.

A long reach rural scenario (point B in Fig. 6.11): The feeder budget is 24.5 dB for 60 km of fiber (18 dB), 2 dB for the diplexer at RN, and 4.5 dB margin which can be used for DCF to partially compensate for the chromatic dispersion. The access budget in this case decreases to 31 dB. This access budget allows the transmission over an AWG demux (5 dB loss), 20 km of fiber (6 dB loss), $1:16$ splitting ratio (14 dB loss), two diplexers (2×2 dB) and 2 dB margin.

Upstream CML configuration

The US experimental setup uses cost-effective chirped managed lasers (CML) as ONUs [52]. As displayed in Fig. 6.12, the US transmitter consists of a 4×10-Gbps DPSK directly modulated CML scheme. The driving signal is encoded in inverse return-to-zero (IRZ) format. By direct modulation, a corresponding frequency shift is generated due to the adiabatic chirp of the laser. As the optical phase is a time integral of the instantaneous frequency, an IRZ pulse creates a phase shift of $\Delta\varphi = 2\pi \int_0^T \Delta f dt$, where Δf is the optical frequency deviation and T is the pulse duration. Consequently, in order to obtain a phase shift of π with a 50%-duty-cycle IRZ signal, a maximum frequency shift of about 10 GHz is required. The wavelengths are at 1535.8 nm, 1536.6 nm, 1537.4 nm, and 1538.1 nm. Figure 6.13(a) shows the BER

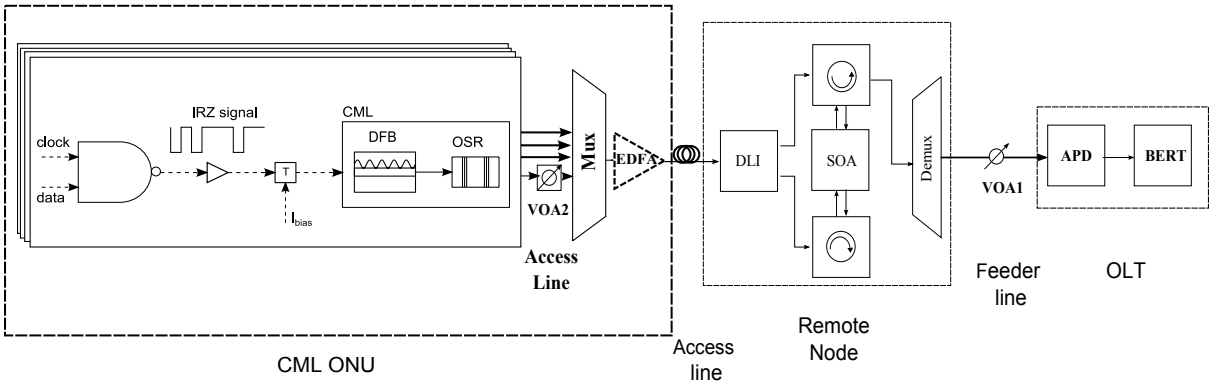

Figure 6.12: Upstream experimental setup.

measurements without the PON extender. The back-to-back transmission is the only scenario considered in this section. Assuming FEC limit at BER 10^{-3}, the receiver sensitivity is -32 dBm. The transmitter output power is 7 dBm at 1538 nm, so, the total optical power budget is 39 dB. Now, the extender is used in the setup and the measurements are repeated. All the neighboring channels are operated relatively at high power levels causing nonlinearities in the SOA. The bias current is 300 mA for the SOA. We can see from Fig. 6.13(b) that the extender can amplify the power budget to 60 dB (30 dB access budget and 30 dB feeder budget). This access power budget allows for 10 km fiber (2 dB), $1 : 128$ splitting ratio (23 dB) and 6 dB reserved for mux/demux. Considering output of both circulators and four channels, $128 \times 2 \times 4 = 1,024$ subscribers can be supported. In order to evaluate the system performance in terms of nonlinearities caused by the amplification, we compared a conventional configuration (only a SOA not SCA) as a PON extender and our SCA setup. Fig. 6.13(c) shows the BER versus optical received power when the conventional configuration is utilized in the RN (before the DLI). The power penalty is obvious specially when the channels have high input power levels. The legend shows the optical input power of one channel and that of the neighboring channel. At larger power levels the SCA even manifest better BER performance. The SCA can obviate the nonlinear impacts occurred in the SOA. In Fig. 6.13(d) as we increase the number channels single SOA configuration fails to work error-free. The SCA extender is less dependent on channel power levels specially when operated in saturation, and it does not distort the signal qualities of the lower power channels. Although, the conventional SOA setup enhances the power budget too, when all channels operate at low input power levels. But, in any case the SCA scheme has better performance than the conventional amplification setup.

Upstream burst-mode

As mentioned in the introduction, in US direction the burst signals are transmitted through different paths (fiber distances) and enter the PON extender with different power levels. Another property of the PON extender is the burst power equalization to reduce the complexity of the burst-mode receiver at the OLT. Figure 6.14 depicts the packet equalization experimental setup. An SOA is used as a preamplifier to partially compensate for high optical path loss in the access lines, and allows the second SOA to operate in saturation regime. The ONU transmitter

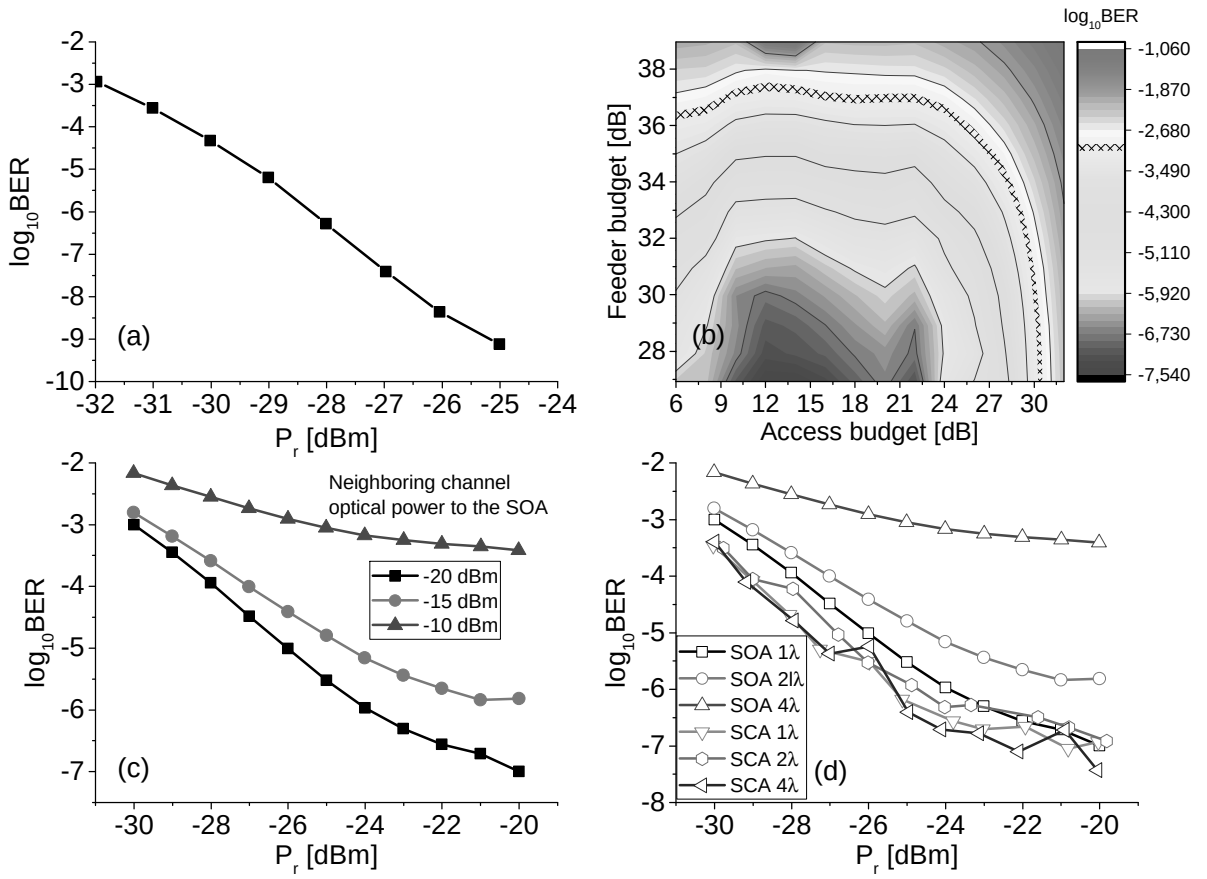

Figure 6.13: (a) back-to-back receiver sensitivity, (b) IsoBER curve for US transmission, c)single SOA configuration with different power on neighboring channels, (d) SCA and SOA comparison.

is composed of a DFB laser operating at 1577 nm which is connected to a bias gating generator (burst control in the Figure 6.14) for burst mode operation. The UL data is generated by a pulse pattern generator (PPG) at a bit rate of 10 Gbps with PRBS $2^7 - 1$. The output power of the laser is 3 dBm. The burst control creates 60μsec bursts, and then a phase modulator (PM) is used to externally modulate the signal. The PM output is split into two paths using the coupler to generate two packets. One is delayed by using a 15 km fiber as a delay line and attenuated compared to the other. Then two packets are coupled back together. The VOA1 is used to control the DR between the two packets. In the inset, the DR is 9 dB. The DLI is located in RN where the phase to intensity conversion takes place. The OLT consists of a VOA denoted as VOA3, an APD, and an error detector (ED). Figure 6.15 shows the BER curves versus receiver input powers without PON extender. The continuous data stream (CW) curve is shown as reference, and in this mode the laser is operated in continuous mode with burst control not connected. We consider the FEC limit for the UL at 10^{-4}, which is described in XG-PON1 standard. The receiver sensitivity for loud and soft packets is -27.5 dBm at BER 10^{-4}. The 2 dB penalty compared to the CW mode is mainly due to the laser thermal chirp which results in intensity deterioration after modulation format conversion [17]. The difference between loud

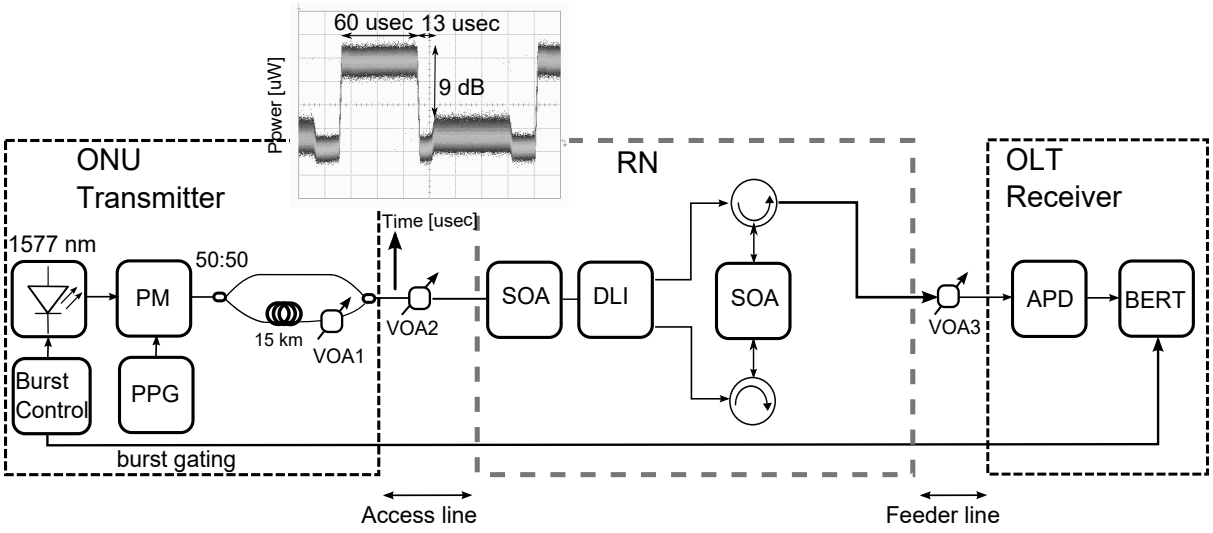

Figure 6.14: Upstream experimental setup for 10 Gbps single channel TDM-PONs.

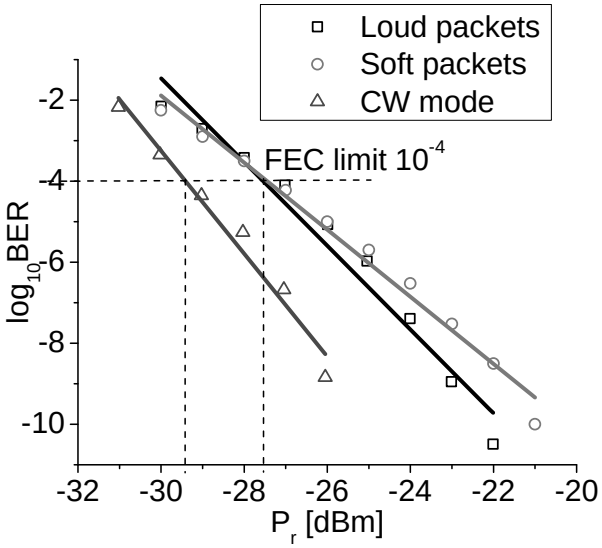

Figure 6.15: 10 Gbps UL BERs versus receiver sensitivity for CW, loud packets, and soft packets.

and soft packet at lower BER (less than 1 dB) is due to 15 km fiber. To increase the access budget and equalize the packets the amplification scheme is used in RN as shown in Fig. 6.14. The optimum bias current of the preamplifier SOA is measured to be I_b=150 mA. The results are illustrated in Fig. 6.16. In Fig. 6.16(a), bias current I_b is set to 100 mA and legend shows different input powers to the SCA. The reference indicates the laser on continuous mode. As it is shown, at lower input powers to the SCA the receiver sensitivity decreases, which is due to the ASE noise of the SOA. In the same manner, the results for bias currents of 150 mA and 200 mA are outlined in Fig. 6.16(b) and (c), respectively. The power penalty at BER 10^{-4} is shown in Fig. 6.16(d). The penalty is the difference between each point on the corresponding input

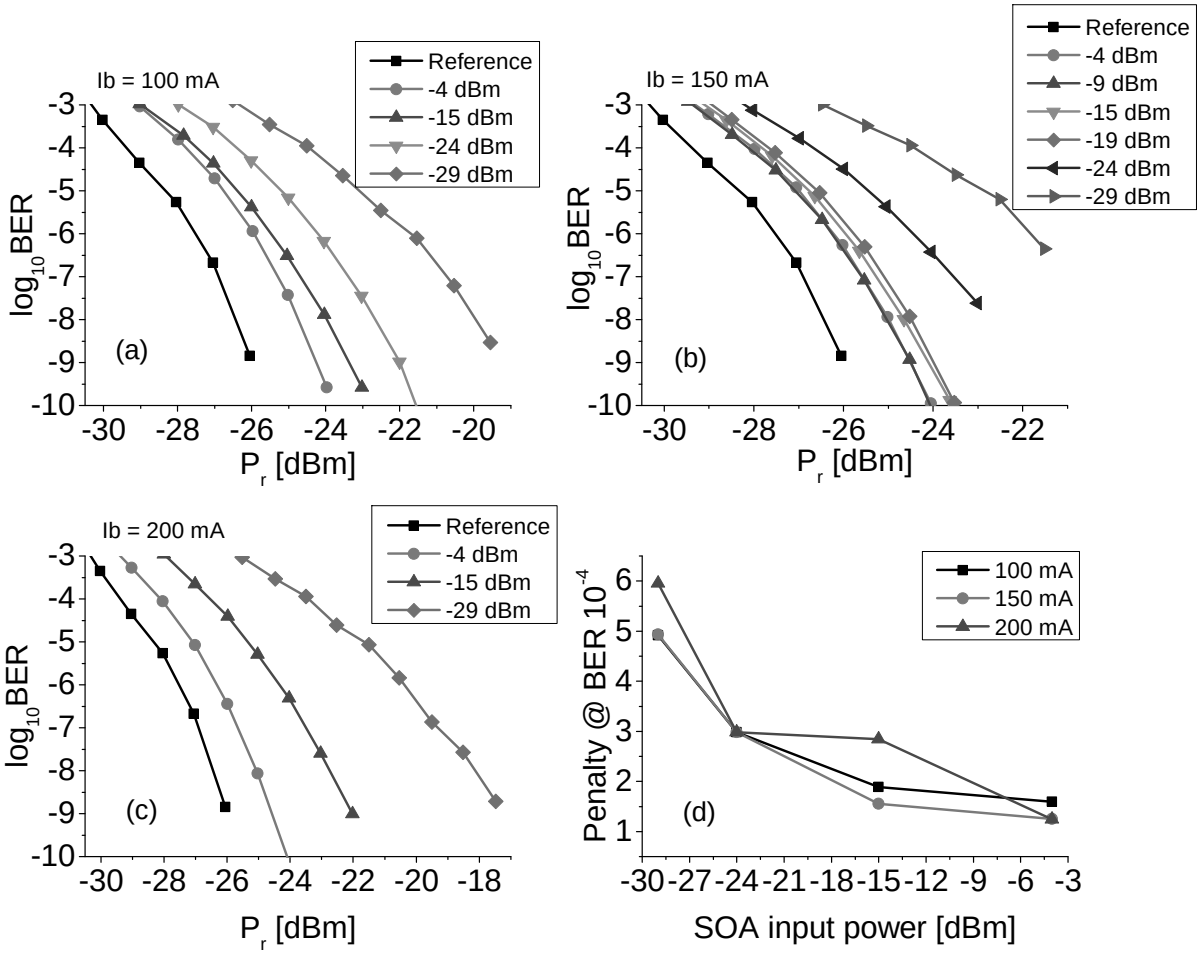

Figure 6.16: Optimization of the SOA with respect to bias currents at different input powers, (a) I_b = 100 mA, (b) I_b=150 mA, (c) I_b=200 mA, (d) penalty at BER of 10^{-4}.

power and the reference at 10^{-4}. The curves show a steady behavior at the SOA input power of -15 dBm onward, since after this point the SOAs operate in saturation and higher optical signal-to-noise ratio is achieved, thus the penalty is reduced below 2 dB.

Figure 6.17 represents BER maps of CW, loud packets, and soft packets. The BER maps are obtained by varying VOA2 (access budget) and VOA3 (feeder budget). The input DR to the first SOA is 9 dB. The CW mode is included in the graph as a reference. The dashed areas show the compatibility of the setup with different XG-PON1 classes represented in Table6.2. The SCA configuration enables extending the power budgets by 29 dB, 30.5 dB, 32.1 dB, and 33.9 dB for E2, E1, N2, and N1, respectively, for both loud and soft packets. For the case of 35-dB access budget, the corresponding feeder budget is 29 dB. The access budget of 35 dB can include 5 dB AWG demux loss, 10 km of fiber (3-dB loss), $1:64$ splitting ratio (20-dB loss), two diplexers to separate up- and downlink signals (4 dB) and 3 dB margin. A feeder budget of 29 dB can cover the insertion loss of AWG at the OLT (5 dB), two diplexers (4 dB) and 60 km of fiber (18 dB) in long reach scenario with 2 dB margin. As shown in Fig. 6.17, the curves bend over at the maximum access budget of 38 dB, this point is limited by the SOAs

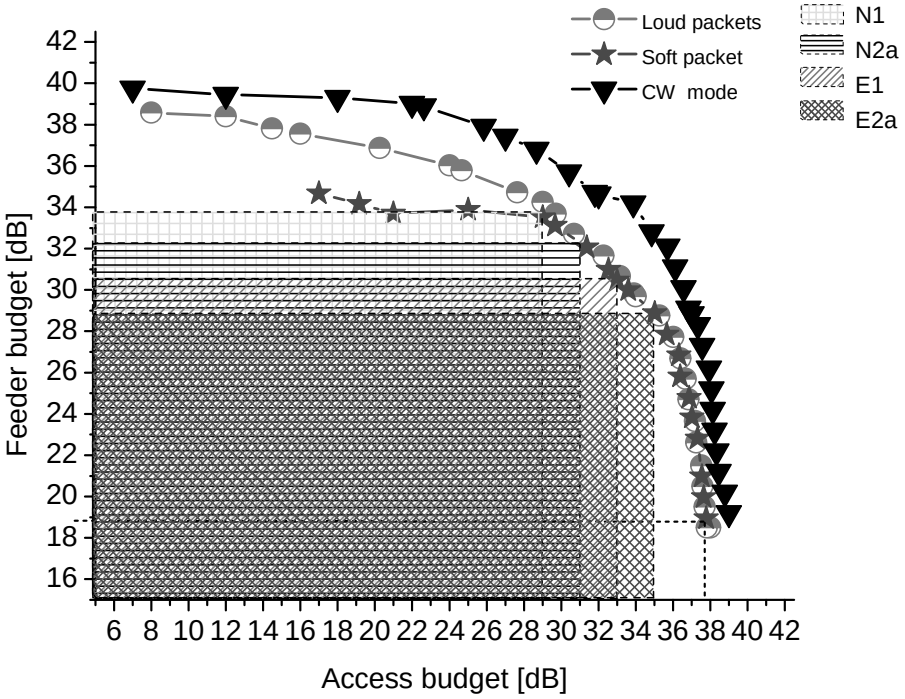

Figure 6.17: 10 Gbps UL BER maps at BER 10^{-4} for CW, loud , and soft packets.

noise figure as well as their gains. The feeder budgets are limited by the SOAs maximum output power. This maximum access budget can be used to double the number of users compared to the previous case. The feeder budget is now 19 dB, which is enough for 20 km of fiber in urban scenario (total of 80 km fiber).

The burst-power equalization capability of the amplification scheme is also investigated. Fig. 6.18 shows output DR versus input DR of the PON extender for different average input power. At 9-dB input DR, the full compression is achieved, and the burst levels are totally equalized. The higher the input power is, the higher compression can be obtained. The maximum DR of 16 dB compression is achievable using this amplification technique (shown at DR input of 21 dB at input power of -8 dBm).

Figure 6.19 shows the equalized burst at different input DR at the output of the SCA, the bursts correspond to the half-rectangle line in Fig. 6.18. As seen at 9 dB DR, the full compression is almost achieved and the bursts are amplified to equal levels (the input bursts are shown in the inset in Fig. 6.14). The sharp overshoots at the beginning of the burst are introduced by laser thermal chirp of the directly modulated laser used in the experiment.

Two-channel US transmission has also been considered to investigate the effect of cross-talk between the burst pulses. The setup is depicted in Fig. 6.20. Now, the ONU consists of two burst-mode lasers at 1530.3 nm, and 1548.5 nm (the only available channels at the time of experiment). The arbitrary waveform generator (AWG) generates a burst of 60μsec to operate each laser in the burst-mode. The mux combines two channels, and then the data are phase

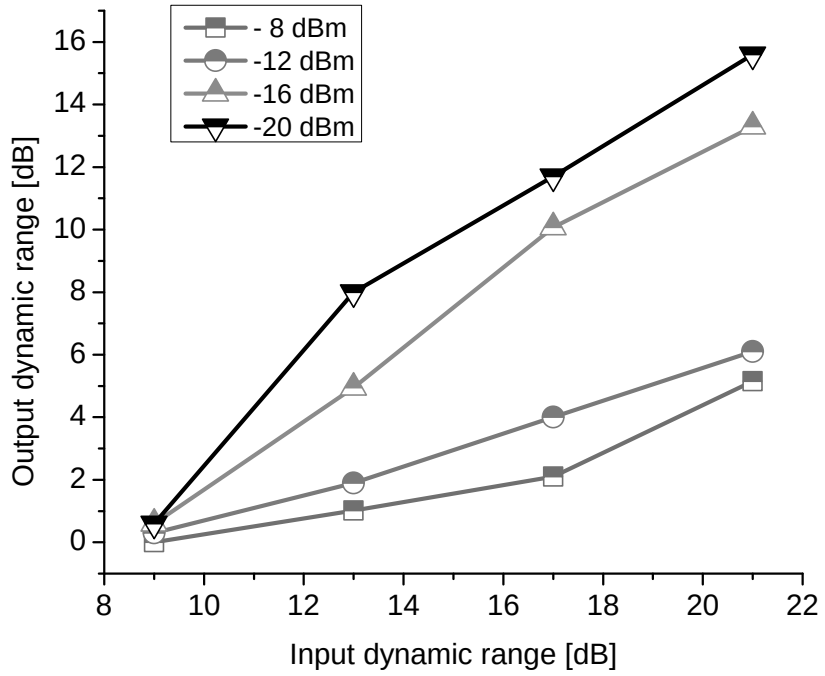

Figure 6.18: Input-output dynamic ranges for different input powers into the SOA.

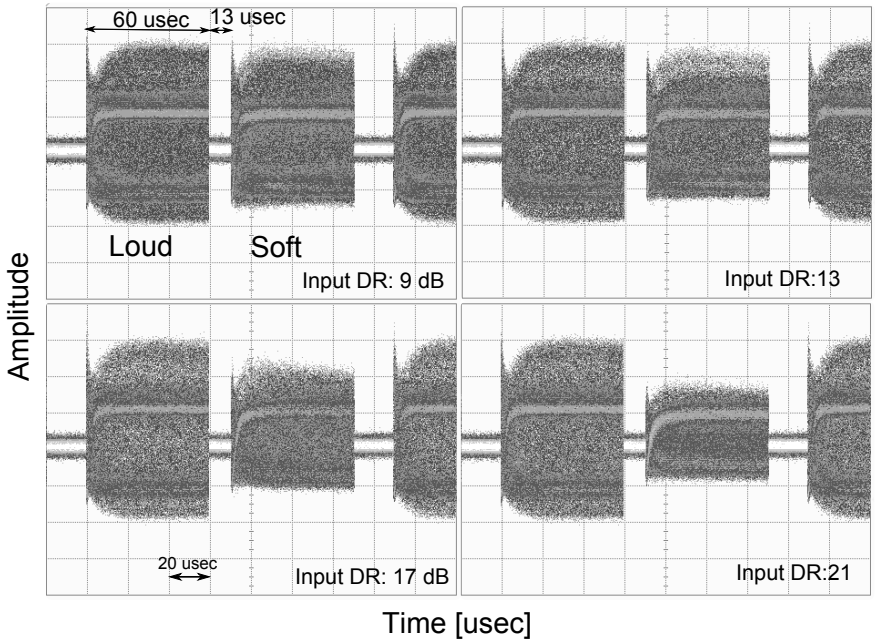

Figure 6.19: Equalized bursts at the input power of -8 dBm, DR: dynamic range.

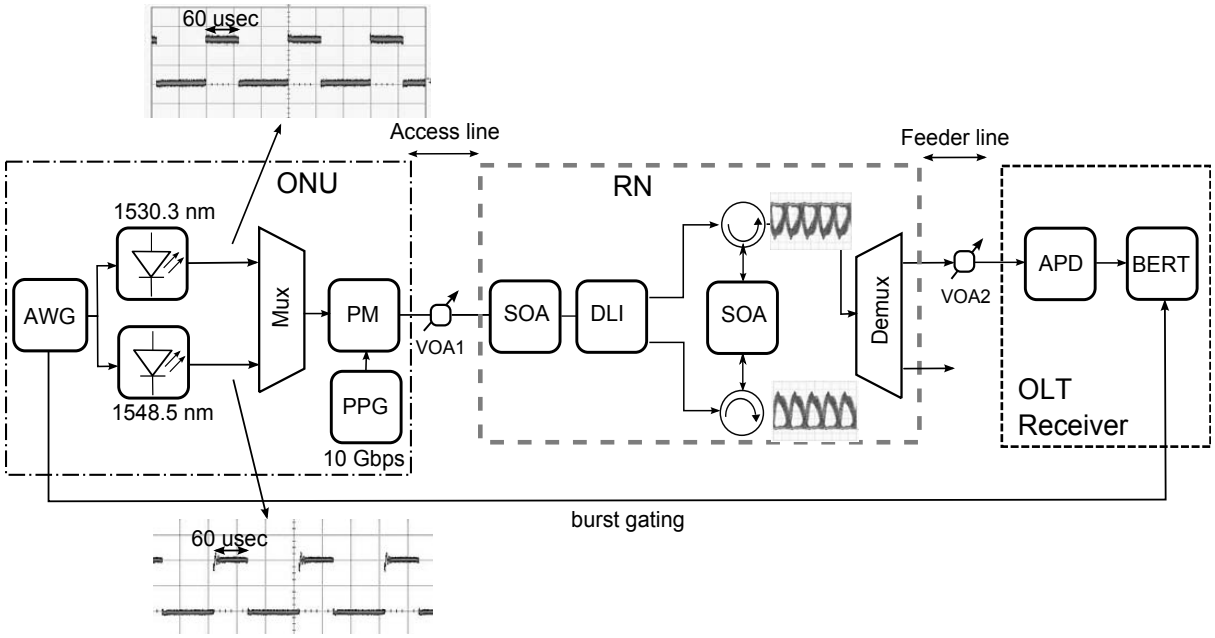

Figure 6.20: TDM uplink setup for two channels scenario.

modulated (one phase modulator was only available during the experiment).

Figure 6.21(a) shows the BER measurements of two channels in back-to-back scenario without any amplification. When two channels are emitting, the receiver sensitivity at the BER of 10^{-4} is -31.2 dBm, the average output of the ONU is 7 dBm, therefore the total optical power budget is calculated as $7 + 31.2 = 38.2$ dB. If only one channel emits, the difference in optical power budget is trivial as shown with the dashed line in Fig. 6.21(a). A small difference between single-channel and two-channel burst-mode transmission is observed. In Fig. 6.21(b) depicts the isoBER curve of both channels in back-to-back scenario. Channel at 1530.3 nm has total optical power budget of $32.7 + 28 = 60.7$ dB the access budget of 32.7 dB can compensate 5-dB mux loss, 10 km of fiber (3 dB), 1:64 splitting ratio (20 dB loss), two diplexers to separate up- and downlink signals (4 dB) and 0.7 dB margin, and channel at 1548.5 nm shows $34 + 27.4 = 61.4$ dB, similarly, 34 dB access budget can be used for 10 km of SMF (3 dB), $1 : 64$ splitting ratio (20 dB loss), two diplexers to separate up- and downlink signals (4 dB) and 2 dB margin.

Single and Multi-wavelength DWDM Performance of NG-PON Extender

Additionally, to single-channel operation, we also investigated the multi-channel (WDM) performance of the proposed PON extender in DS direction. Measurements are evaluated for 1, 2, 4, 8, and 12 channels, respectively. The Back-to-back BER measurement are the results of the measurements in Fig. 6.22. The number followed by λ denotes the number of wavelength channels and the corresponding isoBER curves belong to 1556.55 nm. In other words, we turn off all channels except 1556.55 nm for the 1λ curve, and then turn on the neighboring channels to measure the rest of the isoBERs for 1556.56 nm. Fig. 6.22 indicates that the access

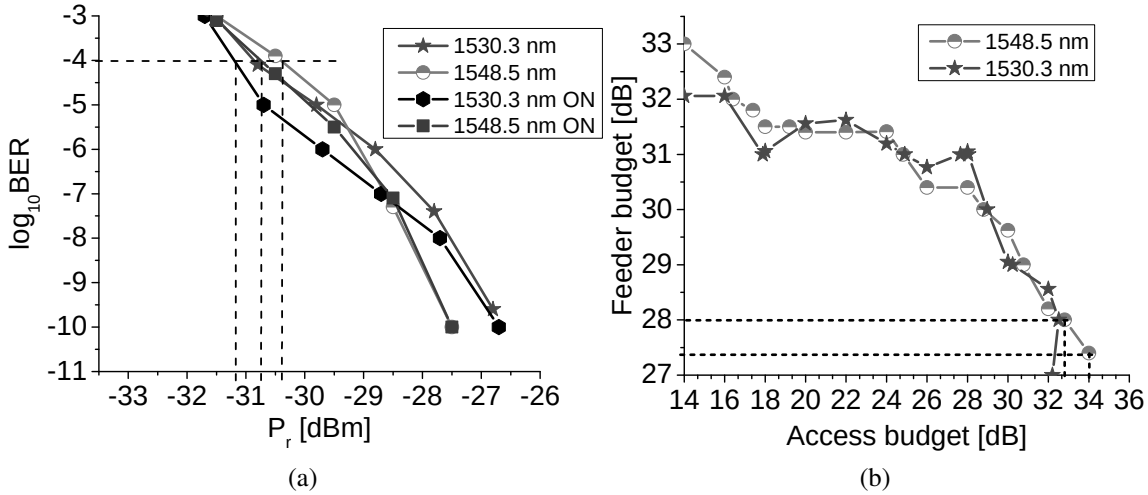

Figure 6.21: Experimental measurements of two-channel uplink transmission,a) BER curves without amplification back-to-back, b) Iso BER curves at BER of 10^{-4}.

budget reduces as we increase the number of channels from 1 to 12. The access budget varies at least 5.2 dB as we go from 1 λ to 12 λs. The wavelength gain competition and ASE noise contribution of the SOA is the main reason for this behavior as explained in the previous section. Accordingly, increasing the number of wavelengths does not necessarily increase the number of subscribers but the data rate can be increased by reducing the splitting ratio. However, the configuration gives the opportunity of converting DPSK to OOK with only one DLI for multiple channels, which is a cost-effective solution in terms of the operational cost at RNs.

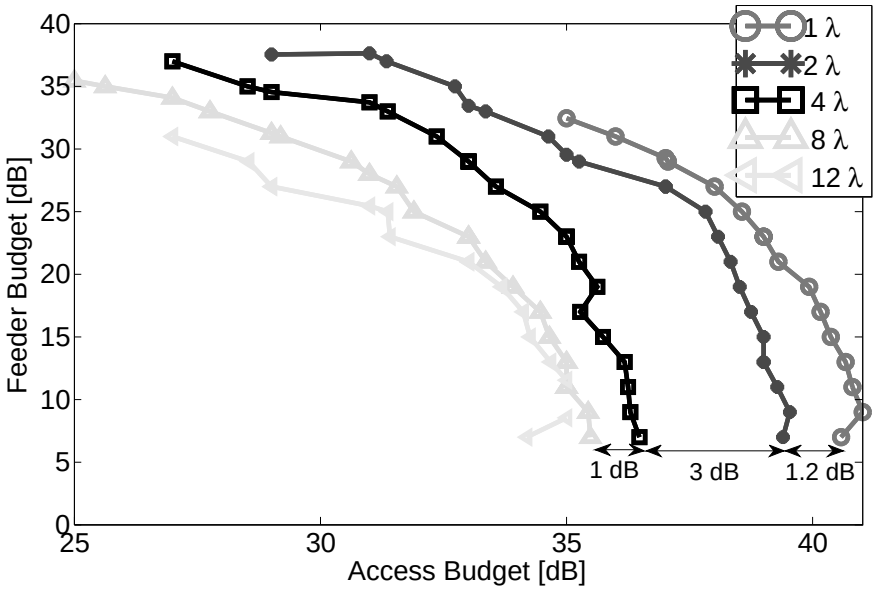

Figure 6.22: IsoBER curves SCA DPSK for different number of channels, all curves are measure at channel 1556.55 nm.

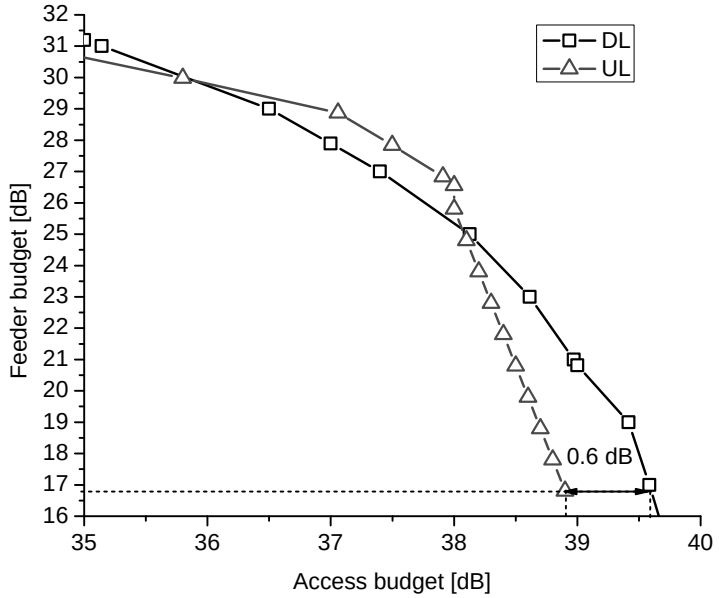

Figure 6.23: Bidirectional BER maps for 10 Gbps single channel transmission.

Bidirectional transmission and Discussions

The bidirectional transmission can be considered by combining DL and UL configurations in Fig. 6.9 and Fig. 6.14 For the DL, one channel is on and the rests are off to compare with the single channel UL (soft packets) transmission. The UL and DL BER maps at 10^{-3} are illustrated in Fig. 6.23. The amplifiers show a symmetry fashion in the opposite directions without any power budget penalty. The difference of less than 1 dB could be due to the measurement inaccuracy. In our experiment setups, the US and DS are transmitted through separate SMFs, in case of bidirectional transmission, back-reflection in components will not affect the performance as DL and UL use different wavelengths. The SCA configuration can extend the optical power bidirectionally to a significant extent. The number of subscribers served in the network reach up to $1,024$ for the single channel configuration. The deployment of the SCA configuration does not need any rigorous modification in optical distribution networks, as it is comprised of a DLI, two SOAs, and two circulators. The modulation format conversion is performed by a single DLI in a multi-wavelength transmission which reduces the cost of DPSK-based DWDM-PON deployments. Additionally, it enables using each output individually leading to a double number of subscribers. The proposed scheme is also suitable for NG-PON2 power budget recommendations [18]. In Ref. [15] it has been shown that the scheme can be expanded to QPSK signals to quadruple the number of subscribers.

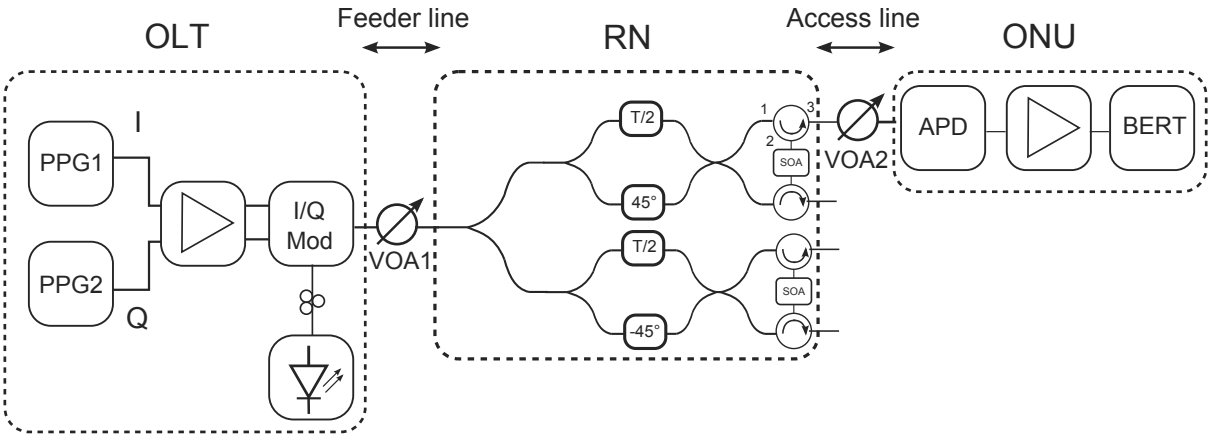

Figure 6.24: DQPSK measurement setup for one channel at 20 Gbps.

6.2.2 DQPSK

The DQPSK configuration can be also employed in both directions based on NG-PON technology requirements. In this section we demonstrate the DS direction. Fig. 6.24 shows the DQPSK measurement setup at 1550 nm. It consists of two PPGs ($2^7 - 1$) for inphase (I) and quadrature (Q), respectively, at 10 Gbps each. The differential encoded data are generate using MATLAB and then loaded on two separate PPGs. A single drive I/Q modulator generates DQPSK signal which is followed by a dual drive amplifier, this amplifier sets the amplitude of the driving voltage to a level appropriate for the quadrature modulation on MZM. The VOA1 emulates the losses of feeder line. The RN consists of a DQPSK optical demodulator and the SCA scheme remains the same, however, there is two separate SOAs for I/Q signals. The DQPSK demodulator has four outputs I_1, I_2, Q_1, and Q_2. Here, isoBER curve corresponds to I_1, no difference were observed among other three outputs. The back-to-back results are demonstrated first without the SCA setup. From Fig. 6.25, the total optical power budget at BER of 10^{-3} (assuming FEC) is 29.8 dB (dashed line in the Fig. 9) when the transmitted power is 3 dBm . 64 (20 dB loss) users can be served assuming 10 km access fiber (3 dB), 10 km feeder fiber (3 dB) and 4.8 dB reserved for mux/demux . In contrast to DPSK, the number of subscribers are doubled, $4 \times 64 = 256$. Higher bit rate, higher bandwidth efficiency (because of the narrower spectrum of DQPSK), and higher number of subscribers are advantages of this scheme over the DPSK configuration. Fig. 6.26 shows isoBER curves for two configurations considered here. Fig. 6.26(a) depicts the SOA configuration with 34 dB total optical power budget and part (b) is SCA isoBER curve with 4 dB more access budget. This allows to doubles the number of subscribers. As, we have been mentioning the maximum value of the access budget is always considered on the curve, the loss in feeder line is lowered.

Looking at the SCA isoBER curve, the total optical power budget is 40 dB (6 dB feeder budget and 34 dB access budget). 20 km feeder fiber, 256 subscribers (26 dB), 10 km access fiber (3 dB), and 5 dB extra losses for mux/demux in US/DS directions. When considering four outputs of the RN, we can serve $4 \times 256 = 1,024$ subscribers per channel. This is the largest number of subscribers reported to our best of knowledge with this unique amplification scheme.

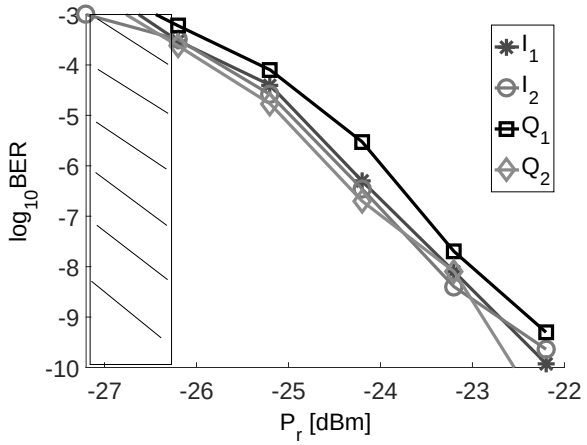

Figure 6.25: DQPSK back-to-back results with no SCA in the RN.

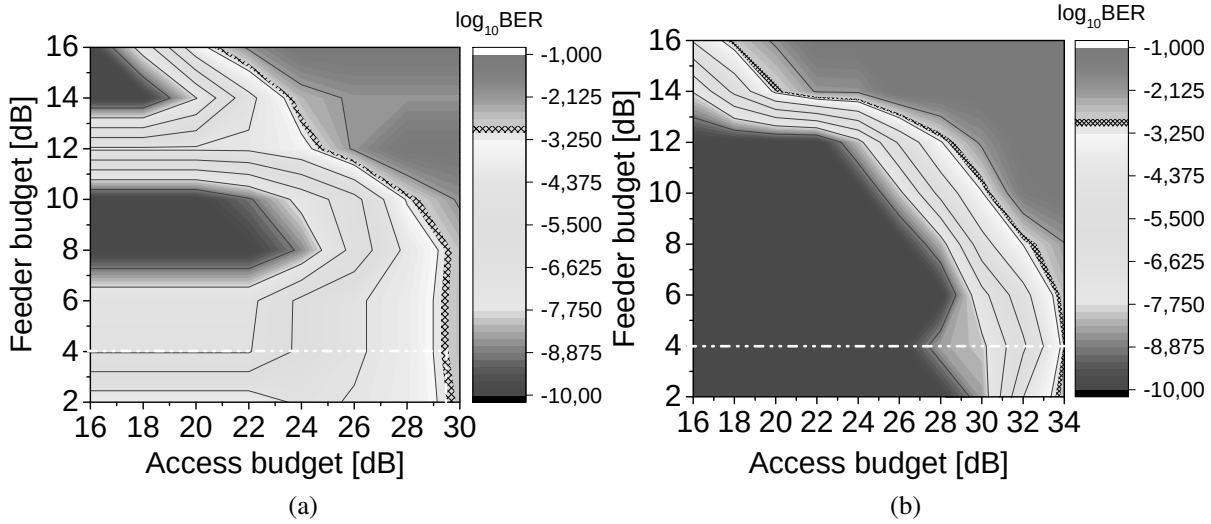

Figure 6.26: Back-to-back isoBER curves DQPSK, a) SOA, b) SCA.

6.3 Seeded TWDM-PON

Passive optical networks (PONs) are the inevitable solution of future access networks to primarily support bandwidth requirements and to accommodate the cost by sharing them among subscribers. Furthermore, it has become extremely important for network operators to utilize the existing fiber infrastructure as efficiently as possible. Two different standards Ethernet PON (EPON) and gigabit-capable PON (GPON) have been largely deployed in different parts of the world. These technologies are attractive due to their high bandwidth capability that meets the short-term subscribers requirements. As an example, the typical bandwidths of triple-play service (internet, TV, and telephone) are between 20 to 100 Mbps per subscriber [53]. In the long term, the existing technologies such as GPON and EPON must provide even higher bandwidth for services such as HDTV, video services, 3D-TV, cloud computing, and HD video

gaming. According to the Cisco visual networking index [15], from 2012 to 2017 the data usage of each subscriber is envisaged to increase by 66% annually. This challenges the network operators, so that they have already started the deployment of additional PON infrastructures in different parts of the world to develop technologies which enable these services [54, 55]. They also consider developing next generation passive optical networks (NG-PON) to allow even more new services with higher bandwidths and lower cost. These NG-PONs need to be developed on the same infrastructure as the existing PON technologies. One promising approach for NG-PON is to employ wavelength division multiplexed-PON (WDM-PON) as it provides large bandwidths, point-to-point connectivity, and higher security to mention only a few advantages [56]. There are some challenges to be solved first, in order to make this technology practical. For instance, optical network units (ONUs) need a wavelength-specific source that should comply with the multiplexer/demultiplexer (mux/demux) channel specifications located in the remote node (RN), now the problem is to identify a cost-efficient solution for such sources in order to enable commercialization and broad deployment of WDM-PON. One attractive approach is downstream (DS) wavelength remodulation for upstream (US) data transmission [28]. The wavelength remodulation enables utilizing cost-efficient colorless sources in ONUs which avoids installation of any wavelength dependent source. Several techniques have been reported, such as spectrum slicing of broad-band amplified spontaneous emission (ASE) sources [57], spectrally sliced Fabry-Pérot laser diodes (FP-LD) [58], ASE injected FP-LD [59], and light-emitting diodes (LED) [39]. The spectral slicing using LEDs suffers from low output power. As reported in [39], the proposed configuration has low power margin so that different techniques must be used to overcome this problem, the distance is limited to 20 km, and the data rate is limited to 622 Mbps per channel. In spectrally sliced FP-LD [60], the mode fluctuations of the laser are converted to intensity noise in the router which limits the performance of the system. Additionally, relative intensity noise (RIN) deteriorates the neighboring ONU channel which is transmitting US data. This requires a power equalization of the DS data at the optical line terminal (OLT) which increases cost significantly. ASE injected FP-LD has been also demonstrated in [61], however, serious limitations are chromatic dispersion (CD) with increasing feeder fiber length (reach beyond 20 km), adjacent channel crosstalk penalty, Rayleigh backscattering of the broadband seed signal, and seed power degradation with increasing feeder fiber length.

In this section we experimentally demonstrate 1.25 Gbps US data remodulation by over-modulating 10 Gbps DS data based on injection locked FP-LD. In this scheme, non-return to zero (NRZ) or differential phase shift keying (DPSK) are used for DS data transmission to compare the introduced cross-talk between DS and US data signals. The transmission through 100 km of single mode fiber (SMF) is successfully demonstrated without any error floor. The experimental results represent total optical power budget of about 30.7 dB for NRZ and 29.2 dB for DPSK after 100 km SMF transmission which enables 128 subscribers per λ-channel to connect to the network. The proposed configuration is also compared with ASE-seeded FP-LD and shows a better performance in terms of transmission distance, signal quality, and setup simplicity. The presented configuration can be counted as a cost-efficient solution for WDM-PONs since it eliminates the wavelength specific light source at the ONU [62].

6.4 Proposed Injection Locked FP configuration

The proposed injected FD-LD WDM PON architecture is illustrated in Fig. 6.27. The OLT consists of transmitters/receivers (Tx/Rx) at specific wavelengths which are connected to an arrayed waveguide grating (AWG) denoted as mux in Fig. 6.27. The DS is generated in OLT and transmitted over a SMF to the demux located in the remote node (RN) where the data are distributed to corresponding ONUs. At the ONU side, the data are split into two paths, one output is directed to ONU's receiver (Rx) and the other output is directed to the colorless FP-LD (Tx). The free-running FP-LD is injected by the DS wavelength and locked, then the data is modulated on the selected wavelength and transmitted in US direction. This configuration allows point-to-point connectivity of the subscriber and the OLT that results in higher quality of service, transparency, and higher bandwidth. Additionally each channel at the RN can be split by passive splitters to serve more subscribers in the network so the time division multiplexing (TDM) technology can also be merged with this architecture. Another advantage is the colorless feature of the ONUs that makes the structure cost-efficient for subscribers since there is no need for a wavelength specific source to be installed at the ONU's site.

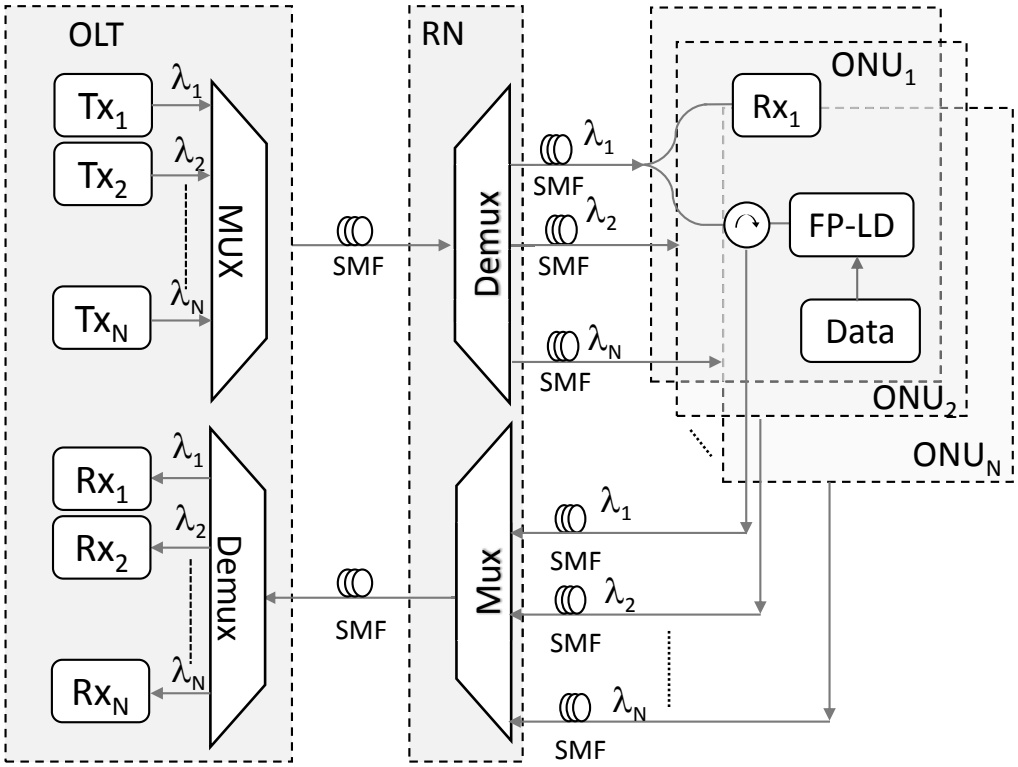

Figure 6.27: The proposed WDM-PON network configuration using FP-LD injection locked as a colorless source in ONUs.

6.5 Experimental Data Remodulation Scheme

6.5.1 NRZ

In OLT, the transmitter generates NRZ signals for DS transmission, as depicted in Fig. 6.28, a distributed feedback (DFB) laser is used as a light source at 1538.33 nm, the output power is 10 dBm. The data stream is generated using a pulse pattern generator (PPG) with pseudo random binary sequence (PRBS) $2^{23}-1$, the bit rate is 10 Gbps. The DS transmitted output power denoted as $P_{Tx\text{-}DS}$ is -0.2 dBm. At ONU side, the DS data is split into two paths by a 50:50 splitter, one is directed to the ONU's receiver, and the other output enters the circulator for the injection of the FP-LD. The transceiver is a 1.25 Gbps based small form-factor pluggable (SFP) module with a free-running FP-LD as a transmitter and an avalanche photodiode (APD) as the receiver. A second variable optical attenuator (VOA2) and polarization controller (PC) before the circulator control the injection power and the polarization of the light to the FP-LD, the PC can be neglected in real transmission scenario as it was used only to investigate how the polarization of the injection light changes the result, only negligible change was observed. The injected FP-LD is then directly modulated with PRBS $2^{23}-1$ using PPG at 1.25 Gbps for US transmission. The US transmitted output power denoted as $P_{Tx\text{-}US}$ is 1 dBm.

Figure 6.29 illustrates the spectrum of FP-LD before and after the injection. In Fig. 6.29(a), the free-running spectrum of FP-LD with no modulation can be observed. The FP-LD is designed for optical C-band, the resolution bandwidth (RBW) of the OSA was set to 0.01 nm. The enlarged spectrum is shown in Fig. 6.29(b) in order to see the modes of the laser and the free spectral range (FSR) which is about 45 GHz. The power spectral density at the injection power of -6 dBm is depicted in Fig. 6.29(c) which has 40 dB side mode suppression ratio (SMSR). At this power the spectrum has the highest SMSR, -5 dBm is the maximum allowed injection power into the SFP modules, here -6 dBm is the highest power that can be injected

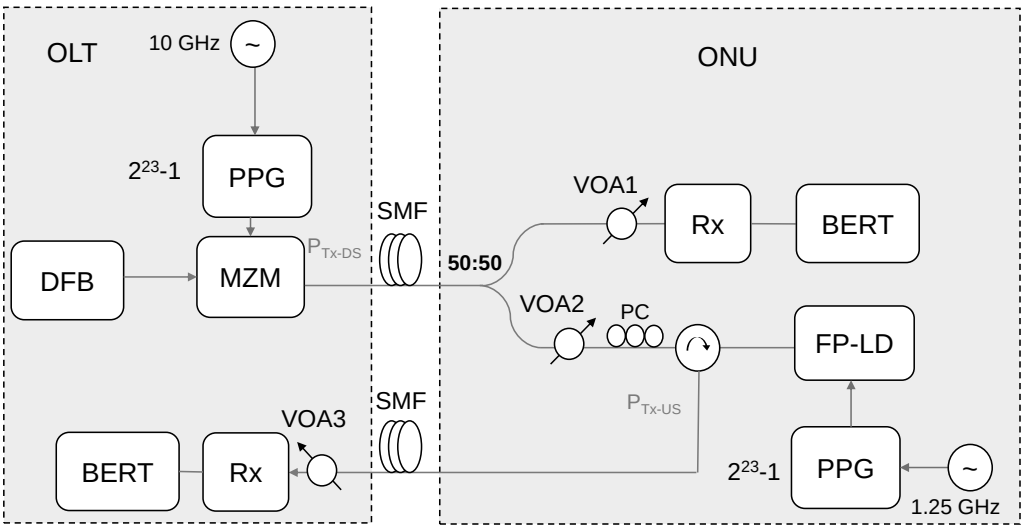

Figure 6.28: The NRZ DS data remodulated for US direction using injection-locked FP-LD.

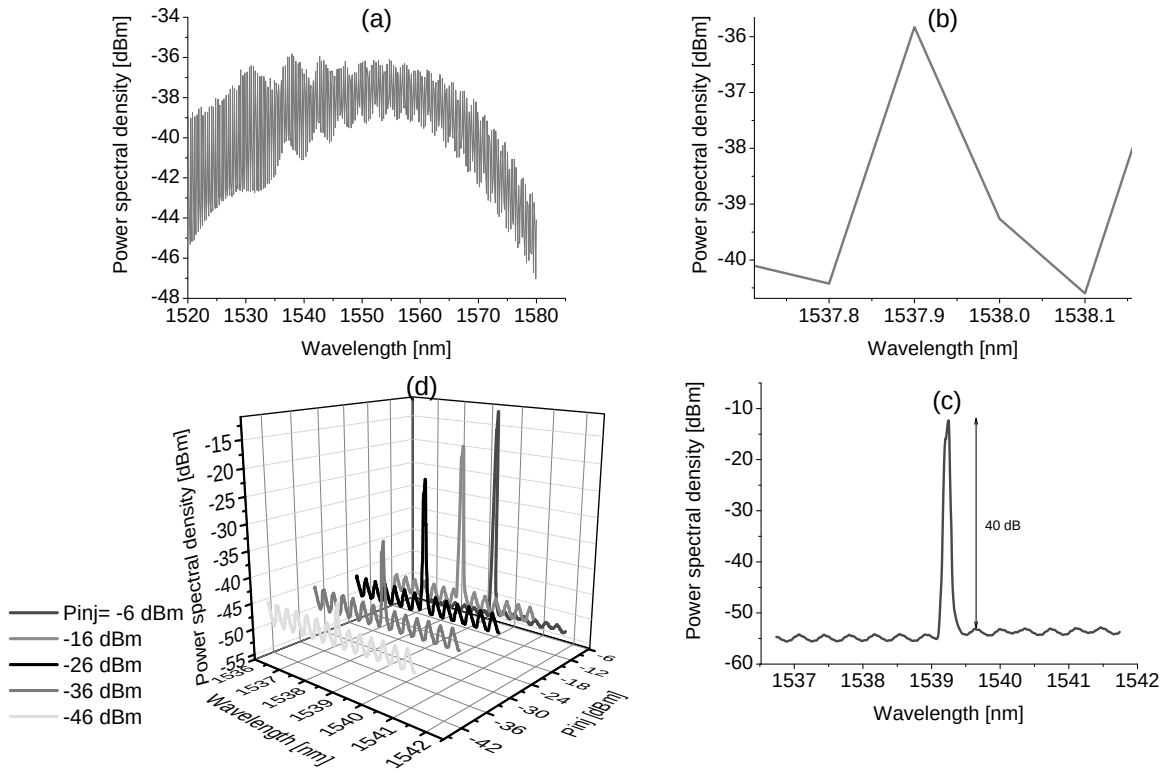

Figure 6.29: Optical spectra of the FP-LD with RBW of 0.01 nm, a) the spectrum of free running FP-LD, 60 nm spanning (multi-longitudinal modes are obvious), b) free running FP-LD spectrum 0.45 nm span (zoomed snapshot of one longitudinal mode), c) injection-locked FP-LD with injection power of -6 dBm, SMSR 40 dB, and d) different injected power to the FP-LD to determine the highest SMSR.

into the FP-LD after passing through the circulator. To clearly see the successful injection locking, Fig. 6.29(d) outlines the power spectral density with respect to wavelengths in terms of different injection powers. The injection power is changed from -6 dBm to -46 dBm using VOA2 in the setup. These values are selected to investigate how the mode locking works, the values lower than -14 dBm did not show good SMSRs, but included to better visualize the mode locking of the FP-LD. As the power increases, the side modes are more suppressed and SMSR increases. The average output power of the injected FP-LD is about -2 dBm. The mode which is locked depends highly on DS laser source wavelength which needs to be centered at one of the FP-LD modes. Frequency detuning of the DS laser results in locking instability and poor bit error ratio (BER).

To visualize the stability of the locked and directly modulated FP-LD, Fig. 6.30 shows 1.25 Gbps eye diagrams. As the master laser frequency located in the OLT is detuned away from the targeted FP-LD mode, the locking is lost and the intensity noise appears as depicted in Fig. 6.30(a). On the contrary, when the frequency of the DFB laser matches exactly the

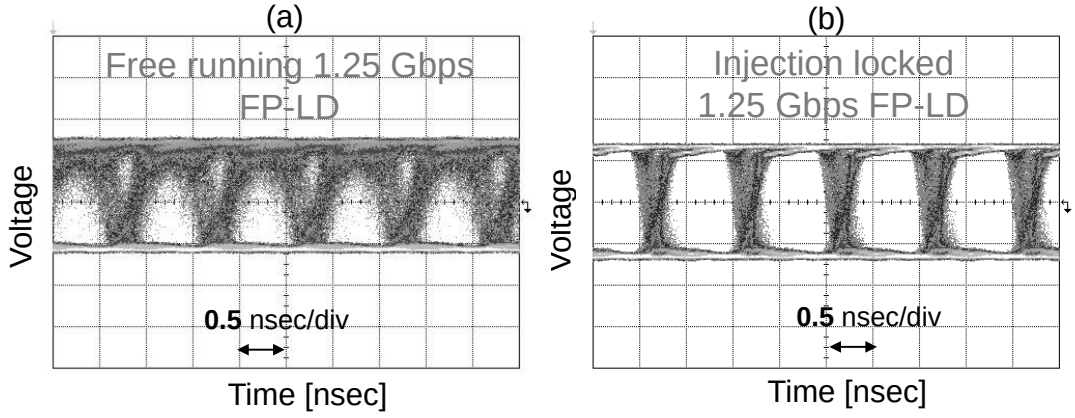

Figure 6.30: Eye diagrams of 1.25 Gbps directly modulated FP-LD, a) free-running, b) injection locked.

targeted FP-LD mode, the locking process is successfully achieved and the side modes are suppressed. When the light is injected into the cavity of FP-LD, the electric field travels in a round-trip manner so that it is amplified. Now if the injected light and the cavity longitudinal mode are coherent, the side modes are suppressed in the cavity and one longitudinal mode is emitted form the FD-LD. The BER curves in Fig. 6.31 illustrate the injection power dynamic range (DR) of the FP-LD in a back-to-back scenario. Figure 6.31(a) shows BER curves versus received power for various injection powers, the injection power can be varied between -6 dBm to -14 dBm. The curves show a DR of 8 dB and the injected power can be kept as low as -14 dBm. The curves have similar performances with respect to receiver sensitivity with less than 0.3 dB difference, as seen in Fig. 6.31(b). As the injection power increases the receiver sensitivity also increases. This is due to the fact that at higher injection power the interference between the back reflected light from the laser and the injected light is also higher. The received power is considered to be at BER of 10^{-4} as it is the forward error correction standard (FEC) for US transmission [51].

The injected FP-LD is directly modulated with 1.25 Gbps NRZ data and transmitted over SMFs having different lengths for US direction and received at the OLT. The experimental BER measurements are depicted in Fig. 6.32. It illustrates the back-to-back transmission as well as different fiber lengths scenarios when the DS data is transmitted over 25 km. An error free transmission is achieved up to 100 km of SMFs (the distance at the time of measurement only limited by the amount of fiber available in the laboratory). In the inset the eye diagram for back-to-back case is shown, the intensity noise is not seen on the mark levels and the eye is completely open. Figure 6.33 illustrates eye diagrams of different transmission distances over SMF. Obviously, the eye diagrams become narrower for longer distances (chromatic dispersion) but remain open and error free, and there is no cross talk from DS data and US, the cross talk should be controlled by keeping the extinction ratio of the DS signals small enough at the input of the FP-LD, in this way, the mark levels are small so that the DS traffic does not interfere the US signals. For further explanation, Fig. 6.34 shows the logBER curves for two cases. First, the US is remodulated when DS wavelength is modulated and the second is the CW light without any modulation. Both BER curves CW and US show negligible difference (0.5 dB), so

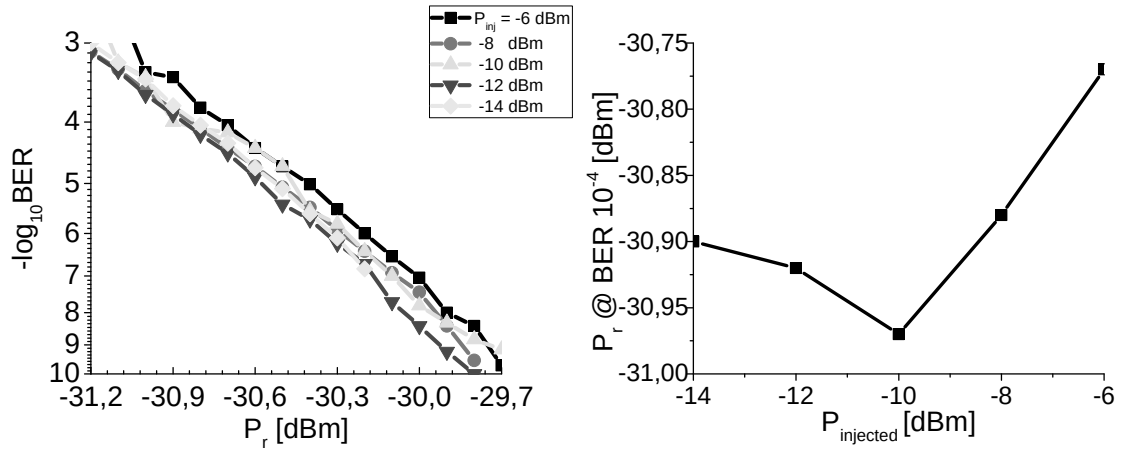

(a) (b)

Figure 6.31: The US back-to-back BER versus receiver sensitivity, a) logBER for different injected powers, b) received power at logBER of -4 in terms of injection power.

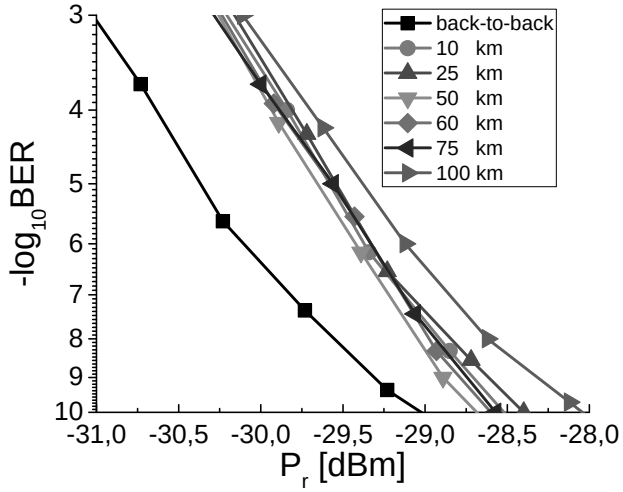

Figure 6.32: Upstream BER curves versus receiver sensitivity.

the cross talk is precisely suppressed by adjusting the DS signals extinction ratio.

It is noteworthy to mention the optical power budget in each direction. By looking at Fig. 6.32, the total optical power budget is 30.7 dB at BER 10^{-4} when US transmitter output power is 1 dBm. The optical power budget allows a $1:128$ splitters (21 dB) at the RN, and 8 dB reserved for mux/demux in WDM scenario (see Fig.6.27).

To see the BER performance of DS data, Fig. 6.35 illustrates 20 km and 50 km transmission with their corresponding eye diagrams in the inset. The unfinished curves are due to the limited received power, nevertheless the error free transmission is possible if higher power is available after 25 km or 50 km of transmission. The DS optical power budgets are 26.6 dB and 26.2

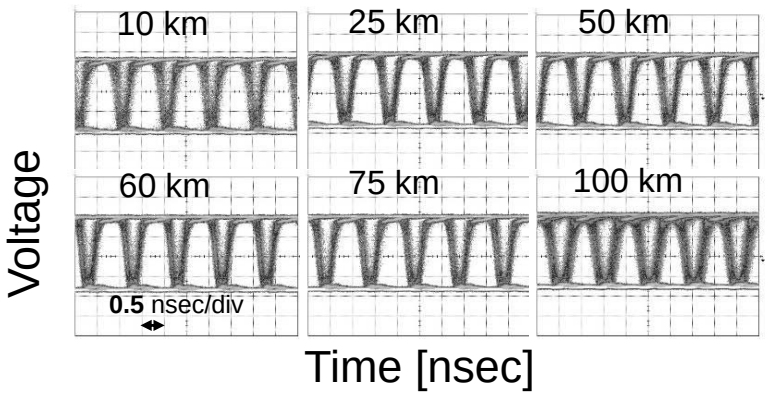

Figure 6.33: Eye diagrams in case of different transmission distances for US scenario, bit rate 1.25 Gbps, received at BER 10^{-9}

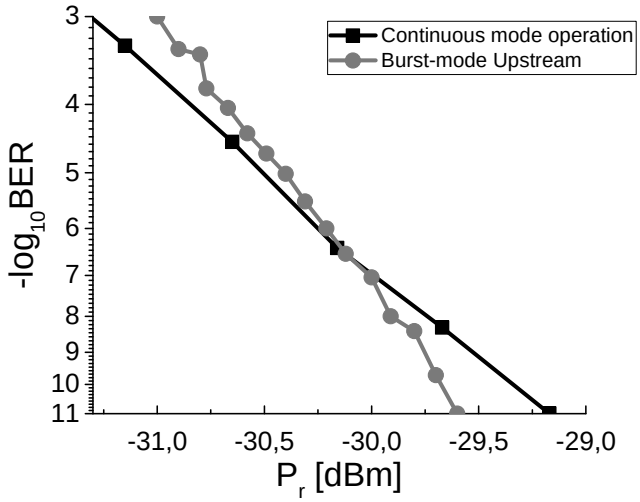

Figure 6.34: Cross talk consideration, BER curves of two different cases. CW: injection of continuous wave light source with no modulation (the downstream light is not modulated), US: the upstream (the downstream light is DPSK modulated) light source is modulated with 1.25 Gbps NRZ.

dB for 25 km (5 dB loss) and 50 km (10 dB loss), respectively, at BER 10^{-3} as shown in Fig. 6.35 (the vertical dashed lines). In DS direction, a 1:64 splitter can be used while 8 dB are still reserved for mux/demux at the RN. The DS optical power budget is less than that of US because of larger chromatic dispersion which is introduced at higher bit rates. To provide longer transmission distances, a dispersion compensation module (DCM) and an optical amplifier are required in DS direction.

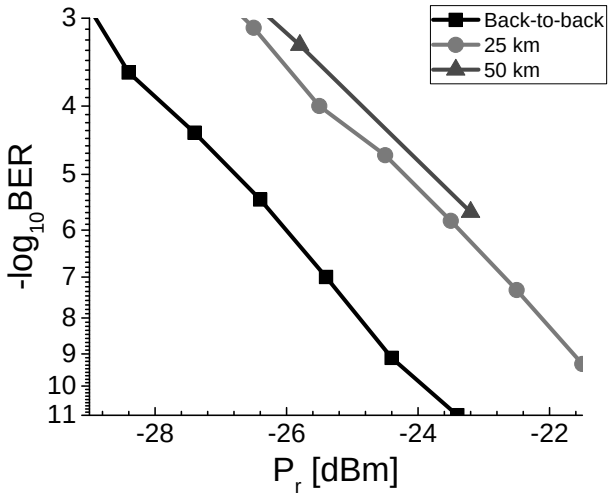

Figure 6.35: BER measurements of DS transmission of 25 km and 50 km.

6.5.2 DPSK

In this section, the FP-LD is locked by using the injection of DS DPSK signals. The ONU transmitter is implemented by modulating the FP-LD with 10 Gbps DS DPSK signals. The US data rate is 1.25 Gbps OOK (on-off keying) signals as before. The proposed scheme in the previous section needs the extinction ratio adjustment and reduction to avoid the cross talk between the DS and the US signals, however, the DPSK signal has constant optical output power which may alleviate this problem and increase the DR of the injection power to the FP-LD.

Figure 6.36 depicts the experimental setup of the proposed scheme. The OLT consists of a clock generator which runs at 10 GHz, a PPG with $2^{23}-1$ PRBS, an NRZ to inverse return-to-zero (IRZ) encoder, an amplifier, a DFB laser at 1534 nm, and an optical reshaping filter. The principle of generating a DPSK signal is as follows: by directly modulating the DFB laser, the frequency shift occurs due to the adiabatic chirp of the laser. The phase of the optical signal is the integral of the instantaneous frequency, $\Delta\varphi = 2\pi \int_0^T \Delta f dt$, where Δf is the optical frequency deviation and T is the pulse duration. The pulse shape must be chosen appropriately to create a DPSK signal. Here, to obtain a phase shift of π between each data symbol, a maximum of 10 GHz is required provided that the IRZ duty cycle is 50%. The optical reshaping filter at the laser output adjusts the optical signal spectrum in order to achieve a constant output intensity, and even more detailed description of the DPSK generation using frequency chirp of the DFB laser is given in [63]. The injection locking is performed in the similar way as in the previous section. The DS transmitted output power denoted as $P_{Tx\text{-}DS}$=1.46 dBm, at ONU side, the DS data is split into two paths by 1×2 50:50 splitter, one is directed to the ONU's receiver, and the other output enters the circulator for the injection of the FP-LD. The transceiver is a 1.25G based small form-factor pluggable (SFP) module with a free-running FP-LD as the transmitter and an avalanche photodiode (APD) as the receiver. The variable optical attenuator

2 (VOA2) and polarization controller (PC) before the circulator control the injection power and the polarization of the light to the FP-LD. The injected FP-LD is then directly modulated with PRBS $2^{23}-1$ using PPG at 1.25 Gbps for US transmission. The US transmitted output power denoted as $P_{Tx\text{-}US}$=1.2 dBm.

The injected power to the FP-LD is varied using VOA2 and the spectra are captured with 0.01 nm optical resolution bandwidth (RBW) for each injected power at the output of FP-LD. Results are illustrated in Fig. 6.37(a). As can be seen, for larger injection powers the SMSR increases, the maximum SMSR is 41.67 dB which is the case at the injection power of -6 dBm, see Fig. 6.37(b). The input power DR is 12 dB in this case which is 4 dB higher than for NRZ remodulation. The injection locking can be performed as low as -18 dBm. This enables longer transmission distances in DS direction without using an optical amplifier. The higher DR results from the optical constant power feature of the DPSK signals. The BER curves are measured and illustrated in Fig. 6.38(a). As the injection power increases, the receiver sensitivity reduces, this is due to the higher SMSR. The receiver sensitivities at BER 10^{-4} versus injection powers is shown in Fig. 6.38(b). There is a maximum of 0.2 dB difference between highest -6 dBm and lowest -18 dBm injection powers which is a negligible penalty. To emulate real transmission scenarios, the data is transmitted through 50 km of SMF in DS direction, and SMFs with different lengths are used for the US direction. The results are shown in Fig. 6.39. In Fig. 6.39(a) depicts the feasibility of the transmission in US up to 100 km, there is a 1.25 dB difference between 10 km and 100 km due to the chromatic dispersion in the SMF. Fig. 6.39(b) shows the receiver sensitivity in terms of transmission distance, obviously, the receiver sensitivity reduces as the data propagate through longer distances.

Figure 6.40 shows the eye diagrams of the DPSK measurements for different fiber lengths, the eye is open and error free for all cases with low intensity noise on 1's levels. The jitter arises from the electronics embedded in the optical receiver. The optical power budget at 100 km (20 dB loss) is 29.2 dB, the number of supported subscribers estimated to be 128 ($3log_2(128) \approx 21$ dB loss) and 8 dB reserved for demux/mux losses in WDM-TDM transmission scenario. The optical power budget at 100 km (20 dB loss) is 29.2 dB, the number

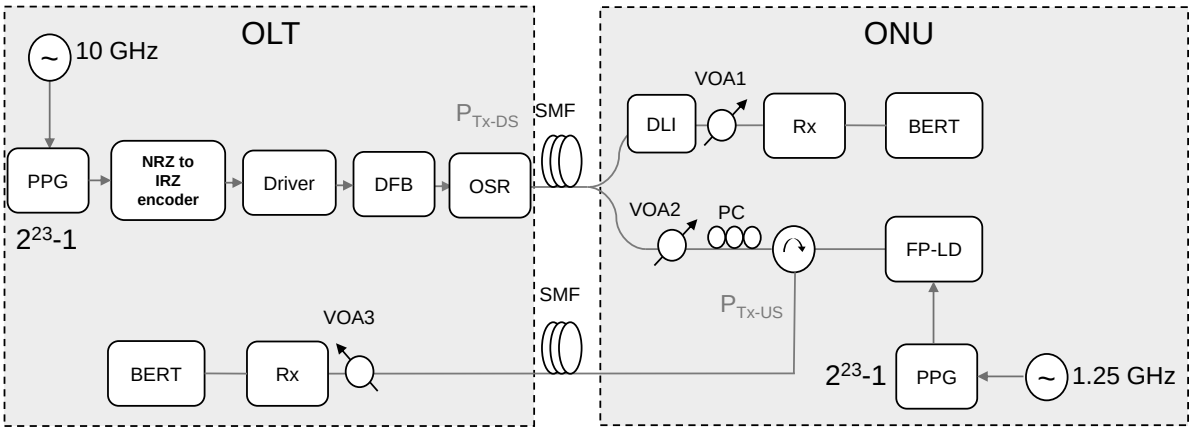

Figure 6.36: Experimental setup of the upstream remodulation with injection locking of FP-LD using downstream DPSK signals.

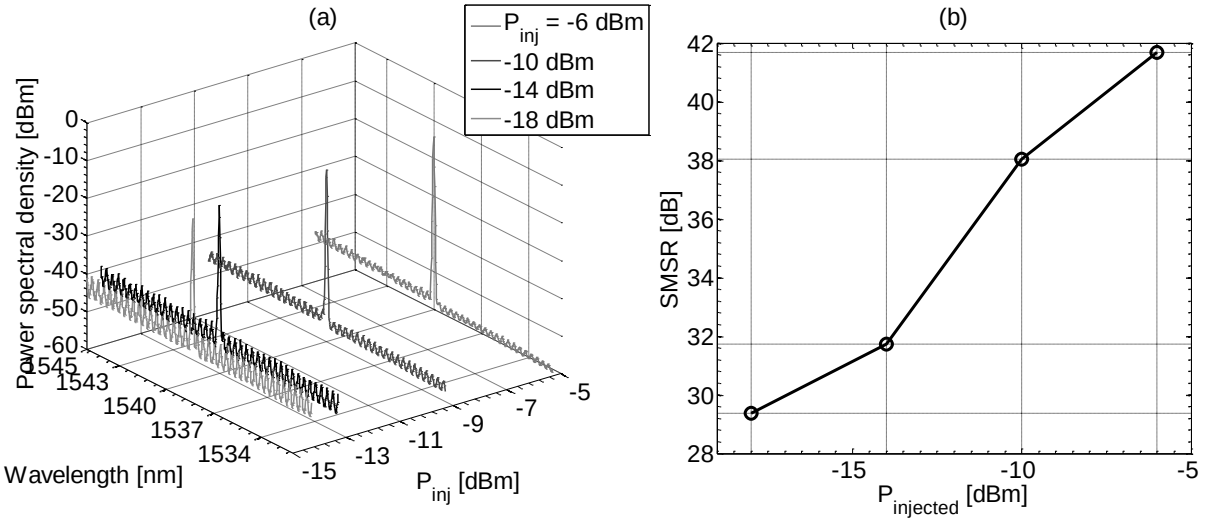

Figure 6.37: BER curves of 1.25 Gbps OOK in US direction with respect to different injection powers to FP-LD.

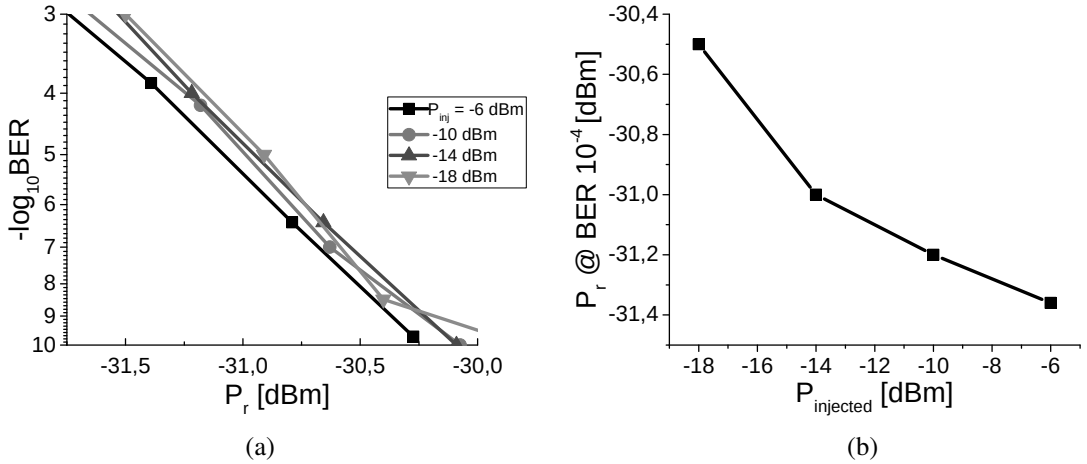

(a) (b)

Figure 6.38: The DSPK remodulation US b-to-b measurements versus receiver sensitivity for different injection powers, a) BER curves, b) Receiver sensitivity @ BER 10^{-4} versus injection power.

of supported subscribers estimated to be 128 ($3log_2(128) \approx 21$ dB loss) and 8 dB reserved for demux/mux losses in WDM-TDM transmission scenario. Table 6.3 summarizes the results of two different transmitter configurations. The needed receive power for two different BER values is given, namely for 10^{-4} FEC limit and for 10^{-9} 100 km US transmission. The 1.5 dB power budget difference arises from the residual intensity variations of the DPSK signals. While generating DPSK, the amplitude of the optical carrier is also modulated. This intensity modulation introduces distortion when the DPSK signals are converted to intensity modulated signals in the DLI. However, in contrast to NRZ configuration, the DPSK configuration results

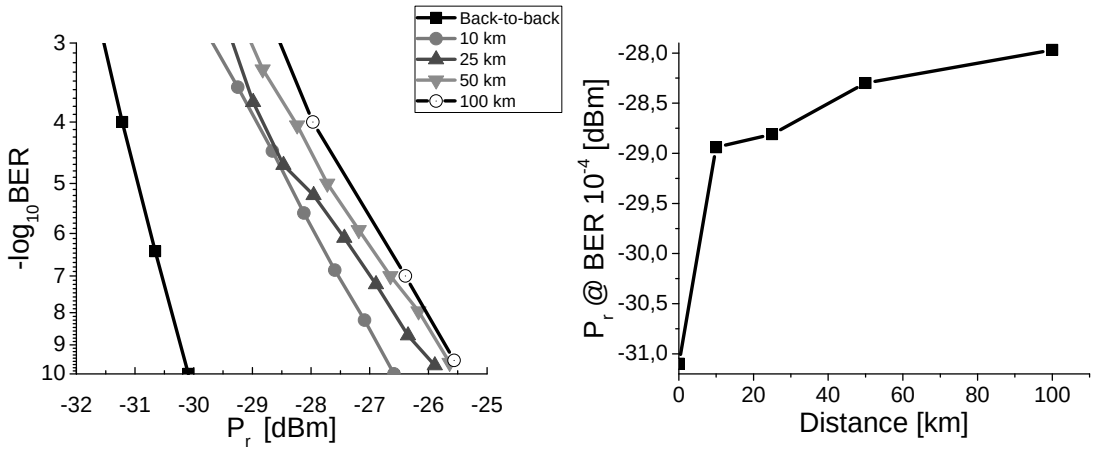

(a) (b)

Figure 6.39: The BER curves of US for different fibers lengths versus sensitivity, a) logBER versus receiver sensitivity, b) Receiver sensitivity in terms of traveled distance in km.

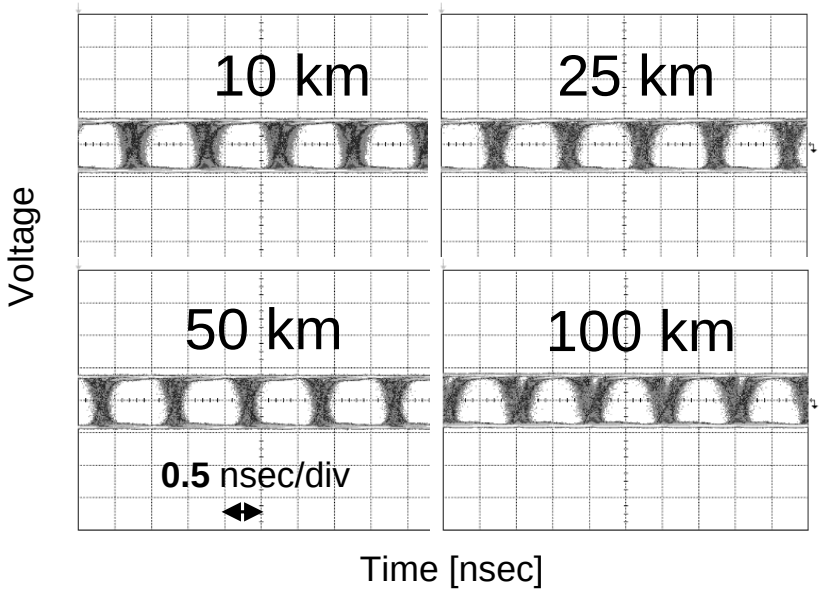

Figure 6.40: The upstream eye diagrams of DPSK remodulation for different SMF lengths.

in more power DR, and it enables the previously designed PON extender box [64] to be utilized in the proposed architecture which increases the optical power budget of WDM-PONs, the extender configuration is compatible with existing PON standards such as, EPON, GPON, and XG-PON1.

Modulation format	Sens. @ BER 10^{-4}	Sens. @ BER 10^{-9}	PB [dB]	DR [dB]
NRZ	-29.6	-28.3	30.7	8
DPSK	-28	-25.7	29.2	12

Table 6.3: Comparison of NRZ and DPSK transmitter configurations for US transmission scenario at 1.25 Gbps, PB: power budget, DR: dynamic range.

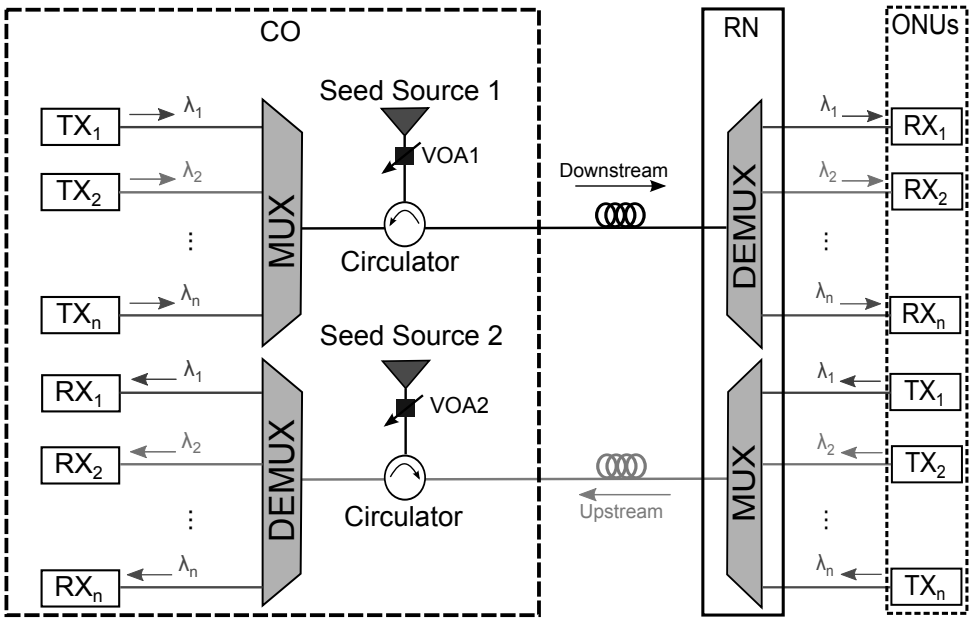

Figure 6.41: The ASE seeded architecture based on FP-LD injection locking.

6.6 Comparison of ASE injected FP-LD and downstream remodulation technique

The ASE seeded system has been reported in [61], we present its basic configuration in Fig. 6.41 in order to show how it differs from the architecture proposed here. The system consists of separate US and DS fibers (SMF), two broadband seed light sources (EDFA) which are connected to two circulators (for US and DS, resp.). The seed light sources are located inside central office (CO) in order to reduce the cost of the local exchanges where the signals are distributed among subscribers. VOAs are used to control the output power of the broadband sources. The spectral slicing of the seed sources are achieved through mux/demux located in CO and ONUs. The spectra are sliced and sent to transceivers (Tx) to lock the free-running FD-LDs. Two separate fiber channels are used for US and DS transmission. After successful injection, a single-longitudinal FP-LD is achieved. Each injected FP-LD is modulated at 1.25 Gbps, and is multiplexed together with neighboring channels through an AWG. The SFP modules in Tx are the same used in the previous configuration, but they are plugged into the Transmode TM-301 module [61]. The modulation format used in this setup is 1.25 Gbps NRZ

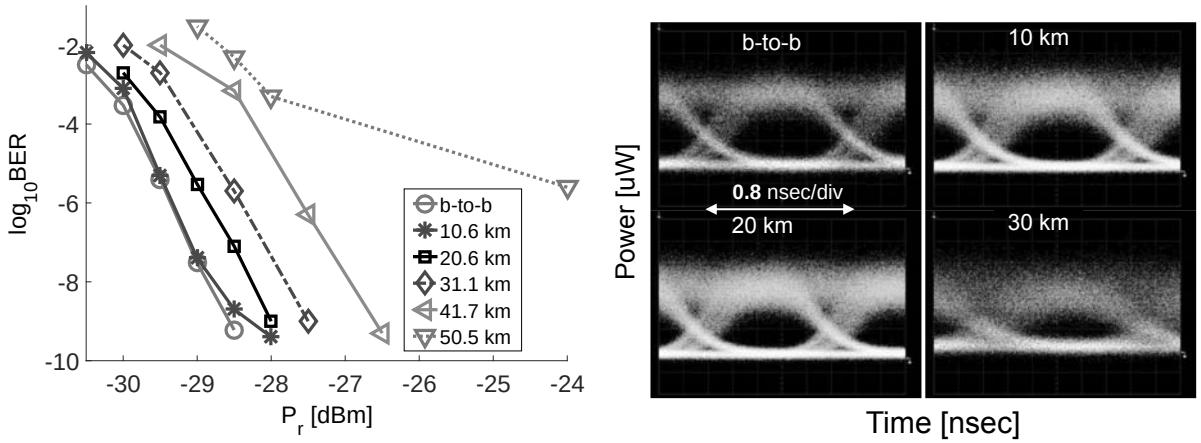

(a) (b)

Figure 6.42: a) BER curves of upstream ASE seeded FP-LD, b) The eye diagrams of upstream ASE seeded FP-LD.

with PRBS $2^{23} - 1$. To compare the proposed and the ASE seeded FP-LD configurations, Fig. 6.42(a) shows the BER curves with respect to different fiber lengths in US direction for ASE seeded FP-LD when only one channel is used. Obviously, the error free transmission is not possible, the maximum achieved distance is 50.5 km in case of ASE seeded FP-LD. In the proposed scheme as mentioned in the earlier parts of this section, the transmission is possible for at least 100 km having error free performance. The major impairments in ASE seeded FP-LD injection locking are seed power, and Rayleigh backscattering. This technique introduces a significant intensity noise on the data stream as demonstrated in Fig. 6.42(b). After 30 km the eye is almost closed and error free transmission is not possible. Furthermore, in terms of cost, the proposed architecture provides inexpensive configuration in operational and management point of view.

Chapter 7

Conclusions and Outlook

This dissertation has investigated state-of-art accomplishments with focus on optical power budget extension techniques for next-generation passive optical networks. As stated in this study, fast increase in broadband services such as video on demand, internet TV, voice over IP , HDTV, IPTV, and so forth require higher data rates delivery to subscribers. NG-PONs aims at responding to these emerging bandwidth-hungry services. The dissertation has illuminated a new amplification concept using higher modulation formats DQPSK for the future optical access networks. It has described a new amplification scheme based on semiconductor optical amplifier for NG-PONs. The SOA-based amplifier has outperformed other techniques presented in the literature to the author's best of knowledge. The scheme compatibility with PON standards such XG-PON, and E-PON have been demonstrated. It has been shown by employing WDM technology in NG-PONs, the guaranteed bit rate can be increased for each user at the cost of higher optical losses introduced by additional optical mux/demux. Additionally, it has been explained WDM can be merged with TDMA technology to significantly enlarge the capacity of PONs, and the number of subscribers. Furthermore, long-reach PON and large splitting ratio have shown a great interest and importance since larger areas can be covered and more subscribers can be served. The proposed concept has shown a promising results to meet these requirements.

The thesis have been organized in seven chapters. The first chapter has outlined the goal of this study and the structure of the thesis. The second chapter has provided an overview of optical fiber communication, electromagnetic fields in a fiber, impairments in a single-mode fiber , and introduction to optical components. It has been explained thoroughly how the light can be generated and propagated through a fiber. The third chapter has completed the second chapter by elaborating the electrical to optical signal generation. The direct and external modulation have been discussed and corresponding advantages and disadvantages have explained. The generation and detection of optical DPSK, DQPSK, and OFDM modulation formats have been explained.

Chapter four has highlighted various broadband access technologies. First, the DSL have been discussed as a widely developed copper-based technology worldwide. Additionally the wireless access network and its corresponding standard have been discussed. This chapter has clarified that the passive optical networks are attracting choice among broadband access technologies.

Chapter five has demonstrated the simulation results of optical power budget extension techniques. The SOA-based has been first presented and provided services for 32 and 128 subscribers in case of DPSK and DQPSK, respectively, for each wavelength. The simulation results has proved that the saturated-collision configuration is a promising option for phase-shift keying signals in long-reach PON scenario. It could provide higher reach, and at the same time higher number of passive splitters. Using SCA, 64 and 256 subscribers could be served in case of DPSK and DQPSK, respectively, for each wavelength. In addition to this, 1 Tbps optical WDM/TDM-OFDM has been discussed using SOA-based and EDFA-based amplifiers. The EDFA amplification configuration has shown remarkably better results compared to SOA, since the EDFA can track the OFDM symbols in time, however, SOA has smaller time constant which cannot be following one OFDM symbol. The EDFA configuration has enabled 64 splitters on each channel with 40 Gbps, but, SOA could only provide 8 splitters on each channel. The distance of 50 km of SMF has been considered for all cases in this chapter.

Chapter six has discussed the experimental 12×10 Gbps DWDM/TDM PONs DL and single wavelength US transmission here with significant power budget enhancements. The total optical power budget of 44 dB can support a very high split ratio of 12×128 subscribers for DS transmission. It has been shown that in bidirectional 10 Gbps single channel transmission, the total optical power budget is measured to be 57 dB that can supports the total of $1,024$ subscribers on a single channel. The SCA configuration has equalized the soft and loud packet in US direction that eases the BMRx employed in OLTs. The 10 Gbps upstream packet equalization based on SOAs has been experimentally shown yielding up to 16 dB dynamic range compression without using a burst mode receiver. It has been proved that full dynamic range compression is possible at 9 dB input dynamic range. The amplification scheme has achieved remarkable 57 dB of access budget for soft and loud packets. Two-channel US scenario has also been experimented, in both cases more than 32-dB access budget has been achieved. The modification costs at the transmitter sides need to be considered, since in the proposed configuration NRZ transmitters must be substituted by DPSK transmitters.

The CML a cost-effective US transmitter configuration has been investigated. This setup could support $1,024$ subscribers on four WDM channels. The saturated-collision scheme extender was less dependent on channel power levels when operated at saturation, and it did not deteriorate the signal qualities of the lower power channels. Although, the conventional SOA setup could boost the optical power budget, but, in any case the SCA scheme outperformed the conventional amplification setup.

Moreover, data remodulation was experimentally demonstrated in two different modulation formats, OOK, and DPSK. The data remodulation was based on the injection of the downstream 10 Gbps optical signals to the FP-LDs in ONUs. The US 1.25 Gbps data transmission for up to 100 km has been demonstrated. The DR has been measured to be 8 and 12 dB for NRZ and DPSK, receptively. The higher optical power budget in DPSK case was due to it constant optical power, this avoided the cross-talk between the DS and US data traffic. The optical power budget in both cases did not show a significant difference. The number of subscribers were estimated to be 128 in both cases. The US bit-rate was 1.25 Gbps which is compatible with EPON and GPON standards. Chapter six also discussed about the comparison of ASE injection and remodulation techniques. The ASE seeded FP-LD injection locking showed worse performance

than remodulation, due to the higher seed power, and Rayleigh backscattering. This high intensity noise on the data stream was another reason. After 30 km the eye diagram was closed and error free transmission was not possible. The remodulation configuration offered an inexpensive architecture in comparison to ASE-seeded technique.

Having described the saturate-collision amplifier, introduced the advantages of this scheme for NG-PON, the new research needs to be conducted in the following directions;

- Usage of **multilevel signaling based coded modulation** which has been introduced in [65], this enables increasing the optical power budget even more, since the bit-error ratio can be shifted to higher values.
- Utilization of the **LDPC codes** [66] in NG-PON to again increase the access budget. This requires deep understanding of such codes and development of the new transceivers.
- In NG-PON, several channels may reach the SCA with different modulation formats, the SCA should be redesigned in a such a way that to support each of them individually without any interruption in the network. Therefore, a **flexible SCA** can be redesigned.
- Transmission of **ultra-wide band** optical signals proposed by [67] along with optical signals with other formats through the SCA scheme can be investigated.
- Finally, **high speed MEMS-VCSELs** proposed by [68] can be modulated directly and be used in the proposed scheme in this study. These devices offer an inexpensive production which reduce the cost of transceivers for NG-PONs

List of Figures

List of Tables

Appendix A

Traveling Wave Equations Proof

Here we prove Eqs. (5.9), (5.10), (5.13), and (5.14). We have inhomogeneous first order differential equations in (5.9), (5.10). The integration factor is used to solve the equations,

$$\frac{\partial S_\nu^+}{\partial z} - (g_\nu - \alpha) S_\nu^+ = \frac{n_g \gamma}{2\tau_{sp} c} D_\nu n_e \tag{A.1}$$

this can be written in the form

$$\dot{y} + p(z)y = g(z) \tag{A.2}$$

We multiply (A.3) by integrating factor $\mu(z)$

$$\mu(z)\dot{y} + \mu(z)p(z)y = \mu(z)g(z) \tag{A.3}$$

we assume that

$$\dot{\mu} = \mu(z)p(z) \tag{A.4}$$

$$\frac{\dot{\mu}}{\mu(z)} = p(z)$$

$$\int \frac{\dot{\mu}}{\mu(z)} dz = \int p(t)dz$$

$$\ln \mu(z) = \int p(t)dz + c_1$$

$$\mu(z) = \exp\{\int p(t)dz + c_1\} \tag{A.5}$$

Now we go back to Eq. A.3

$$\underbrace{(\mu(z)y(z))'}_{\mu(z)\dot{y}+\dot{\mu}y} = \mu(z)g(z) \tag{A.6}$$

$$\int (\mu(z)y(z))'dz = \int \mu(z)g(z)dz \tag{A.7}$$

$$\mu(z)y(z) + c_2 = \int \mu(z)g(z)dz \tag{A.8}$$

$$y(z) = \frac{\int \mu(z)g(z)dz - c_2}{\mu(z)} \tag{A.9}$$

Now substitute $\mu(z)$ we have our complete solution to the equation.

$$y(z) = \frac{\int \exp\{\int p(t)dz + c_1\}g(z)dz - c_2}{\exp\{\int p(t)dz + c_1\}} \tag{A.10}$$

Thus, the photon density can be obtained as

$$S_\nu^+(z) = \exp\{\int_0^z (g_\nu(x) - \alpha)dx\}\times \left[S_\nu^+(0) + \frac{n_g\gamma D_\nu}{2\tau_{sp}c}\int_0^z (\exp\{-\int_0^z (g_\nu(x) - \alpha)dx\}n_e(y))dy)\right] \tag{A.11}$$

Similarly,

$$S_\nu^-(z) = \exp\{-\int_z^L (g_\nu(x) - \alpha)dx\}\times \left[S_\nu^-(L) + \frac{n_g\gamma D_\nu}{2\tau_{sp}c}\int_0^z (\exp\{\int_z^L (g_\nu(x) - \alpha)dx\}n_e(y))dy)\right] \tag{A.12}$$

To simplify the mathematical expressions, photon density equations can be written as [40]

$$S_\nu^+(z) = G_\nu^+(z)[S_\nu^+(0) + I_{\nu_1}^+(z)] \tag{A.13}$$

$$S_\nu^-(z) = G_\nu^-(z)[S_\nu^-(L) + I_{\nu_2}^-(z)] \tag{A.14}$$

$$\tag{A.15}$$

$I_{\nu_1}^+(z)$, and $I_{\nu_2}^-(z)$ correspond to second terms in Eqs. (A), and (A.12) respectively. It is significant to find $S_\nu^+(0)$, and $S_\nu^-(L)$ by applying boundary conditions in Fig. 5.1.

$$
\begin{aligned}
S_\nu^+(0) &= R_1 S_\nu^-(z) = R_1 G_\nu^-(z)[S_\nu^-(L) + I_{\nu_2}^-(z)] \\
&= R_1 G_\nu^-[R_2 S_\nu^+(L) + I_{\nu_2}^-(z)] \\
&= R_1 G_\nu[R_2 G_\nu S_\nu^+(0) + R_2 G_\nu I_{\nu_1}^+(L) + I_{\nu_2}^-(0)] \\
&= \frac{R_1 G_\nu[I_{\nu_2}^-(0) + R_2 G_\nu I_{\nu_1}^+(L)]}{1 - R_1 R_2 G_\nu^2}
\end{aligned} \tag{A.16}
$$

Similarly,

$$
S_\nu^-(0) = \frac{R_2 G_\nu[I_{\nu_1}^+(L) + R_1 G_\nu I_{\nu_2}^-(0)]}{1 - R_1 R_2 G_\nu^2} \tag{A.17}
$$

where $G_\nu = G_\nu^-(0) = G_\nu^+(L)$.

Now we solve for $E^+(0)$ and $E^-(L)$ in Eqs. (5.13), (5.14). Figure 5.1 obeys the following boundary conditions

$$
E^+(0) = \sqrt{1 - R_1} E_{in} + \sqrt{R_1} E^-(0) \tag{A.18}
$$

$$
E^-(L) = \sqrt{R_2} E^+(L) \tag{A.19}
$$

$$
E_r = \sqrt{1 - R_1} E_{in} + \sqrt{1 - R_1} E^-(0) \tag{A.20}
$$

$$
E_{out} = \sqrt{1 - R_2} E^+(L) \tag{A.21}
$$

After substitution and simplifications we obtain

$$
\begin{aligned}
E^+(0) &= \sqrt{1 - R_1} E_{in} + \sqrt{R_1} E^-(L) \exp\{-i\beta L + \frac{1}{2}\int_0^L (g_s(x) - \alpha) dx\} \\
&= \sqrt{1 - R_1} E_{in} + \sqrt{R_1 R_2} E^+(0) \exp\{-2i\beta L + \int_0^L (g_s(x) - \alpha) dx\} \\
&= \frac{\sqrt{1 - R_1} E_{in}}{1 - \sqrt{R_1 R_2} \exp\{-2i\beta L + \int_0^L (g_s(x) - \alpha) dx\}}
\end{aligned} \tag{A.22}
$$

$E^-(L)$ is also solved in a similar way

$$
\begin{aligned}
E^-(L) &= \sqrt{R_2} E_0^+ \exp\{-i\beta L + \frac{1}{2}\int_0^L (g_s(x) - \alpha) dx\} \\
&= (\sqrt{(1 - R_2) R_1} E_{in} + \sqrt{R_1 R_2} E^-(0)) \exp\{-2i\beta L + \int_0^L (g_s(x) - \alpha) dx\} \\
&= \frac{\sqrt{(1 - R_2) R_1} E_{in} \exp\{-i\beta L + \frac{1}{2}\int_0^L (g_s(x) - \alpha) dx\}}{1 - \sqrt{R_1 R_2} \exp\{-2i\beta L + \int_0^L (g_s(x) - \alpha) dx\}}
\end{aligned} \tag{A.23}
$$

The signal gain of the amplifier can be obtain by using Eqs. (A.18), and (A.21)

$$
\frac{|E_{out}|^2}{|E_{in}|^2} = \frac{(1 - R_2)(1 - R_1) G_\nu}{(1 - \sqrt{R_1 R_2 G_\nu})^2 + 4\sqrt{R_1 R_2} G_\nu \sin^2(\beta L)} = G_{sig} \tag{A.24}
$$

Bibliography

[1] ITU-T G984.1, *Gigabit-capable passive optical networks (GPON): General characteristic*, International Telecommunication Union Std., 2008.

[2] M. Hajduczenia and H. da Silva, "IEEE 802.3av^{TM}-2009 10G-EPON and support for loss budgets beyond 29db," in *Optical Fiber Communication (OFC), collocated National Fiber Optic Engineers Conference, 2010 Conference on (OFC/NFOEC)*, March 2010, pp. 1–3.

[3] P. Chanclou, J.-P. Lanquetin, S. Durel, F. Saliou, B. Landousies, N. Genay, and Z. Belfqih, "Investigation into optical technologies for access evolution," in *Optical Fiber Communication - incudes post deadline papers, 2009. OFC 2009. Conference on*, March 2009, pp. 1–3.

[4] Z. Belfqih, P. Chanclou, F. Saliou, N. Genay, and B. Landousies, "Enhanced optical budget system performance of an burst extended PON at 10.7gbit/s over 60km of fibre," in *Optical Communication, 2008. ECOC 2008. 34th European Conference on*, Sept 2008, pp. 1–2.

[5] F. Ponzini, F. Cavaliere, G. Berrettini, M. Presi, E. Ciaramella, N. Calabretta, and A. Bogoni, "Evolution Scenario Toward WDM-PON [Invited]," *Optical Communications and Networking, IEEE/OSA Journal of*, vol. 1, no. 4, pp. C25–C34, September 2009.

[6] F. Effenberger, "The XG-PON System: Cost Effective 10 Gb/s Access," *Lightwave Technology, Journal of*, vol. 29, no. 4, pp. 403–409, Feb 2011.

[7] "IEEE Standard Wireless LAN Medium Access Control (MAC) and Physical Layer (PHY) Specifications," *IEEE Std. 802.11*, 2012.

[8] "IEEE Standard for Air Interface for Broadband Wireless Access Systems," *IEEE Std. 802.16*, 2012.

[9] ITU-T G992.1, "Asymmetric digital subscriber line (ADSL) transceivers," 1999.

[10] ITU-T G993.1, "Very high speed digital subscriber line transceivers (VDSL)," 1999.

[11] ITU-T G9701, *Fast access to subscriber terminals (G.fast): Physical layer specification*, International Telecommunication Union Std., 2016.

[12] P. Chanclou, B. Capelle, B. Charbonnier, J.-L. Courant, Y. Denis, N. Genay, S. Gosselin, D. Kurz, B. Landousies, E. Le Bris, B. Le Guyader, A. Pizzinat, and F. Saliou, "France telecom's pon deployment, learnt lessons and next steps," in *Optical Fiber Communication Conference and Exposition and the National Fiber Optic Engineers Conference (OFC/NFOEC), 2013*, March 2013, pp. 1–3.

[13] J. Park, G. Y. Kim, H. J. Park, and J. H. Kim, "Ftth deployment status &; strategy in korea: Gw-pon based ftth field trial and reach extension strategy of ftth in korea," in *Global Telecommunications Conference, 2008. IEEE GLOBECOM 2008. IEEE*, Nov 2008, pp. 1–3.

[14] P. Solina, "European pon deployments: A carrier view of the technical, regulatory, and economic challenges," in *Optical Communication (ECOC), 2010 36th European Conference and Exhibition on*, Sept 2010, pp. 1–20.

[15] Cisco VNI: Forecast and Methodology, 20142019, 2015.

[16] L. Spiekman, D. Piehler, P. Iannone, K. Reichmann, and H.-H. Lee, "Semiconductor optical amplifiers for fttx," in *Transparent Optical Networks, 2007. ICTON '07. 9th International Conference on*, vol. 2, July 2007, pp. 48–50.

[17] N. Genay, T. Soret, P. Chanclou, B. Landousies, L. Guillo, and F. Saliou, "Evaluation of the budget extension of a gpon by edfa amplification," in *Transparent Optical Networks, 2007. ICTON '07. 9th International Conference on*, vol. 4, July 2007, pp. 76–79.

[18] D. Nesset and P. Wright, "Raman extended gpon using 1240 nm semiconductor quantum-dot lasers," in *Optical Fiber Communication (OFC), collocated National Fiber Optic Engineers Conference, 2010 Conference on (OFC/NFOEC)*, March 2010, pp. 1–3.

[19] F. Saliou, P. Chanclou, F. Laurent, N. Genay, J. Lazaro, F. Bonada, and J. Prat, "Reach extension strategies for passive optical networks [invited]," *Optical Communications and Networking, IEEE/OSA Journal of*, vol. 1, no. 4, pp. C51–C60, September 2009.

[20] G. de Valicourt, D. Make, J. Landreau, M. Lamponi, G. Duan, P. Chanclou, and R. Brenot, "High gain (30 db) and high saturation power (11 dbm) rsoa devices as colorless onu sources in long-reach hybrid wdm/tdm-pon architecture," *Photonics Technology Letters, IEEE*, vol. 22, no. 3, pp. 191–193, Feb 2010.

[21] B. Schrenk, F. Bo, J. Bauwelinck, J. Prat, and J. Lazaro, "Energy-efficient optical access networks supported by a noise-powered extender box," *Selected Topics in Quantum Electronics, IEEE Journal of*, vol. 17, no. 2, pp. 480–488, March 2011.

[22] C. Antony, P. Ossieur, G. Talli, P. Townsend, H. Krimmel, A. Poustie, R. Wyatt, B. Harmon, I. Lealman, G. Maxwell, D. Rogers, and D. Smith, "Upstream burst-mode operation of a 100km reach, 16×512 split hybrid dwdm-tdm pon using tuneable external cavity lasers at the onu-side," in *Optical Communication, 2009. ECOC '09. 35th European Conference on*, Sept 2009, pp. 1–2.

[23] P. Ossieur, C. Antony, A. Clarke, A. Naughton, H.-G. Krimmel, Y. Chang, C. Ford, A. Borghesani, D. Moodie, A. Poustie, R. Wyatt, B. Harmon, I. Lealman, G. Maxwell, D. Rogers, D. Smith, D. Nesset, R. Davey, and P. Townsend, "A 135-km 8192-split carrier distributed dwdm-tdma pon with $2\times32\times10$gb/s capacity," *Lightwave Technology, Journal of*, vol. 29, no. 4, pp. 463–474, Feb 2011.

[24] S. Porto, C. Antony, P. Ossieur, and P. Townsend, "An upstream reach-extender for 10gb/s pon applications based on an optimised semiconductor amplifier cascade," in *Optical Communication (ECOC), 2011 37th European Conference and Exhibition on*, Sept 2011, pp. 1–3.

[25] P. O. S. Porto, C. Antony and P. D. Townsend, "An upstream reach-extender for 10Gb/s PON applications based on an optimized semiconductor amplifier cascade," *Optics Express*, vol. 20, no. 1, pp. 186–191, Dec. 2012. [Online]. Available: http://dx.doi.org/10.1364/OE.20.000186

[26] K.-I. Suzuki, Y. Fukada, T. Nakanishi, N. Yoshimoto, and M. Tsubokawa, "Burst-mode optical amplifier for long-reach 10 gbit/s pon application," in *Optical Fiber communication/National Fiber Optic Engineers Conference, 2008. OFC/NFOEC 2008. Conference on*, Feb 2008, pp. 1–3.

[27] S. Pato, R. Meleiro, D. Fonseca, P. Andre, P. Monteiro, and H. Silva, "All-optical burst-mode power equalizer based on cascaded soas for 10-gb/s epons," *Photonics Technology Letters, IEEE*, vol. 20, no. 24, pp. 2078–2080, Dec 2008.

[28] N. Frigo, P. Iannone, P. Magill, T. Darcie, M. Downs, B. Desai, U. Koren, T. Koch, C. Dragone, H. Presby, and G. Bodeep, "A wavelength-division multiplexed passive optical network with cost-shared components," *Photonics Technology Letters, IEEE*, vol. 6, no. 11, pp. 1365–1367, Nov 1994.

[29] S.-M. Lee, K.-M. Choi, S.-G. Mun, J.-H. Moon, and C.-H. Lee, "Dense wdm-pon based on wavelength-locked fabry-pe acute;rot laser diodes," *Photonics Technology Letters, IEEE*, vol. 17, no. 7, pp. 1579–1581, July 2005.

[30] M. Leeson and S. Sun, "Spectrum slicing for low cost wavelength division multiplexing," in *Mediterranean Winter, 2008. ICTON-MW 2008. 2nd ICTON*, Dec 2008, pp. 1–4.

[31] A. Ghatak, *Optics*. 1221 Avenue of the Americas, New York, NY 10020: McGraw-Hill, 2008.

[32] Corning ®SMF-28 ® Optical fiber, *Product Information*, Corning® Std., 2002.

[33] C. Doerr and K. Okamoto, "Advances in silica planar lightwave circuits," *Lightwave Technology, Journal of*, vol. 24, no. 12, pp. 4763–4789, Dec 2006.

[34] M. Hayee and A. Willner, "Nrz versus rz in 10-40-gb/s dispersion-managed wdm transmission systems," *Photonics Technology Letters, IEEE*, vol. 11, no. 8, pp. 991–993, Aug 1999.

[35] A. Gnauck and P. Winzer, "Optical phase-shift-keyed transmission," *Lightwave Technology, Journal of*, vol. 23, no. 1, pp. 115–130, Jan 2005.

[36] *Application Note DQPSK Bit Error Test Solution*, SHF, Wilhelm-von-Siemens-Str. 23D, 12277, Berlin, Germany, 2010.

[37] W. Shieh and I. Djordjevic, *OFDM for Optical Communications*. 30 Corporate Drive, Suite 400, Burlington, MA 01803, USA: Elsevier, 2010.

[38] A. Combe, "FTTH Council Europe," 2015.

[39] K. Han, E. Son, H. Choi, K. Lim, and Y. Chung, "Bidirectional wdm pon using light-emitting diodes spectrum-sliced with cyclic arrayed-waveguide grating," *Photonics Technology Letters, IEEE*, vol. 16, no. 10, pp. 2380–2382, Oct 2004.

[40] D. Marcuse, "Computer model of an injection laser amplifier," *Quantum Electronics, IEEE Journal of*, vol. 19, no. 1, pp. 63–73, Jan 1983.

[41] M. Connelly, "Wideband semiconductor optical amplifier steady-state numerical model," *Quantum Electronics, IEEE Journal of*, vol. 37, no. 3, pp. 439–447, Mar 2001.

[42] M. Adams, J. Collins, and I. Henning, "Analysis of semiconductor laser optical amplifiers," *Optoelectronics, IEE Proceedings J*, vol. 132, no. 1, pp. 58–63, February 1985.

[43] G. P. Agrawal, *Nonlinear Fiber Optics*. 525 B Street, Suite 1900, San Diego, California, 92101-4495, USA: Academic press, 2001.

[44] J. Armstrong, "Ofdm for optical communications," *Lightwave Technology, Journal of*, vol. 27, no. 3, pp. 189–204, Feb 2009.

[45] B. Lin, J. Li, H. Yang, Y. Wan, Y. He, and Z. Chen, "Comparison of dsb and ssb transmission for ofdm-pon," in *Optical Fiber Communication Conference and Exposition (OFC/NFOEC), 2012 and the National Fiber Optic Engineers Conference*, March 2012, pp. 1–3.

[46] X. Li, Y. Shao, S. Zou, C. Hou, X. Zheng, X. Liu, J. Zhang, W. Fang, and N. Chi, "Study of iq imbalance effect in direct-detection optical ofdm systems," in *Communications and Photonics Conference and Exhibition (ACP), 2009 Asia*, vol. 2009-Supplement, Nov 2009, pp. 1–6.

[47] Q. T. Le, F. Saliou, R. Xia, , P. Chanclou, T. von Lerber, A. Tervonen, M. Mattila, W. Weiershausen, S. Honkanen, and F. Küppers, "TDM/DWDM PON extender for 10 Gbit/s Downstream Transmission," in *Proc. ECOC'11*, 2011, paper Th.12.C.2, pp. 1–3.

[48] R. Vodhanel, A. Elrefaie, M. Iqbal, R. Wagner, J. Gimlett, and S. Tsuji, "Performance of directly modulated dfb lasers in 10-gb/s ask, fsk, and dpsk lightwave systems," *Lightwave Technology, Journal of*, vol. 8, no. 9, pp. 1379–1386, Sep 1990.

[49] R. Maher, L. Barry, and P. Anandarajah, "Cost efficient directly modulated dpsk downstream transmitter and colourless upstream remodulation for full-duplex wdm-pons," in *Optical Fiber Communication (OFC), collocated National Fiber Optic Engineers Conference, 2010 Conference on (OFC/NFOEC)*, March 2010, pp. 1–3.

[50] A. Tervonen, M. Mattila, W. Weiershausen, T. von Lerber, E. Parsons, H. Chaouch, A. Marculescu, J. Leuthold, and F. Kueppers, "Dual output soa based amplifier for pon extenders," in *Optical Communication (ECOC), 2010 36th European Conference and Exhibition on*, Sept 2010, pp. 1–3.

[51] ITU-T G987.2, *10-Gigabit-capable passive optical networks (XG-PON): Physical media dependent (PMD) layer specification*, International Telecommunication Union Std., 2010.

[52] Q. T. Le, A. Emsia, D. Briggmann, and F. Küppers, "Direct DPSK modulation of chirp-managed laser as cost-effective downstream transmitter for symmetrical 10-Gbit/s WDM PONs," *Optics Express*, vol. 20, no. 26, pp. B470–B478, Dec. 2012. [Online]. Available: http://dx.doi.org/10.1364/OE.20.00B470

[53] P. Rigby, "FTTH report," FTTH Handbook D&O Committee, Tech. Rep. Edition 6, August 2014.

[54] D. Breuer, F. Geilhardt, R. Hulsermann, M. Kind, C. Lange, T. Monath, and E. Weis, "Opportunities for next-generation optical access," *Communications Magazine, IEEE*, vol. 49, no. 2, pp. s16–s24, February 2011.

[55] R. Herber, "Changing the network structure-leaving the past behind," in *Proc. SPIE*, 2010, pp. 1–4.

[56] C.-H. Lee, W. Sorin, and B. Y. Kim, "Fiber to the home using a pon infrastructure," *Lightwave Technology, Journal of*, vol. 24, no. 12, pp. 4568–4583, Dec 2006.

[57] S.-M. Lee, K.-M. Choi, S.-G. Mun, J.-H. Moon, and C.-H. Lee, "Dense wdm-pon based on wavelength-locked fabry-pe acute;rot laser diodes," *Photonics Technology Letters, IEEE*, vol. 17, no. 7, pp. 1579–1581, July 2005.

[58] M. Leeson and S. Sun, "Spectrum slicing for low cost wavelength division multiplexing," in *Mediterranean Winter, 2008. ICTON-MW 2008. 2nd ICTON*, Dec 2008, pp. 1–4.

[59] J. young Kim, H.-S. Cho, S.-G. Mun, H.-K. Lee, and C.-H. Lee, "High-capacity dwdm-pon using triple-contact f-p lds," *Photonics Technology Letters, IEEE*, vol. 23, no. 2, pp. 127–129, Jan 2011.

[60] K. youl Park and C.-H. Lee, "Noise characteristics of a wavelength-locked fabry perot laser diode," *Quantum Electronics, IEEE Journal of*, vol. 44, no. 11, pp. 995–1002, Nov 2008.

[61] E. In de Betou, C.-A. Bunge, H. Ahlfeldt, and M. Olson, "140 km long-reach wdm-pon experiment for ring-based access network architectures," in *Optical Communication (ECOC 2013), 39th European Conference and Exhibition on*, Sept 2013, pp. 1–3.

[62] A. Emsia, Q. T. Le, R. E. Guendogdu, M. Malekizandi, E. I. de Betou, M. Olson, J. Keck, R. Herber, K. Rienecker, M. Fricke, and F. Kueppers, "Cost-efficient upstream transmitter using injection locked fabry-perot laser diodes for multi-gbit/s wdm-pon," *17. ITG-Symposium; IEEE Proceedings of, Photonic Network*, pp. 1–8, Mar 2016.

[63] Q. T. Le, A. Emsia, D. Briggmann, and F. Küppers, "Direct dpsk modulation of chirp-managed laser as cost-effective downstream transmitter for symmetrical 10-gbit/s wdm pons," *Opt. Express*, vol. 20, no. 26, pp. B470–B478, Dec 2012. [Online]. Available: http://www.opticsexpress.org/abstract.cfm?URI=oe-20-26-B470

[64] A. Emsia, Q. T. Le, M. Malekizandi, D. Briggmann, I. B. Djordjevic, and F. Kueppers, "WDM-TDM NG-PON Power Budget Extension by Utilizing SOA in the Remote Node," *IEEE Photon. J.*, vol. 6, no. 2, pp. 1–10, Apr. 2014. [Online]. Available: http://dx.doi.org/10.1109/JPHOT.2014.2314108

[65] I. Djordjevic, T. Liu, and T. Wang, "Multinary-signaling-based coded modulation for ultrahigh-speed optical transport," *Photonics Journal, IEEE*, vol. 7, no. 1, pp. 1–9, Feb 2015.

[66] I. B. Djordjevic and T. Wang, "Multiple component codes based generalized ldpc codes for high-speed optical transport," *Opt. Express*, vol. 22, no. 14, pp. 16 694–16 705, Jul 2014. [Online]. Available: http://www.opticsexpress.org/abstract.cfm?URI=oe-22-14-16694

[67] M. Malekizandi, Q. T. Le, D. Briggmann, A. Emsia, and F. Küppers, "Radio transmission and ber performance of uwb pulse generation based on directly modulated semiconductor laser," in *Optical Interconnects Conference (OI), 2015 IEEE*, April 2015, pp. 74–75.

[68] M. T. Haidar, S. Preu, S. Paul, C. Gierl, J. Cesar, A. Emsia, and F. Küppers, "Widely tunable telecom mems-vcsel for terahertz photomixing," *Opt. Lett.*, vol. 40, no. 19, pp. 4428–4431, Oct 2015. [Online]. Available: http://ol.osa.org/abstract.cfm?URI=ol-40-19-4428

Acronyms

ADC	Analog to Digital Converter
ADSL	Asymmetric Digital Subscriber Line
APD	Avalanche Photodiode
APON	Asynchronous Transfer Mode Passive Optical Network
ASE	Amplified Spontaneous Emission
AWG	Arrayed Waveguide Grating
AWG	Arbitrary Waveform Generator
BER	Bit Error Ratio
BLS	Broadband Light Source
BMRx	Burst-mode Receiver
BPL	Broadband Powerline
BPON	Broadband Passive Optical Network
CAGR	Compound Annual Growth Rate
CML	Chirped Managed Laser
CO	Central Office
CW	Continuous Wave Laser
DAC	Digital to Analog Converter
DBR	Distributed Bragg Reflector
DFB	Distributed Feedback Laser
DL	Downlink
DLI	Delay Line Interferometer
DPSK	Differential Phase Shift Keying
DQPSK	Differential Quadrature Phase Shift Keying
DR	Dynamic Range

DS	Downstream
DSB	Dual Side Band
DWDM	Densed Wavelength Division Multiplexing
EAM	Electroabsorption Modulator
EDFA	Erbium Doped Fiber Amplifier
ER	Extinction Ratio
DSL	Digital Subscriber Line
DSLAM	Digital Subscriber Line Access Multiplexer
EPON	Ethernet Passive Optical Networks
FEC	Forward Error Correction
FFT	Fourier Transform
FP-LD	Fabry-Pérot Laser Diode
FSAN	Full Service Access Network
FSR	Free Spectral Range
FTTdp	Fiber-to-the-Distribution Point
FTTx	Fiber-to-the-x
FWHM	Full Width Half Maximum
G-PON	Gigabit-Passive Optical Networks
GVD	Group Velocity Dispersion
10GE-PON	10 Gigabit Ethernet Passive Optical Networks
HDTV	High Definition Television
HFC	Hybrid Fiber Coax
IFFT	Inverse Fourier Transform
ISI	Inter-symbol Interference
ITU-T	International Telecommunication Union-Telecommunication Standardization Sector
LiNbO3	Lithium Niobate
LTE	Long Term Evolution
MCM	Multi-carrier Modulation
MZI	Mach-Zehnder Interferometer
MZM	Mach-Zehnder Modulator

NRZ	Non-Return-to-Zero
NG-PON	Next-Generation Passive Optical Network
ODN	Optical Distribution Unit
O-E-O	Optical-Electrical-Optical
OFDM	Orthogonal Frequency Division Multiplexing
OLT	Optical Line Terminal/Termination
OOK	On-Off Keying
ONU	Optical Network Unit
P2P	Point-to-Point
P2M	Point-to-Multipoint
PPG	Pulse Pattern Generator
PRx30	Refer to the OLT/ONU optical interface specifications
RZ	Return-to-Zero
Rx	Receiver
SCA	Saturated Collision Amplifier
SCR	Subcarrier to Carrier Ratio
SMF	Single Mode Fiber
SPM	Self-Phase Modulation
SSB	Single Side Band
SOA	Semiconductor Optical Amplifier
TDM	Time Division Multiplexing
TIR	Total Internal Reflection
Tx	Transmitter
UMTS	Universal Mobile Telecommunication System
UL	Uplink
US	Upstream
VCSEL	Vertical Cavity Surface Emitting Diode
VDSL	Very High Data Rate Digital Subscriber Line
VOA	Variable Optical Attenuator
VoD	Video-on-Demand
WDM	Wavelength Division Multiplexing

WiFi	Wireless Fidelity
WLAN	Wireless Local Area Network
WiMAX	Worldwide Interoperability for Microwave Access
WPAN	Wireless Personal Area Network
WWAN	Wireless Wide Area Network
XG-PON	10 Gigabit-capable Passive Optical Network

Symbols

α	The absorption coefficient/ fiber attenuation
β	Propagation mode parameter
γ	Fraction of spontaneously emitted photons
ε	Permittivity of a material
η	Quantum efficiency
λ	Wavelength
μ	Permeability of a material
τ_g	Group delay of pulse broadening
τ_{sp}	Electron lifetime due to spontaneous photon emission
ϕ	Phase shift
ω	Angular frequency
Δ	Fractional index change
Λ	Period of the grating
Ψ	Field components
B	Magnetic flux density
c	The speed of light
D	Electric displacement charge
D	Chromatic dispersion
E	Electric field
f	Frequency
g_ν	Gain coefficient at λ_ν
g_s	Gain coefficient (general)
G_ν	Gain function at λ_ν
H	Magnetic field

n	Refractive index of a medium
n_e	The total electron density in the conduction band contributing to interaction with photons
n_g	Group refractive index
NA	Numerical aperture
P_λ	Optical power per wavelength
PB	Optical power budget
R	Responsivity of a photodiode
R_F	Mirror reflectivity of the cavity
S_ν	Photon density at λ_ν
U	Waveguide mode parameter
V	Normalized waveguide parameter
V_π	Mach-zehnder modulator characteristic voltage
W	Waveguide mode parameter
z	z coordinate of the travelling-wave

Own Publications

Journal

1. **Emsia, A.**; Le, Q. T. ; Malekizandi, M.; Briggmann, D.; Djordjevic, I. B.; and Küppers, F., "WDM-TDM NG-PON Power Budget Extension by Utilizing SOA in the Remote Node," *IEEE Photon. J.*, vol. 6, no. 2, pp. 110, Apr. 2014. [Online]. Available: http://dx.doi.org/10.1109/JPHOT.2014.2314108

2. Malekizandi, M.; Le; Q. T.; **Emsia, A.**, Briggmann, D.; Chipouline, A; Küppers, F., "TDM-PON compatible generation of 10 Gbps NRZ and 1.25 Gbps UWB signals by a single light source", Opt. Express, vol. 24, pp. 17018, 2016, ISSN 1094-4087. [Online]. Available: http://dx.doi.org/10.1364/OE.24.017018

3. Malekizandi, M.; Le, Q. T.; **Emsia, A.**; Briggmann, D.; Küppers, F., " Generation of UWB Doublet Pulse Based on Directly Modulated Laser and Chromatic Dispersion," in *IEEE Photonics Technology Letters*, vol. 28, no. 3, pp. 343-346, Feb.1, 1 2016.

4. Haidar, M. T.; Preu, S.; Paul, S.; Gierl, C.; Cesar, J.; **Emsia, A.**; and Küppers, F., "Widely Tunable Telecom MEMs-VCSEL for Terahertz Photomixing," *Opt. Lett.*, vol. 40, no. 19, pp. 44284431, Oct 2015. [Online]. Available: http://ol.osa.org/abstract.cfm?URI=ol-40-19-4428

5. Le, Q. T.; **Emsia, A.**; Briggmann, D.; and Küppers, F., "Direct DPSK Modulation of Chirp-Managed Laser as Cost-effective Downstream Transmitter for Symmetrical 10-Gbit/s WDM PONs," Opt. Express, vol. 20, no. 26, pp. B470-B478, Dec 2012. [Online]. Available: http://www.opticsexpress.org/abstract.cfm?URI=oe-20-26-B470

Conference

1. **Emsia, A.**; Q. T.; Guendogdu, R. E. ; Malekizandi, M.; In de Betou, E.; Olson, M.; Keck, J.; Herber, R; Rienecker, K.; Fricke, M.; and Küppers, F., Cost-efficient upstream transmitter using injection locked fabry-perot laser diodes for multi-gbit/s wdm-pon, in *IEEE Proceedings of Photonic Network, 17. ITG-Symposium*, pp. 18, Mar 2016.

2. Malekizandi, M.; Le, Q. T.; Briggmann, D. ; **Emsia, A.**; and Küppers, F., "Radio transmission and ber performance of uwb pulse generation based on directly modulated

semiconductor laser," in Optical Interconnects Conference (OI), 2015 IEEE, April 2015, pp. 7475.

3. Malekizandi, M.; Le, Q. T.; Nessling, H.; **Emsia, A.**; Briggmann, D.; and Küppers, F., "Adaptive UWB Pulse Generation with Accumulated Chromatic Dispersion Variations in Optical Fiber Networks ," in CLEO Europe 2015.

4. **Emsia, A.**; Le, Q. T., Malekizandi, M.; Briggmann, D.; and Küppers, F., "10 Gbit/s PON Upstream Burst-mode Equalization Based on SOAs," in Asia Communications and Photonics Conference 2014, OSA Technical Digest (online) (Optical Society of America, 2014), paper ATh1H.2.

5. **Emsia, A.**; Malekizandi, M.; Briggmann, D.; Le, Q. T.; Djordjevic, I. B.; Küppers, F. : "Experimental Demonstration of NG-PONs Power Budget Enhancement Techniques," in Photonics West, SPIE 2014, February 2014, San Francisco, California, USA.

6. Malekizandi, M. ; **Emsia, A.** ; Briggmann, D. ; Le, Q. T. ; Djordjevic, I. B. ; Küppers, F. : "Power budget extension for higher order modulation formats in PONs," in Photonics West, SPIE 2014, February 2014, San Francisco, California, USA.

7. **Emsia, A.**; Malekizandi, M.; Le, T. Q.; Djordjevic, I. B.; Küppers, F. : "1 Tb/s WDM-OFDMA-PON Power Budget Extension Techniques," in 2013 IEEE Photonics Conference (IPC) , Sep 2013 , Bellevue, WA, USA .

8. Malekizandi, M.; **Emsia, A.**; Briggmann, D.; Le, Q. T.; Djordjevic, I.B. ; Küppers, F. : "Power budget extension for OFDM-TDM-WDM PON," in DokDok 2013, Oktober 2013, Jena, Germany.

9. **Emsia, A.** ; Malekizandi, Mohammadreza ; Briggmann, Dieter ;Le, Q. T.; Küppers, Franko : "DPSK-based reach extension for NGbit/s NG-PON," in DokDok 2013, Oktober 2013, Jena, Germany.

10. **Emsia, A.**; Le, Q. T.; Briggmann, D.; Küppers, F. : "WDM-PON Budget Extension Techniques for Nx10 Gbit/s DPSK Signals," in SPIE Photonics West 2013, February 2013, San Francisco, California, USA.

11. **Emsia, A.**; Le, Q. T.; von Lerber, T.; Briggmann, D. ; Küppers, F. : "WDM-PON Upstream Budget Extension for 4x10 Gbit/s DPSK Directly Modulated Lasers," in 2013 IEEE Photonics Conference (IPC), Sep 2013 , Bellevue, WA, USA .

12. **Emsia, A.** ; Le, Q. T.; von Lerber, T.; Briggmann, D.; Küppers, F. : "Budget extension schemes for nx10 Gbits/s DPSk-Based TDM/WDM DPSK-BASED TDM/WDM PON." in OPTICS 2012 , July 2012 , Rome, Italy.

Award

- **Best Student Paper Award**

  A. Emsia, Q. T. Le, M. Malekizandi, D. Briggmann, and F. Küppers,“ *10 Gbit/s PON Upstream Burst-mode Equalization Based on SOAs*,” in Asia Communications and Photonics Conference 2014, OSA Technical Digest (online) (Optical Society of America, 2014), paper ATh1H.2.

Supervised Master Thesis

- M. Malekizandi: “Higher Order Modulation Formats for PON Systems”, Master thesis, D 2199-M, Note= 1,3.
- C. Ersoy, “Digital coherent receivers in passive optical WDM networks”, Master thesis, D 2217-M, Note= 1,7.
- E. Slama, “Investigation and implementation of a measurement method to determine the optical modulation index in RFoG networks”, Master thesis, D 2248-M, Note= 1,3.

Curriculum Vitae

Personal Profile

Name:	Ali Emsia
Date of Birth:	01.07.1986
Place of Birth:	Tehran, Iran

Education and Work Experience

2003-2007	B.Sc. in Electrical Engineering, Eastern Mediterranean University, North Cyprus
2007-2009	M.Sc. Master of Digital Communications, Faculty of Engineering, Christian-Albrechts-Universität zu Kiel, Germany
2009-2010	Electrical Engineering and Information Technology, Chair for Communication, Christian-Albrechts-Universität zu Kiel, Germany
2010-2011	Digital Signal Processing and System Theory, Faculty of Engineering Kiel University
2011-2016	Research assistant at the Department for Photonics and Optical Communications, Institute for Microwave Engineering and Photonics, Technische Universität Darmstadt
04.2013-10.2013	Visiting researcher at College of Optical Sciences, University of Arizona , USA.
2016-	Product manager at ASC-TEC Delta Electronics Company, Bodman-Ludwigshafen, Germany.